U.S. Department of the Interior
U.S. Geological Survey

RESISTIVITY OF LAKE VALLEY FAULT FROM AUDIOMAGNETOTELLURIC MEASUREMENTS, SIERRA COUNTY, SOUTHERN NEW MEXICO

by

Douglas P. Klein and Richard A. Wise
U.S. Geological Survey
Denver, Colorado

U.S. Geological Survey Open-File Report 98-334

RESISTIVITY OF LAKE VALLEY FAULT
FROM AUDIOMAGNETOTELLURIC MEASUREMENTS,
SIERRA COUNTY, SOUTHERN NEW MEXICO

CONTENTS

INTRODUCTION 1

DATA 4

RESULTS 6

Line 100: South of Monument Peak 6

Sites 325 and 326: Relation of Geoelectric Units Northeast of Monument Peak to Line 100 12

Line 200: Measurements Along Berrenda Crrek North of Town Mountain 17

SUMMARY 21

REFERENCES 22

APPENDIX: Data and Model Response Fits 23

LIST OF FIGURES AND TABLES

FIGURES

Figure 1--Map of AMT survey sites and lines. 2
Figure 2--AMT data for line 100. 8
Figure 3--Resistivity model for line 100. 10
Figure 4--AMT data and inversion results for sites 124, 325, and 326 ... 13
Figure 5--Bostick transform and resistivity model for sites 124, 325 and 326. 16
Figure 6--AMT data and model for line 200. 19

Appendix Figures

Figure 7--Data for site 111. 24
Figure 8--Data for site 112. 27
Figure 9--Data for site 114. 30
Figure 10--Data for site 116. 33
Figure 11--Data for site 117. 36
Figure 12--Data for site 118. 39
Figure 13--Data for site 119. 42
Figure 14--Data for site 120. 45
Figure 15--Data for site 121. 48
Figure 16--Data for site 122. 51
Figure 17--Data for site 124. 54
Figure 18--Data for site 203. 57
Figure 19--Data for site 204. 60
Figure 20--Data for site 205. 63
Figure 21--Data for site 206. 66
Figure 22--Data for site 325. 69
Figure 23--Data for site 326. 72

TABLES

Table 1--Resistivity ranges of geologic materials in the southwest U.S... 3
Table 2--Chief lithologic units in the vicinity of Lake Valley Mining Area. 7

RESISTIVITY OF LAKE VALLEY FAULT FROM AUDIOMAGNETOTELLURIC MEASUREMENTS, SIERRA COUNTY, SOUTHERN NEW MEXICO

by

Douglas P. Klein and Richard A. Wise
U.S. Geological Survey
Denver, Colorado

INTRODUCTION

This report describes the results of geoelectromagnetic measurements (2-23,000 Hz) in the Lake Valley area, southern New Mexico (fig. 1). Measurements were made in October 1997 to determine subsurface resistivity structure to aid geologic investigations of the Lake Valley Fault. The fault forms the western boundary for Silver-Manganese (Ag-Mn) mineralization in the Lake Valley Mining area. The study area is near State Route 27, a driving distance of about 39 km (24 mi.) SW of the town of Truth-or-Consequences or 65 km (40 mi.) NE of the town of Deming. Traverses across the NW-trending Lake Valley Fault were established south and north of the Lake Valley mining area. This work is part of investigations by the U.S. Geological Survey (USGS) for the Bureau of Land Management. The combined work focuses on understanding the geological setting and mineralization within and surrounding Lake Valley Ag-Mn Mining area.

The geoelectrical method used for the present study is audiomagnetotellurics (AMT) (Vozoff, 1972, 1991; Strangway and others, 1973). The AMT technique uses long horizontal-wavelength (approximating a plane wave) electromagnetic fields at many frequencies to map the distribution of electrical resistivity versus depth in the Earth. Geological inferences are based on the relationships between electrical resistivity to rock types and their physical structures (Table 1). AMT measurements are made of both time-varying magnetic and electric (telluric) fields having frequencies that overlap the audio (acoustic) frequency band of 20 to 20,000 Hz. There are continuous natural electromagnetic signals at these frequencies nearly everywhere on Earth. These electromagnetic signals are generated by lightning and similar atmospheric electric disturbances. Electromagnetic fields from controlled manmade sources are also used. AMT

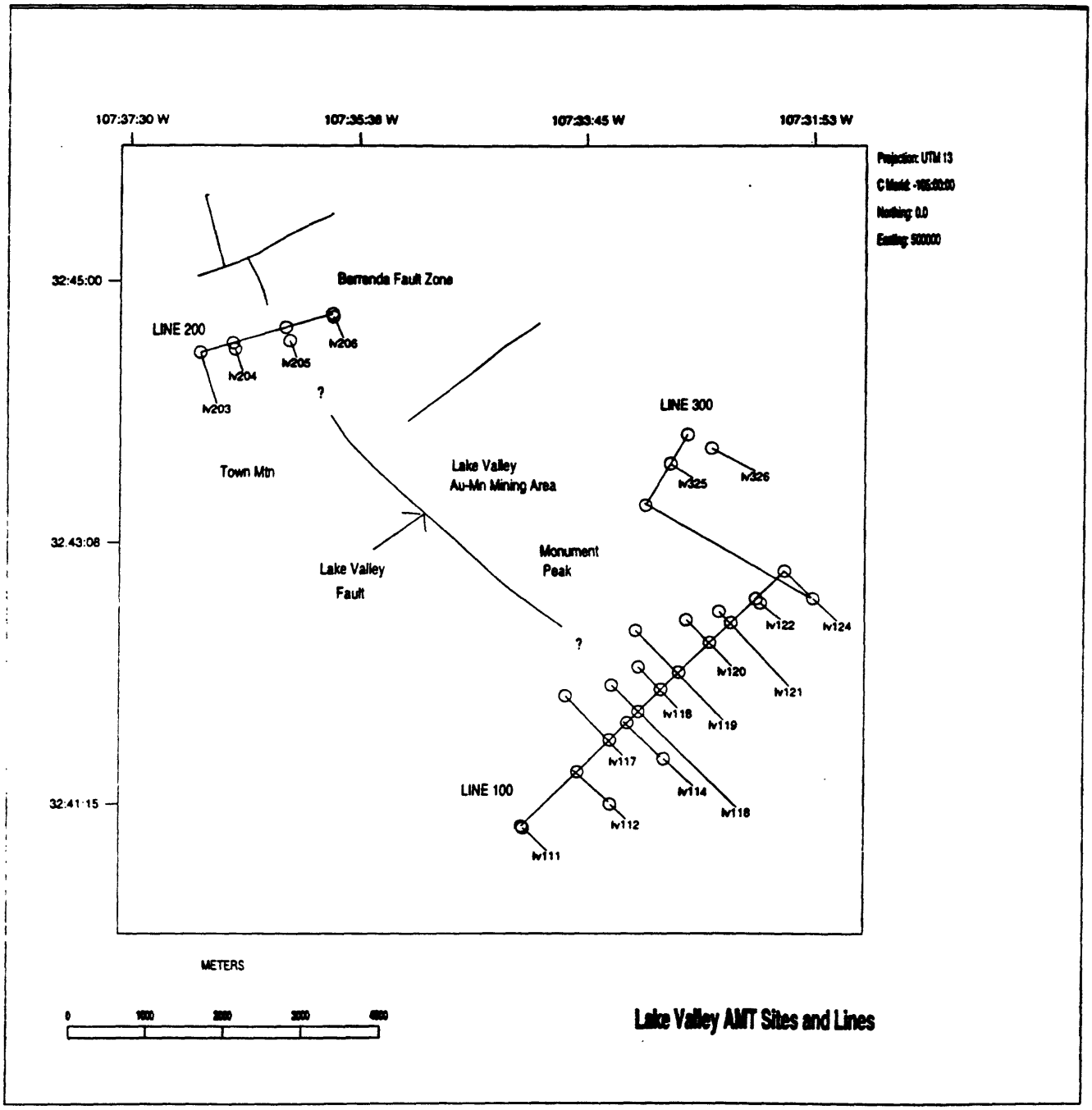

Figure 1--Map of AMT survey sites and lines in relation to prominent faults and topographic features. Line 100, 200, and 300 are shown with the projected locations of measurement sites.

Table 1--Resistivity ranges of geologic materials in the southwest U.S. (Keller and Frischknecht, 1966, p.1-55; Brant, 1966; Klein, 1996). The lower 1/3 (approximate) of these ranges takes into account saturation by ground water (10-50 Ohm-m). The upper 2/3 of these ranges represent low-porosity, dry and unaltered, rock. Ranges shown may not account for the presence of conductive metallic sulfide minerals and hot saline water (0.1 - 10 Ohm-m) or resistive alteration such as silicification. Single geologic units may exhibit a range in resistivity caused by a variations in weathering, alteration, and pore-fluid content.

Geologic Material	Resistivity Range (Ohm-m)
Alluvium	10 - 100
Gravel and conglomerate	20 - 400
Argillite and shale	20 - 500
Tertiary volcanic rock	20 - 1000
Sandstone	40 - 1000
Mesozoic-Tertiary intrusions	50 - 2000
Proterozoic schist	50 - 5000
Limestone and dolomite	200 - 5000
Quartzite and Proterozoic granite and gneiss	200 - 5000

signals penetrate into the Earth to depths ranging to about 3,000 m dependent on the resistivity of the Earth. The depth penetrated is proportional to the resistivity along the path of the signal, and inversely proportional to the frequency of the signal, so that measurements at multiple frequencies allow interpretation of resistivity at various depths.

DATA

Data were acquired along roads and jeep trails using a single vehicle and a field crew of two. Positions were established (+/- 30 m) using a Magellan ProMark X geographic positioning (GPS) unit. Instrumentation consisted of an "MT-1" system with acquisition and processing software from Electromagnetic Instruments Incorporated (EMI). Acquisition components included "BF-6" ferrite-cored induction coils to sense the magnetic field (H) variations, and titanium alloy electrical grounding stakes separated by 30 m to sense the horizontal electrical field (E). Sensors where laid out to measure horizontal components of H and E in orthogonal X and Y directions, selected as true north and east respectively. Sensors connect to filters, amplifiers, and digitizers that electronically condition the signals and route them to a computer for storage and digital processing. To supplement natural signals at frequencies above 900 Hz, electromagnetic signals were artificially generated using a battery-powered, dual-loop "IMX-1" transmitter system from EMI. This transmitter was deployed at a distance of about 300 m from the measurement. Except for site 124 (fig. 1) where a local H reference was employed (Gamble and others, 1979a), data were acquired with single site procedures.

Data at frequencies lower than 300 Hz were acquired as time-series and processed into Fourier series. Higher frequency data were acquired directly as Fourier series. Auto- and cross-spectra estimates were computed and used to estimate AMT (or MT) impedances (E/H; units of Ohm) and various derived response parameters (Vozoff, 1972; 1991). Typically, response estimates were acquired at 39 equal-log-spaced frequencies from 2.2 to 24,000 Hz. Data are presented as derived apparent resistivity, Rij (Ohm-m; proportional to the square of impedance) (Cagniard, 1953) and impedance phase Pij (degrees), where the subscripts i,j may be "x" or "y" to indicate the relationship of the electric field component ("i") to the magnetic field component ("j"). Rij have the units of resistivity, but cannot be construed as the physical resistivity of the Earth (additional analysis is required to estimate physical resistivity). Additional parameters on data quality and dimensionality are shown in the Appendix.

Data analysis, modeling, and plotting were accomplished with "Geotools MT" software. Impedances along traverses were rotated so that the XY component was nearly perpendicular the projected trend of the target (Lake Valley fault). In many cases the data had characteristics common to layered subsurface conditions. In other cases, this direction corresponded to the direction of electrical strike where the XX and YY impedance elements are minimized in a 2-D situation. Some data showed indications of 3-D structure, particularly on part of a traverse north of Town Mountain.

Data associated with coherency less than 0.8 were usually discarded, as well as much of the data that deviated significantly from the trend of the response function versus frequency. Site 325 (fig. 1) showed an appreciable static shift (a constant offset between Rxy and Ryx for all acquired frequencies). Here Rxy and Ryx curves paralleled each other with a 0.3 log-cycle offset. This indicates a nearby (10's of meters) and shallow (10 m or less from the surface) inhomogeneity. Rxy for site 325 was arbitrarily shifted downward to agree with the Ryx curve. The processed data show a mean scatter of about 0.10 (log cycle, or 10-percent relative error).

Rxy data, after editing, were fit by a layered Earth model response using both the method of Bostick (1977) (applied to phase variations and scaled to apparent resistivity) and that of Constable and others (1979) (applied to both amplitude and phase). The component perpendicular to the Lake Valley fault was used for all analysis. The Bostick transform is an analytic procedure useful to obtain a first estimate of signal penetration range and subsurface resistivity. The inversion of Constable and others (1979) weights the modeling based analytical error estimates of the data (Gamble and others, 1979b). This inversion of forms the core of the analysis. Neither 2-D nor 3-D modeling is presented. The majority of 1-D models fit the data satisfactorily, and models usually show consistent resistivity variation along the profiles indicating that conclusions on the resistivity structure are probably adequate for inferring preliminary geological models.

RESULTS

Data are discussed along three lines (100, 200, 300; fig. 1). Sites are designated by a alphabetic prefix indicating the survey (lv for Lake Valley) and a 3 digit number; the first digit indicates the line number and the last two numbers are unique site numbers. For instance, lv123 indicates site number 23 which is used in line 100; lv124 was used for both line 100 and 300. The site designation prefix "lv" is omitted on the cross-sections to be presented, and will likewise not be further specified in the text. Line 100 crosses the projected trend of the Lake Valley fault south of Monument Peak. Line 300, east of Monument Peak, is discussed in the context of the resistivity structure associated with line 100. Line 200 crosses the projected trend of the Lake Valley fault north of Town Mountain. Remarks on the mapped geology that accompany this interpretation are based on discussions with USGS geologists working in the area concurrently with the electrical surveys (J.M. O'Neill, C.J. Nutt, and D.A. Lindsey, verbal and written communications, April 1998), as well as previous local and regional geologic maps by Creasey and Granger (1953) and Jicha (1954).

Line 100: South of Monument Peak

Geological strata west of Lake Valley fault (fig. 1) is composed of Tertiary volcanic rocks of unknown thickness. Strata east of Lake Valley fault consists of a cover of Tertiary volcanic rocks underlain by Paleozoic sedimentary units that outcrop in and north of the Lake Valley mining area. Precambrian rocks in the study area are unknown except by inference from distant outcrops and inferences on the estimated thickness of the overlying Tertiary and Paleozoic rocks. Lithologic units encountered are listed in table 2 . Geologic units in the vicinity of the Lake Valley mining area (fig. 1, table 2) have been estimated from geological mapping to dip about 20° SE. Such a dip may result in a differential depth to units of about 350 m per km.

Data along line 100 are shown in figure 2. Site locations have been projected onto the line as shown in figure 1. Figure 2 shows apparent resistivity and impedance phase vs. frequency and distance and a Bostick transform showing a preliminary view of resistivity versus depth and distance. Frequency decreases downward in the direction of greater penetration. Phase and apparent resistivity are generally antithetic in that phases less than 45° indicate transitions to higher apparent resistivity, whereas phases greater than 45° indicate transitions to

Table 2—Generalized sequence of the chief lithologic units in the vicinity of Lake Valley Mining area along with their relative resistivity (low, medium and high). Table 1 lists typical ranges of resistivity values for various lithologies. See text for actual resistivities encountered.

Gravel, float and alluvium (Quaternary-Tertiary): variable thickness, probably less than 30 m; low resistivity

Tertiary volcanic rock (Tertiary, mainly Rubio Peak formation, lumped with about 20 m of various Mississippian calcareous rocks east of Lake Valley fault): 100 m thick east of Lake Valley fault; unknown thickness west of Lake Valley fault; moderate resistivity

Percha shale (Devonian): 40 m thick; low resistivity

Dolomites and Limestone (Ordovician-Silurian): 300 m thick; high resistivity

Granite and gneiss (Proterozoic): high resistivity

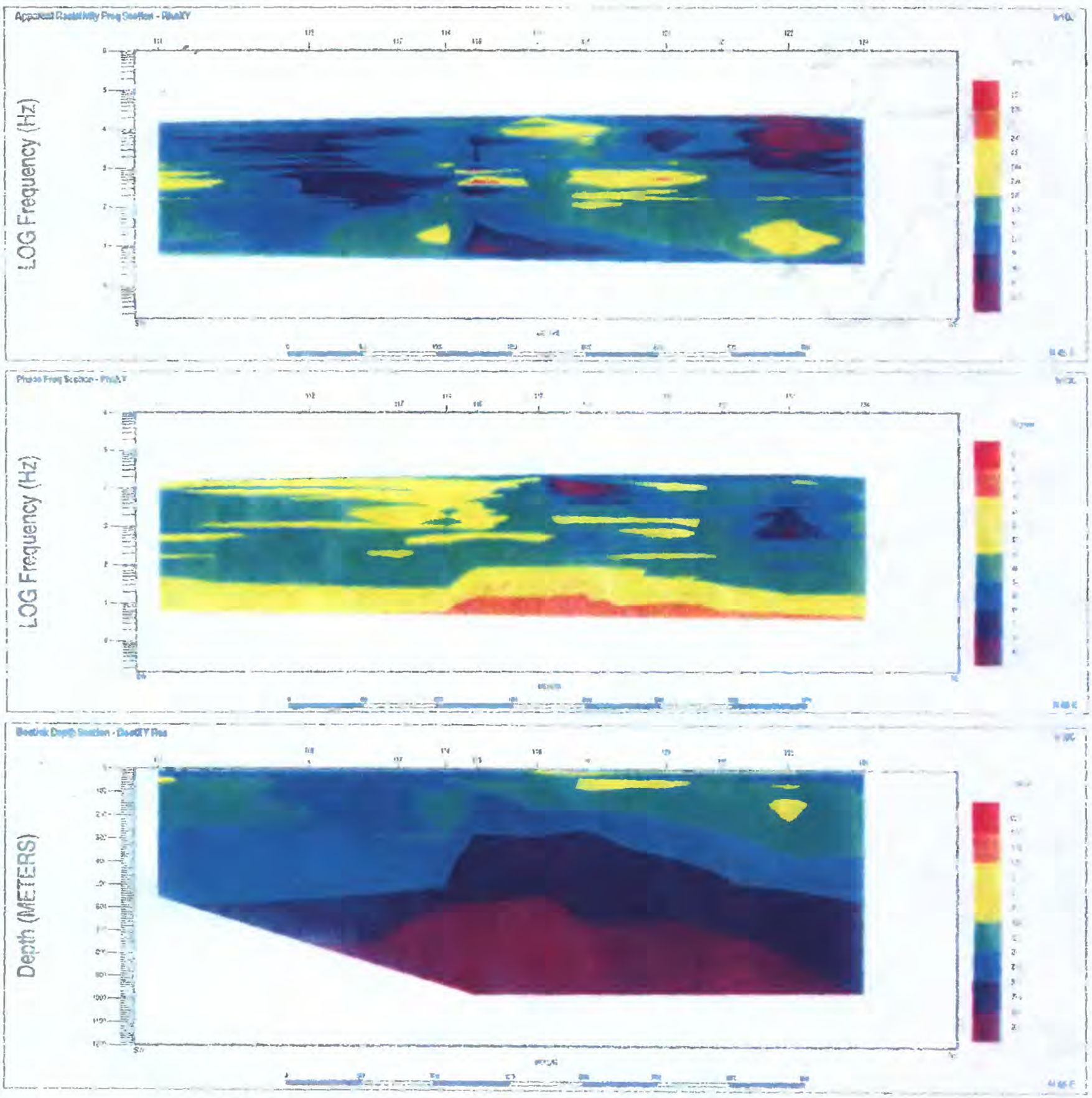

Figure 2--AMT Data for line 100. **TOP**-apparent resistivity (Rxy) vs. distance and frequency; **CENTER**-impedance phase (Pxy) vs. distance and frequency; **BOTTOM**-Bostick transform vs. distance and depth; Bostick transform based on phase (Pxy) with X rotated approximately perpendicular to Lake Valley fault. Frequency plotted as logarithm base 10; decreases downward. Color codes shown on bars. Labeled ticks along top of sections show projected location of AMT sites

lower apparent resistivity. The Bostick transform shows depth of penetration to be 1.1 km, a picture of generally increasing resistivity with depth with superimposed low-resistivity layers, an indication of a lateral discontinuity in the vicinity of site 16, and an apparent eastward dip in the strata east of site 16.

Figure 3 shows a resistivity-depth-distance model for line 100. This model is an estimated cross-section of the physical distribution of resistivity beneath line 100. Resistivity is color coded with lower to higher resistivity associated with the progression from reds-yellows-greens-blues-purples. A similar color progression is used in other figures of this report, but the colors may represent different resistivity ranges. The model was formed as a composite of 1-D inversions for each site therefore the section is portrayed with a block of layers beneath each site. The plot shows a transition zone between models of adjacent sites. The transition zone is arbitrarily plotted midway between sites and spans a distance of 30-percent of the separation between sites. Figure 3 (top) shows the upper 250 m of the model with a vertical exaggeration of about 10; the bottom shows the section to 2,000 m with no vertical exaggeration. The depth of resolution for the data is about 1,200 over most of the section, shallower under sites 117 and 122. Vertical banding at depths greater than 1,200 m is an artifact; for the deepest layer, only depth and resistivity are resolved; thickness is unknown and, for the present data, physically indistinguishable in the present data from being infinite in thickness.

. In figure 3, interpretative lines labeled as A. B, C, U, V mark inferred interfaces between electrical resistivity units . These units may differ from geologic units. Site 118 is near the inferred southward extension of the Lake Valley fault. The discontinuity in the data (fig. 2), and in various lines on the model (fig. 3) is an expression of this fault. To the west of the fault, where geologic mapping indicates an sequence of andesitic volcanic rocks of unknown thickness, there are definable electrical units that are as clear as those to the east where there is a thinner volcanic cover overlying a succession of Paleozoic rocks. To the east of the fault, the uppermost strata is inferred to be andesitic volcanic flows based on float in the overburden, and outcrop on Monument Peak.

Line A (fig. 3, top, NE of site 118) at 10 to 50 m depth marks the top of a low-resistivity unit (3-10 ohm-m). This is interpreted to represent the bottom of the of unconsolidated gravel,

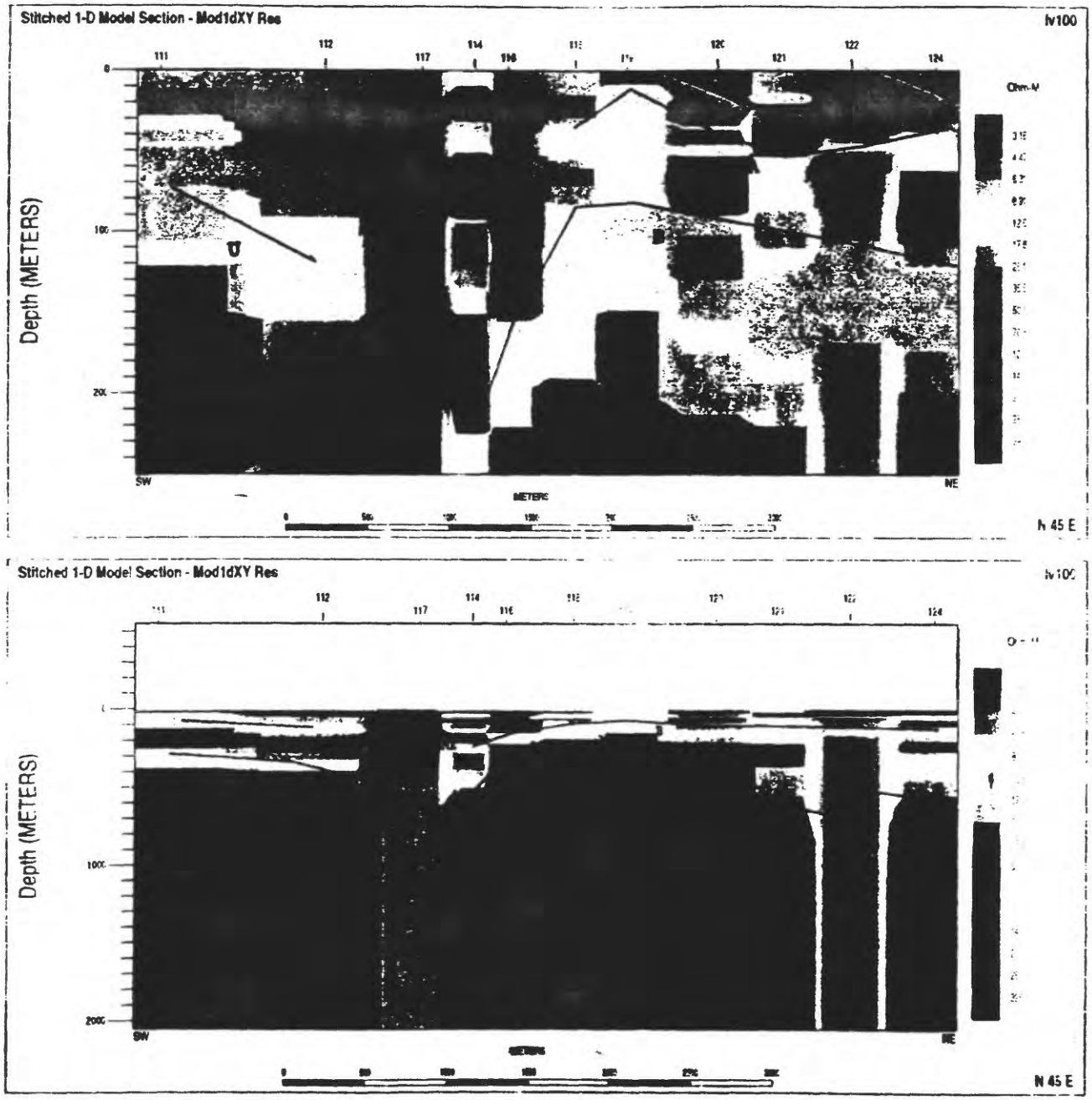

Figure 3--Resistivity model for line 100. **TOP**-model to 250 m depth with vertical exaggeration of 10; **BOTTOM**-model to 2,000 m depth with no vertical exaggeration . Model is composite of 1-D resistivity inversions based on error-weighted apparent resistivity (Rxy) and phase (Pxy). X rotated approximately perpendicular to Lake Valley fault. Resistivity color codes shown on bars. Labeled ticks along top of sections show projected location of AMT sites. Lines labeled A, B, C, U, and V show interpreted top of geoelectric units.

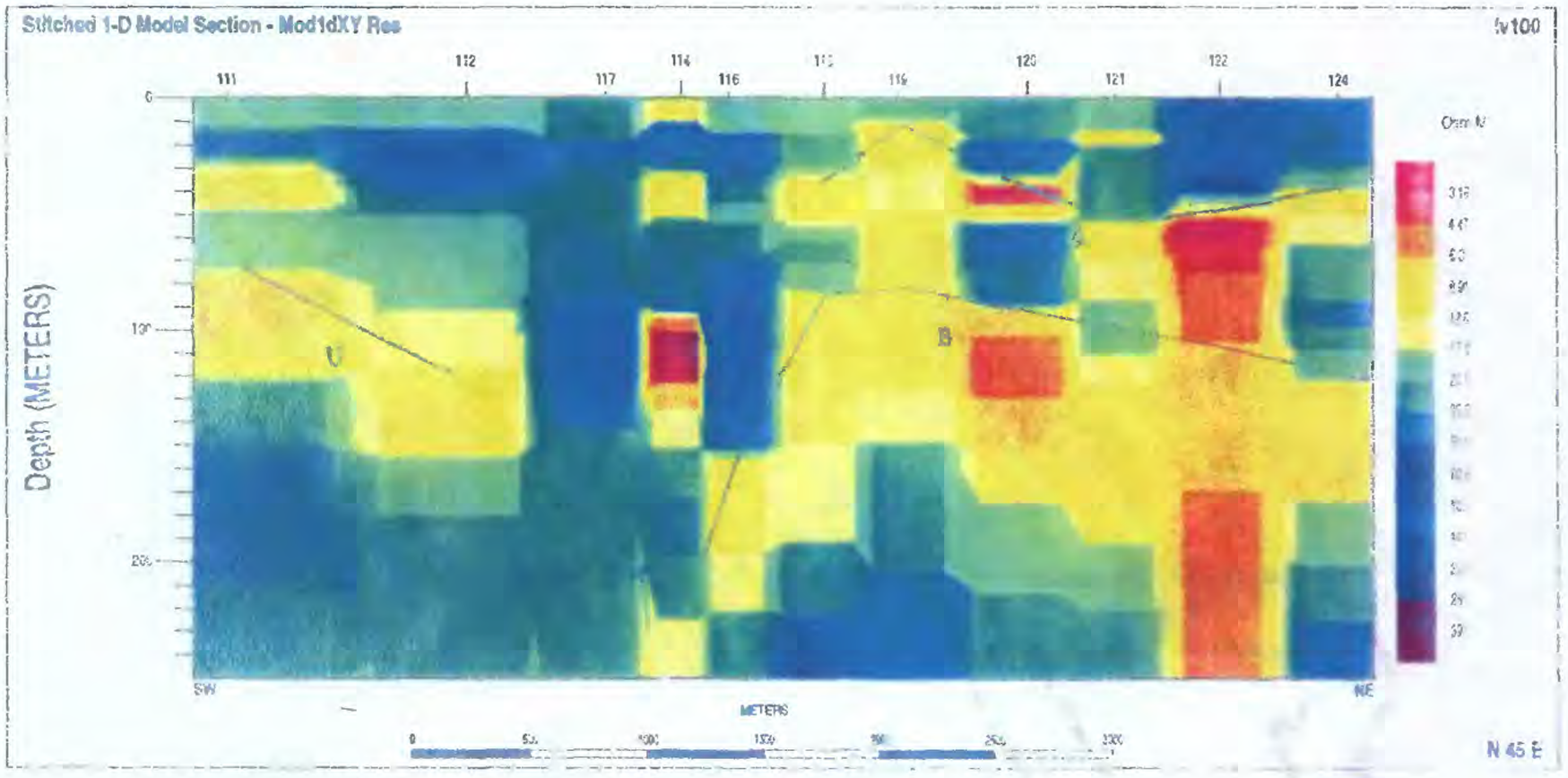

Figure 3--Resistivity model for line 100. **TOP**-model to 250 m depth with vertical exaggeration of 10; **BOTTOM**-model to 2,000 m depth with no vertical exaggeration . Model is composite of 1-D resistivity inversions based on error-weighted apparent resistivity (Rxy) and phase (Pxy). X rotated approximately perpendicular to Lake Valley fault. Resistivity color codes shown on bars. Labeled ticks along top of sections show projected location of AMT sites. Lines labeled A, B, C, U, and V show interpreted top of geoelectric units

float, and alluvium, a zone that is or has been conducive to weathering, and the collection of wet silts or clays.

Line B, shown on both the top and bottom of fig. 3 at a depth of 80 to 110 m NE of site 118, and seemingly west-dipping west between sites 118 and 114, marks a conductive unit (10-15 Ohm-m) that is interpreted to represent the top of the Percha shale. The westward dip indicates possible vertical offset of this unit amounting to about 140 m between sites 118 and 114. Site 114 is about 1 km southeast of station 118 (fig. 1), and the 140 m offset of the unit could be accounted for by a SE dip of the unit of 7°. Likewise, apparent dip on B NE of 118 (fig. 3) may in part be related to the differential SE offsets of sites over dipping stratigraphy.

Line C (fig. 3, bottom) marks the top of resistive units (50 to 300 Ohm-m). The true resistivity within this unit is probably 300 Ohm-m or greater, inasmuch as the modeling algorithm creates a smoothly varying resistivity (Constable and others, 1979). The average depth of C is about 600 m SW of site 117 compared to 200-m depth to the NE from sites 116 to 120. Northeast of site 120, C deepens to an average depth of about 500 m. On the average, C is about 150 m deeper than B (inferred to mark the top of the Percha shale). Taking the geologic estimate of thickness of the Percha as 40 m, C is about 100 m into the Ordovician-Silurian dolomite and limestone whose combined thickness is estimated at about 300 m (table 2). Line C probably presents a boundary over a resistive unit in the sequence of Paleozoic strata. Line C shows a likely disruption of the carbonate units between sites 118 and 112 across a horizontal distance of about 1.5 km with an apparent cumulative downthrow of the carbonate units by 400 m W. Correcting for an assumed maximum regional dip of 20° SE, and using an average offset between sites east and west of site 117 as one km, the interpreted fault throw would be about 50 m. Resistivity values extending downward below about 600 m below site 117 can be ignored because the data here are incomplete at low frequencies.

Apparent deepening of C by about 300 m NE of site 120 may be partially accounted for by a 20° SE dip of beds, but the largest downthrow occurs between sites 120 and 121, suggesting an uplift between sites 116 and 121. In conjunction with this postulated uplift, the low resistivity (3 to 8 Ohm-m) beneath site 122 suggests a fault zone. Low resistivity beneath site 122 is consistent with increased porosity with increased pore-fluid content, and alteration due to fluid flow along a fault. A north-trending fault beneath site 122 would be along the east edge of

Monument peak. At shallow depth, B shows a smaller displacement of about 50 m from sites 120 to 124 (fig. 3, top); if a fault zone exists below 122, it must have had recurrent motion during deposition of the Paleozoic rocks. Beneath site 124, there is a conductive geoelectric layer between B and C (fig. 3, bottom) that has no counterpart west of site 122. This localized conductive layer might reflect an eastward slump block or deposition of conglomerate from the inferred uplift to the west during faulting.

West of Lake Valley fault, low-resistivity zones (8-10 Ohm-m, fig. 2) indicated by U and V at depths of about 100 and 300 m are probably indicating higher fluid fraction and clay content due to weathering and alteration at interfaces between different episodes of volcanism. An indication of apparent NE downthrow of V and C amounting to 50 to 100 m occurs from 111 to 112. This indicates faulting down to the NE or graben formation on the west side of Lake Valley fault. The 300 m N horizontal offset of site 112 from 111 (fig. 1) is in the opposite sense to account for the vertical differential as due to geologic dips which are about 20° S within 1.5 km NW of site 111.

Proterozoic basement is not identified in the present results. Geologic consideration of the thickness of the Paleozoic rocks and their dip, indicates that the Proterozoic rocks are probably present at a depth of 1,100 to 1,700 m beneath the profile. The nearest outcrops the Proterozoic rocks (granite and gneiss) are about 15 km SW in the vicinity of Cooks Range (Jicha, 1954, plate 1). Granitic and carbonate rocks may have overlapping resistivity (table 1) so the basement may be within reach of the electromagnetic fields, but indistinguishable from the overlying carbonates.

Sites 325 and 326 - Relation of Geoelectric Units Northeast of Monument Peak to Line 100

Sites 321 and 326, NE of Monument Peak (fig. 1), along with site 124 provide insight into the average apparent dip of geoelectric units in the survey area. Figures 4.1-4.3 shows the layered models for these sites (fig. 4.1-4.3, left), as well as the apparent resistivity (fig. 4.1-4.3, top right) and phase data (fig. 4.1-4.3, bottom right). The symbols and curves on these figures are representative of the data, layered models, and the model response fits from the present survey (see Appendix). Line 300 was established at an azimuth of 30° to show the projection of sites 124, 325, and 326 as approximately equally spaced (fig. 5). This does not represent the cross-section in correct horizontal perspective; the line was constructed to provide a visual

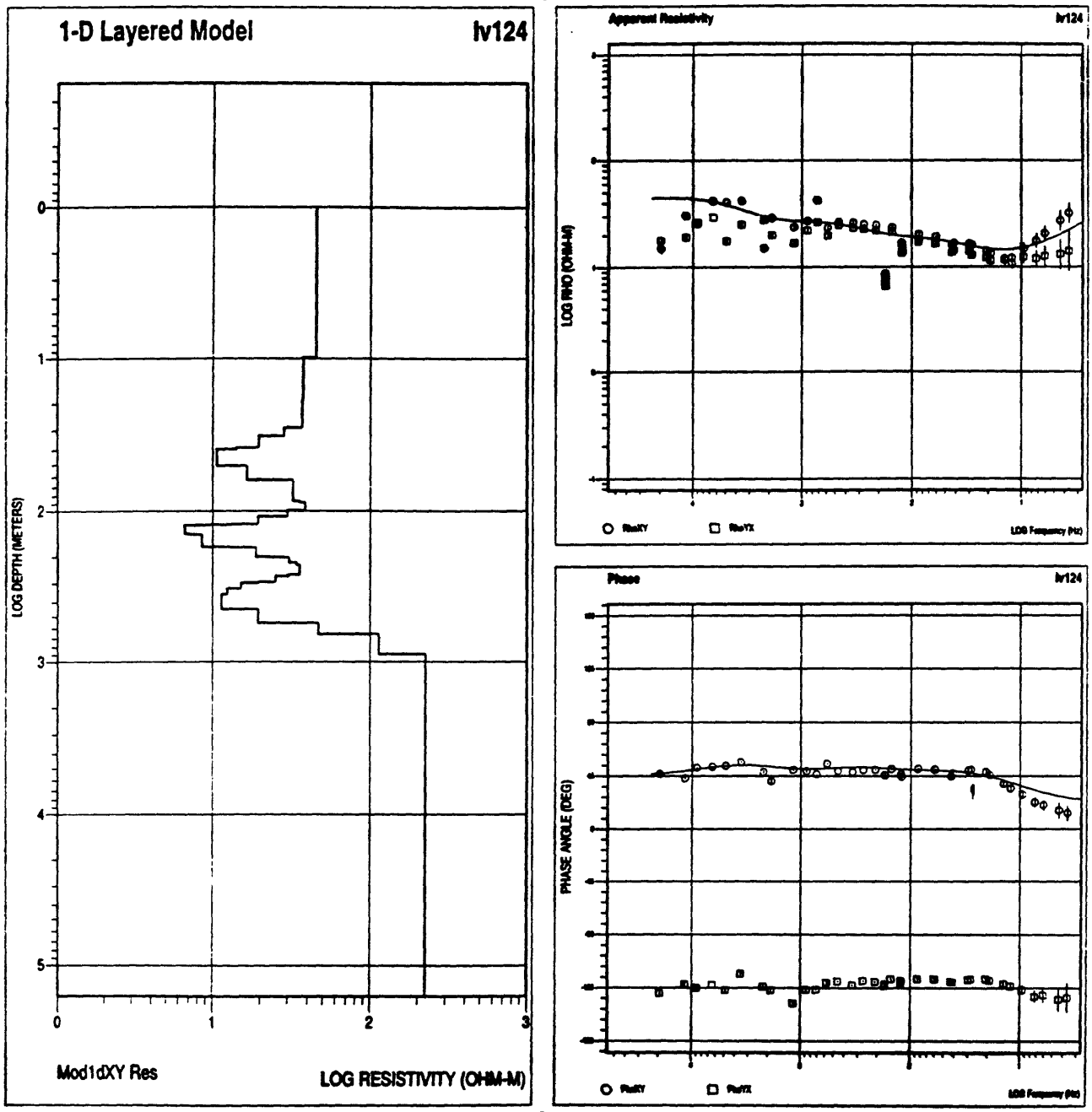

Figure 4.1--AMT data and inversion results for site 124. **LEFT**-layered model; **TOP RIGHT**-apparent resistivity (symbols) and response of model (line); **BOTTOM RIGHT**-phase (symbols) and response of the model (line). Inversion based on error-weighted apparent resistivity and phase. Circles indicate Rxy (X rotated approximately perpendicular to the Lake Valley fault); squares indicate Ryx.

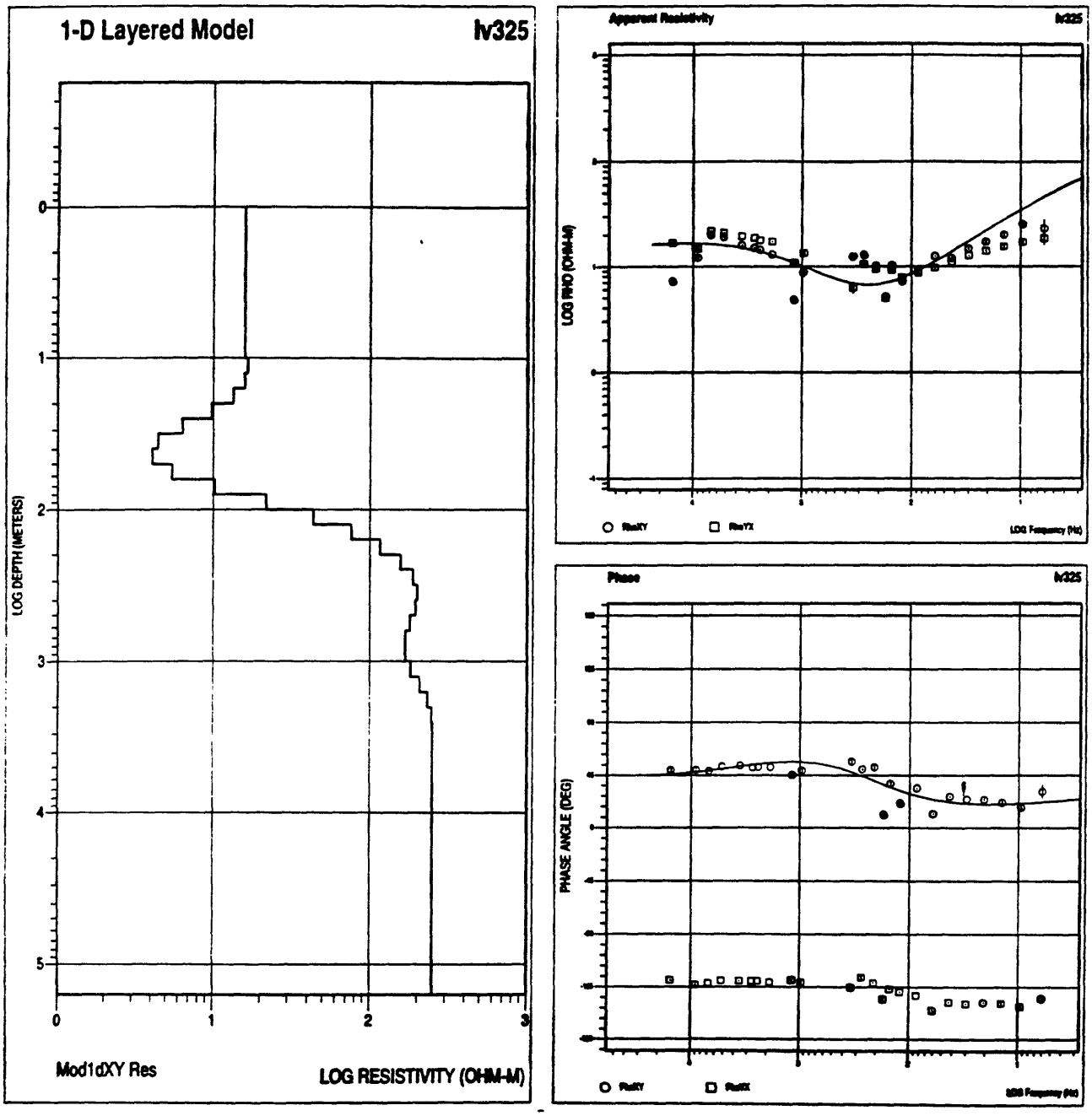

Figure 4.2--AMT data and inversion results for site 325. See caption figure 4.1

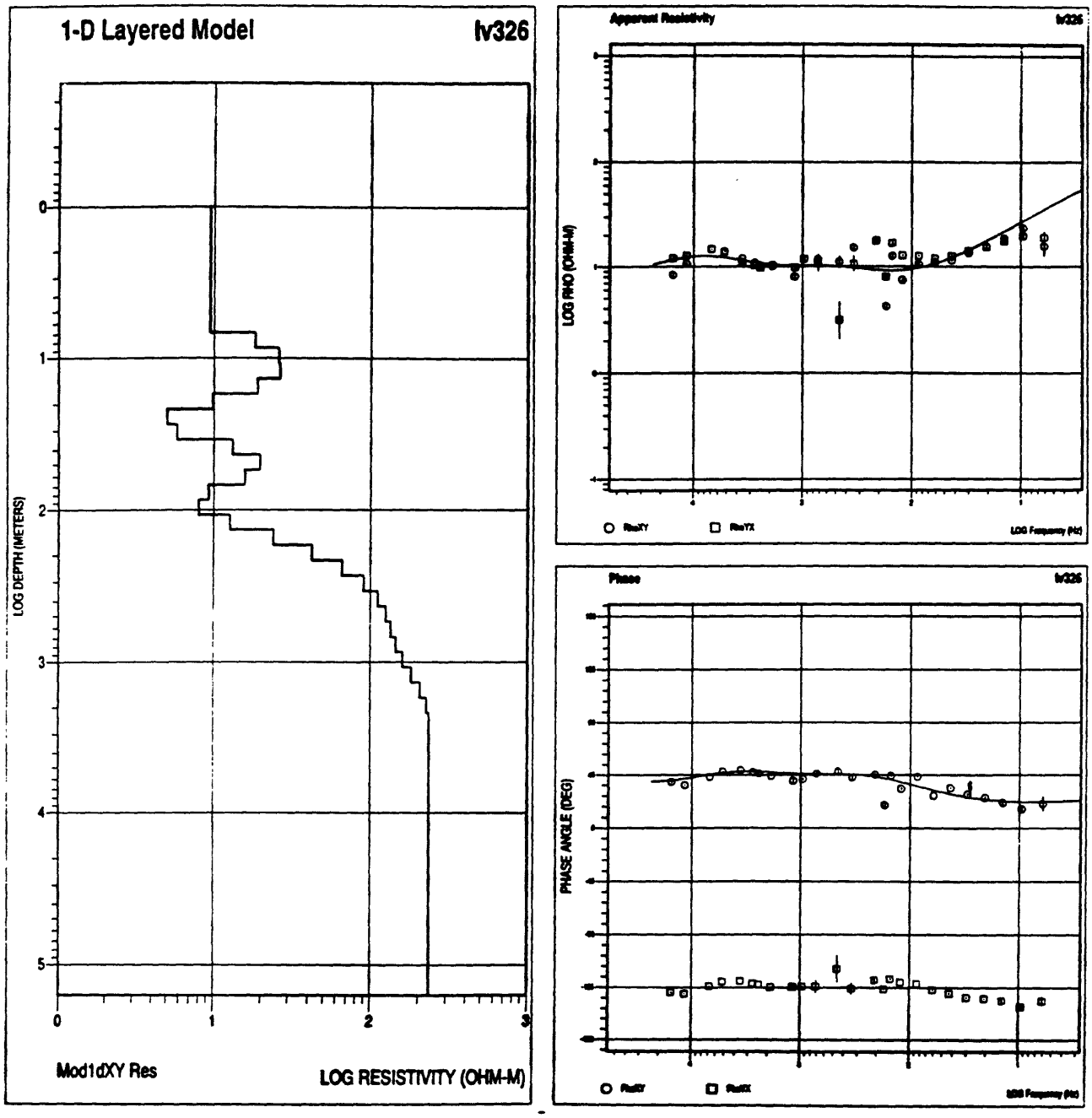

Figure 4.3--AMT data and inversion results for site 326. See caption figure 4.1.

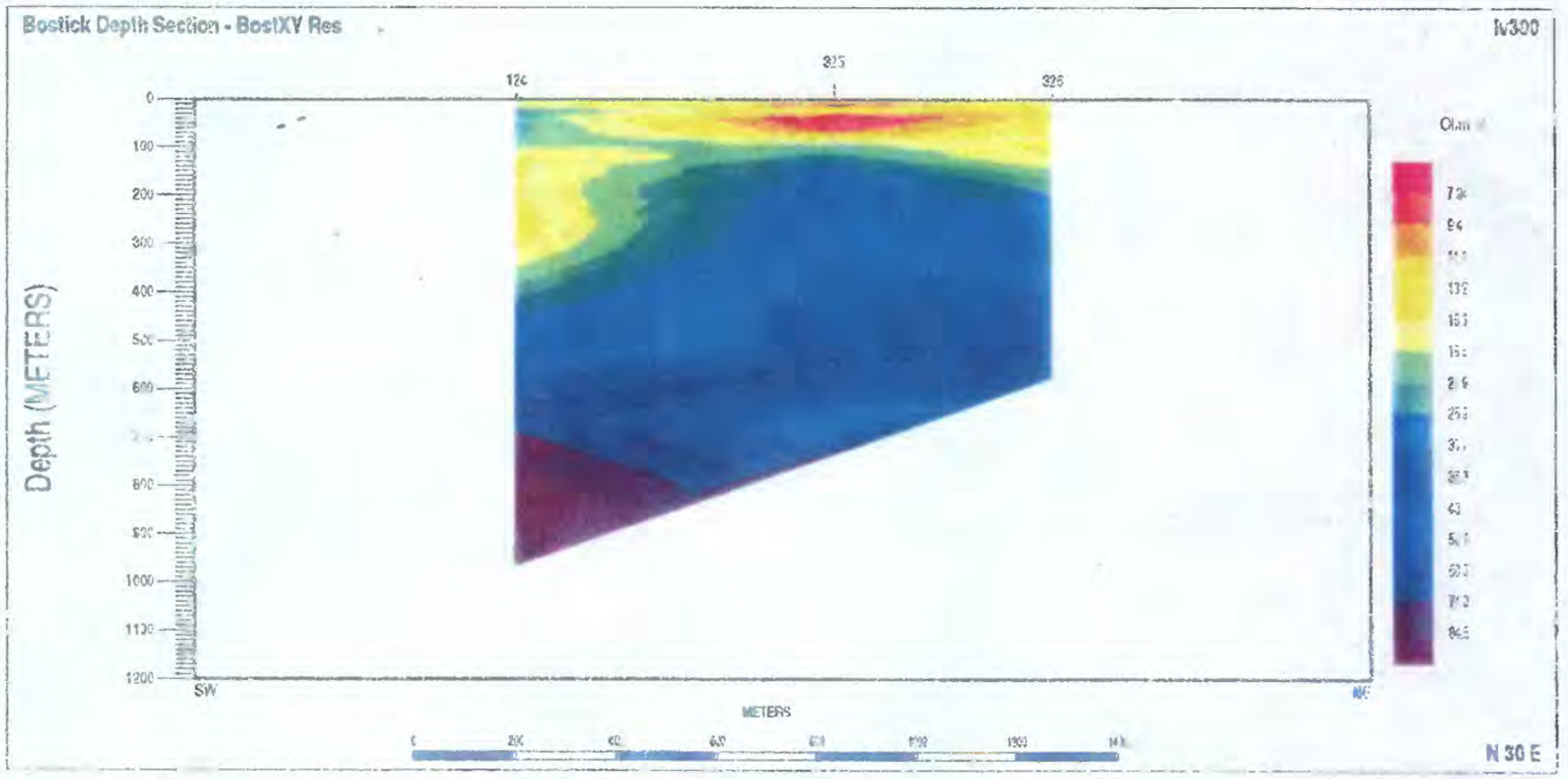

Figure 5--Bostick transform and resistivity model for sites 124, 325 and 326. TOP-Bostick transform based on phase showing resistivity vs. depth and distance; BOTTOM-resistivity model with no vertical exaggeration. Model is composite section of 1-D resistivity inversions based on error-weighted apparent resistivity (Rxy) and phase (Pxy). X rotated approximately perpendicular to Lake Valley fault. Resistivity color codes shown on the bars. Labeled ticks along top of sections show projected locations of AMT sites

correlation of electrical units. A Bostick transform of the data (fig. 5, top) and a composite section of the 1-D models (fig. 5, bottom) show a gross similarity as expected. Considering the model (fig.5, bottom), the upper two layers of low resistivity at site 124, at depths of about 30 m and 120 m respectively, have been interpreted as the base of overburden and the Percha Shale respectively (discussion accompanying fig.3). A deeper conductive layer starting at about 300 m beneath site 124 was unique to this site on line 100. It is apparently missing at sites 325 and 326 as well. At site 325, the shallower conductive layers converge at a depth of less than 100 m implying that the basin cover and volcanic rocks may be thinner here compared to line 100. Both conductive units and deeper resistive units (about 50 Ohm-m or greater) at sites 325 and 326 indicate an apparent eastward dip.

The geoelectric marker within carbonate section used for line 100 was the top of resistivity greater than about 50 ohm-m, located at a depth of about 500 m beneath site 124 (C, discussion of fig. 3). At station 325, the top of geoelectric units with resistivity greater than 50 ohm-m is at a depth of about 120 m (fig. 5). This apparent vertical offset of 380 m between 325 and 124 is consistent with an average south apparent dip of 8° from site 325 to 124 (fig. 1). This is about half of the geologically estimated dip, but may be appropriate for estimating the maximum vertical throw across the Lake Valley fault. The previously estimated minimum throw, using a dip of 20° for strata beneath the measurements of line 100 is about 50 m. Using an 8° dip, a maximum throw of about 250 m is possible.

Line 200: Measurements Along Berrenda Creek North of Town Mountain

Line 200 (fig.1) should intersect the NW extension of Lake Valley fault near site 205. The Lake Valley fault disappears beneath cover about 1 km SE of line 200 and reappears in outcrop again about 1 km to the NW. AMT measurements lay on the Berrenda Fault system that is bounded by two mapped NE-trending strands roughly orthogonal to the Lake Valley fault (fig. 1). A factor that weighs on this data is a power line about 1 km NW of sounding 206 that is sub-parallel to the line of sites. In the vicinity of sites 203 and 204, this power line is tapped to provide electricity to a ranch SE of line 200. The subsidiary power line is about 150 m from site 204, and about 50 m from site 203. Nearby power line signals at 60 Hz and it's harmonics can produce deterioration of the signal-to-noise ratio for data at frequencies less than a few thousand

Hz. Power lines may also carry induced electric currents that distort the electromagnetic response of the Earth.

Figure 6 shows the results from line 200 - apparent resistivity and phase data (fig. 6.1, top and bottom respectively), skew (fig. 6.2, top), and a composite section of layered models (fig. 6.2, bottom). The layered models show resistivity varying from about 60 to 600 Ohm-m to depths of about 500 m. Apparent resistivity and phase data (fig. 6.1, top and bottom respectively) indicate a low resistivity surface layer, consonant with alluvium along Berrenda Creek, and an increase in resistivity with depth that is broken by a conductive layer corresponding to a frequencies near 4,000 Hz. Skew, a measure of the relative amplitudes of XX and YY impedances compared to XY and YX impedances, is anomalously high west of sounding 205 (fig. 6.2, top). This indicates a three-dimensional geometry, a small signal-to-noise ratio, or both. Because of probable 3-D geoelectric structure and power lines, only the higher-frequency part of the 1-D models (penetrating to less than about 500 m) will be considered.

The model (fig. 6.2 bottom) appears comparable to that part of line 100 located NE of the Lake Valley fault (fig. 2). There is a conductive zone (about 50 Ohm-m) starting at about 100 m depth, possibly associated with the Percha Shale, and increased resistivity with depth probably associated with the Paleozoic carbonates and Proterozoic basement. The conductive zone inferred to be Percha Shale appears to have an vertical offset (down to the SW) of 100 m between sites 205 and 204, and again between sites 204 and 203. The apparent offsets may be an indication of faulting, or a westerly dip of the strata. Lateral changes in skew between site 205 and 204 (fig. 6.2, top) may be in part due to the orthogonal intersection of the Lake Valley Fault with the Brenda fault system. Based on the shallower results, a throw of near 100 m down west for the Lake Valley fault between 204 and 205, and indication of a second fault (a splay of the Lake Valley fault) with a throw of about 50 m between 203 and 204 seems likely.

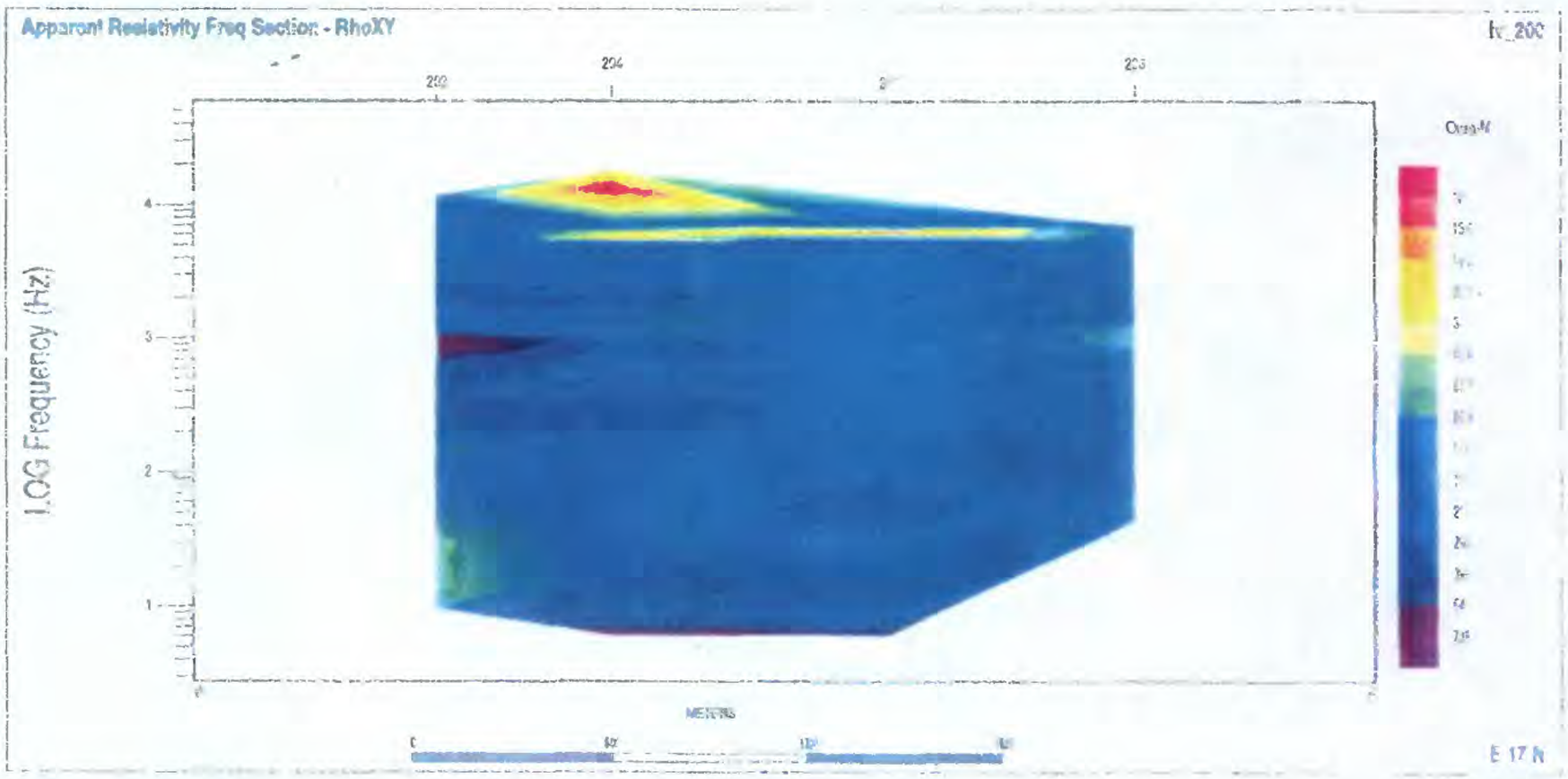

Figure 6.1--AMT data and model for line 200. **TOP**-apparent resistivity vs. distance and frequency; **BOTTOM**: phase vs. frequency. Frequency plotted as logarithm base 10 and decreases downward . Ticked labels along top of sections show projected site locations. Data are colored coded as shown on bars.

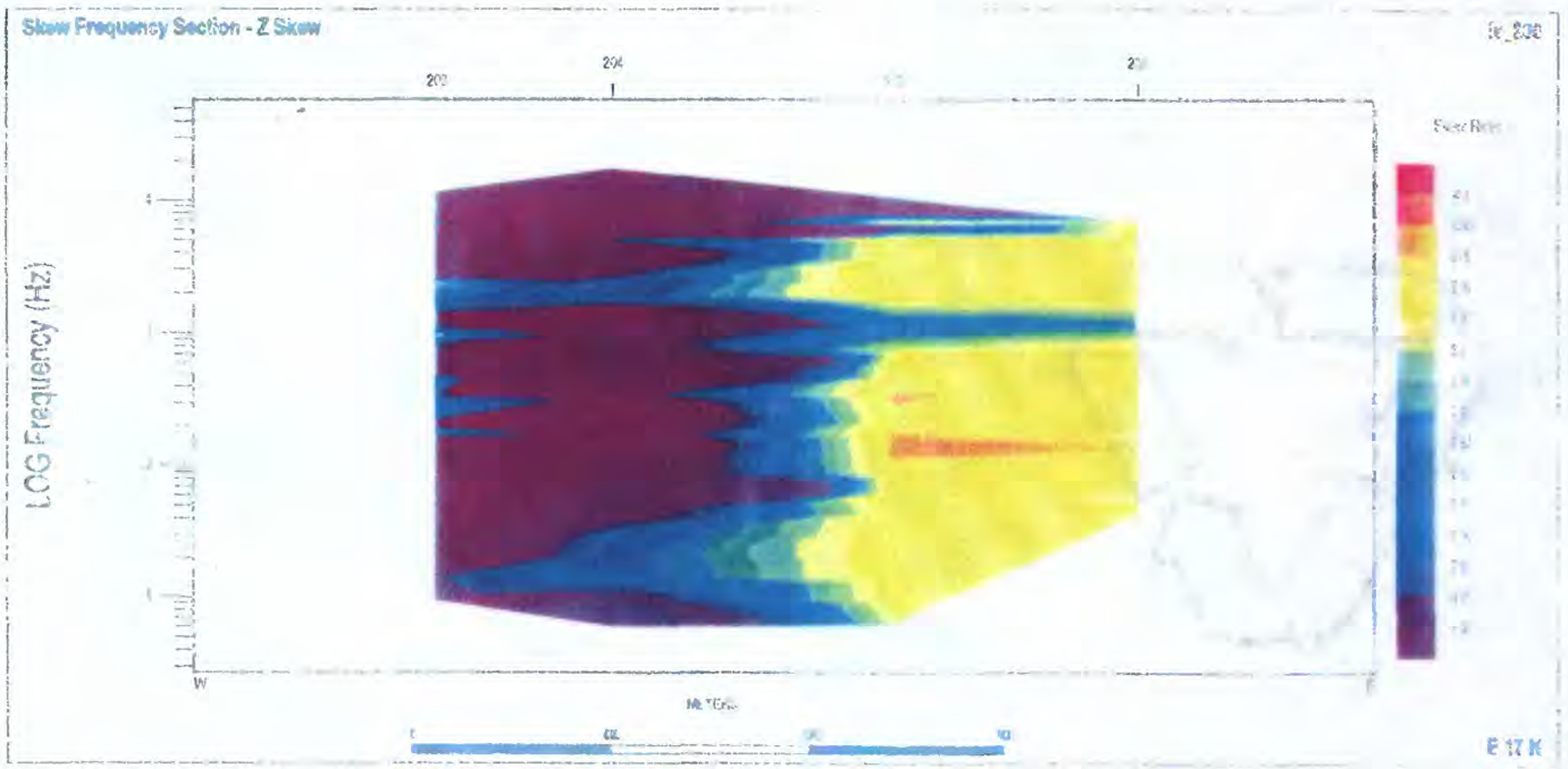

Figure 6.2--AMT data and model for line 200. TOP-skew plotted vs. distance and frequency. Frequency plotted as logarithm base 10 and decreases. BOTTOM-model resistivity vs. distance and depth with no vertical exaggeration. Model composed of composited 1-D inversions based on error-weighted apparent resistivity (Rxy) and phase (Pxy) where X oriented approximately normal to Lake Valley fault. Dashed labels along top of sections show projected site locations. Data are colored on log...

SUMMARY

Seventeen AMT sites were established along two traverses south and north of Lake Valley Mining district to investigate resistivity structure and it's geologic implications. Measurements south of Monument Peak address the question of whether Lake Valley fault extends southward beneath cover. Measurements along Berrenda Creek, north of Town Mountain, were made to investigate the fault structure as it extends north.

South of Monument Peak, the east half of the traverse identified two widespread conductive units. The upper conductive unit (3-10 Ohm-m) at depths varying from 10-50 m is inferred to be associated with the base of the unconsolidated alluvium, gravel and float. The next lower conductive unit (10-15 Ohm-m) is interpreted to represent Percha Shale at a depth of about 200 m. Conductive units on the west half of the traverse are probably reflecting interfaces between andesitic flow units. Discontinuities in these units indicate the southward continuation of Lake Valley fault. Apparent eastward dip of the inferred flow units indicates graben development along the fault. An additional fault is suggested about 2 km east of the Lake Valley Fault, possibly in line with the east flank of Monument Peak. This fault is inferred from contrasts in resistivity near the east end of the traverse. Deep units detected had high resistivities that may be associated either with limestone or igneous-metamorphic rocks. Proterozoic basement could not be separately identified. Vertical offset across the deep resistive unit provided the chief evidence of total throw across the Lake Valley fault. Dip of strata, which is known only in the mining area and to the north, was a factor in interpretation of throw. Using an average 20° SW dip gave the minimum displacement of 50 m to the west. The largest displacement that can be inferred is 250 m based on comparing resistivity structure east of Monument Peak with that on line 100 to establish an apparent dip of 8°.

Measurements north of the Lake Valley mining area on a traverse along Berrenda Creek were influenced by power lines and intersecting faults. Shallower penetrating data affected least by these complications provide hints on the northward extension of Lake Valley fault. The upper 500 m of the model suggests an apparent westward dip of strata of about 20° that may be associated with multiple faults with a combined throw of 100-150 m.

REFERENCES

Brant, A.A., 1966, Geophysics in the exploration for Arizona porphyry coppers, in Titley, S.R., and Hicks, C.L., eds., Geology of the porphyry copper deposits, southwestern North America: Tucson, Ariz., University of Arizona Press, p.87-110.

Bostick, F.X., Jr., 1977, A simple almost exact method of MT analysis; appendix, Workshop on evaluation of electrical methods in the geothermal environment (WEEMGE) Snowbird, Utah: University of Utah, Depart. Geol. Geophys., Contract report for U.S. Geological Survey: Geothermal Workshop, Jan. 1977, p.174-177.

Cagniard, Louis, 1953, Basic theory of the magneto-telluric method of geophysical prospecting: Geophysics, v.18, p.605-635.

Constable, S.C., Parker, R.L., and Constable, D.G., 1979, Occam's inversion: a practical algorithm to generating smooth models from electromagnetic data: Geophysics, v.52, p.289-300.

Creasey, S.C., and Granger, A.E., 1953, Geologic map of the Lake Valley Manganese District Sierra County, New Mexico: U.S. Geological Survey Mineral Investigations Field Studies Map MF-9, scale 200 ft/in.

Gamble, T.D., Goubau, W.M., and Clarke, J., 1979a, Magnetotellurics with a remote reference: Geophysics, v.44, p. 53-68.

Gamble, T.D., Goubau, W.M., and Clarke, J., 1979b, Error analysis for remote reference magnetotellurics: Geophysics, v.44, p.959-968.

Jicha, Henry L., 1954, Geology and mineral deposits of Lake Valley quadrangle, Grant, Luna, and Sierra Counties, New Mexico: Socorro, New Mexico Bureau Mines and Mineral Resources, New Mexico Inst. Mining and Technology, Bull.37, 93 p., 5 plates (plate 1: Geologic Map, scale 1:62,500).

Keller, G.V., and Frischknecht, F.C., 1996, Electrical methods in geophysical prospecting: New York, Pergamon Press, 519 p.

Klein, D.P., 1996, Electrical geophysical surveys of Coronado National Forest: U.S. Geological Survey Bulletin 2083-E, p.105-127.

Strangway, D.W., Swift, C.M., Jr., and Holmer, R.C., 1973, The application of audio-frequency magnetotellurics (AMT) to mineral exploration: Geophysics, v.38, p. 1159-1175.

Vozoff, Keeva, 1972, The magnetotelluric method in the exploration of sedimentary basins: Geophysics, v.37, p.98-141.

Vozoff, Keeva, 1991, The magnetotelluric method, in Nabigian, M.N., ed., Electrical methods in applied geophysics, v.2, Applications, Part A, Chapter 8: Tulsa, Society Exploration Geophysicist, p.641-712.

APPENDIX

DATA AND MODEL RESPONSE FITS

Lake Valley Area, Southern New Mexico

AMT data parameters from each site (fig. 1) are presented as frequency or polar plots. Sites are presented sequentially by identification number. The site identification notation indicates the survey "lv" (Lake Valley), the profile line (first digit), and unique site identification number (digits 2 and 3). Parameters shown are derived using standard tensor AMT computations (Vozoff, 1972, 1991, Constable and others, 1979). Data parameters shown for each site are:

* Apparent resistivity (Rxy and Ryx, or RhoXY and RhoYX)
* Impedance phase (Pxy and Pyx, or PhsXY and PhsYX)

  Apparent resistivity and phase are shown with curves resulting from 1-D inversions for each mode (XY or YX)
* E-predicted coherency (or multi-coherency) for the XY and YX modes
* Impedance skew
* Electrical strike (computed rotation +/- 90°) and rotation angle employed for analysis
* Polar diagrams showing the relative changes of magnitude of the XY and YX impedance elements as rotated through 360°.

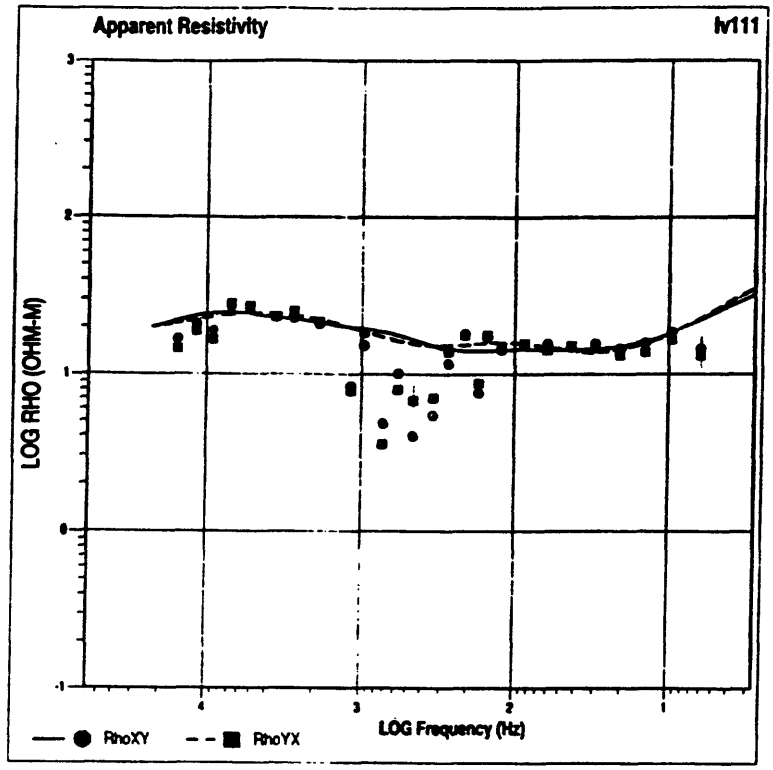

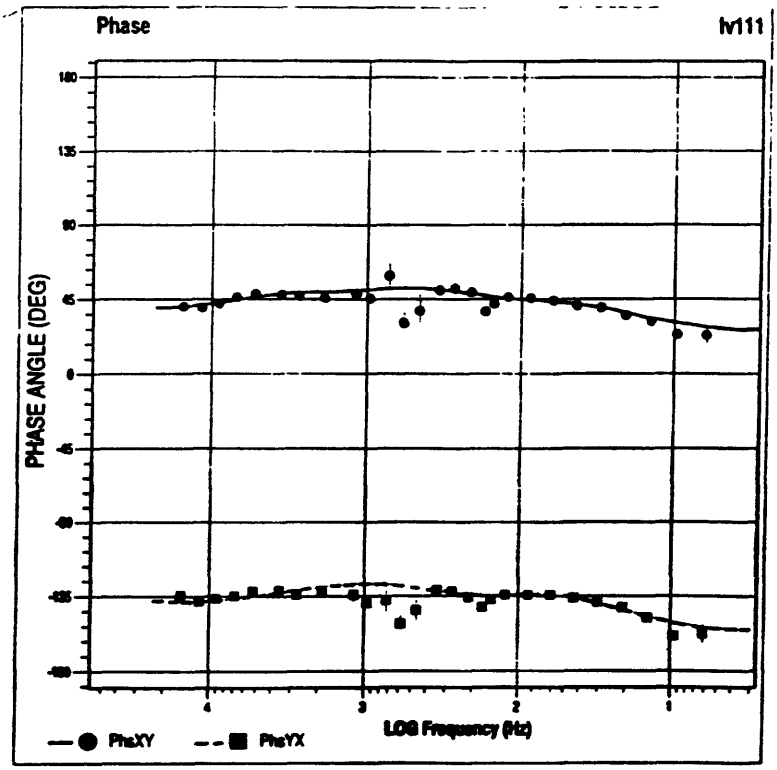

Figure 7-A–Data parameters for site 111. Apparent resistivity (TOP) and impedance phase (BOTTOM) plotted against frequency. Scales are logarithmic base 10; frequency decreasing (deeper penetration) toward right. Data for XY and YX modes shown by symbols as labeled. Computed response of layered models for observed modes shown by lines as labeled. Vertical lines show statistic errors on parameter estimates.

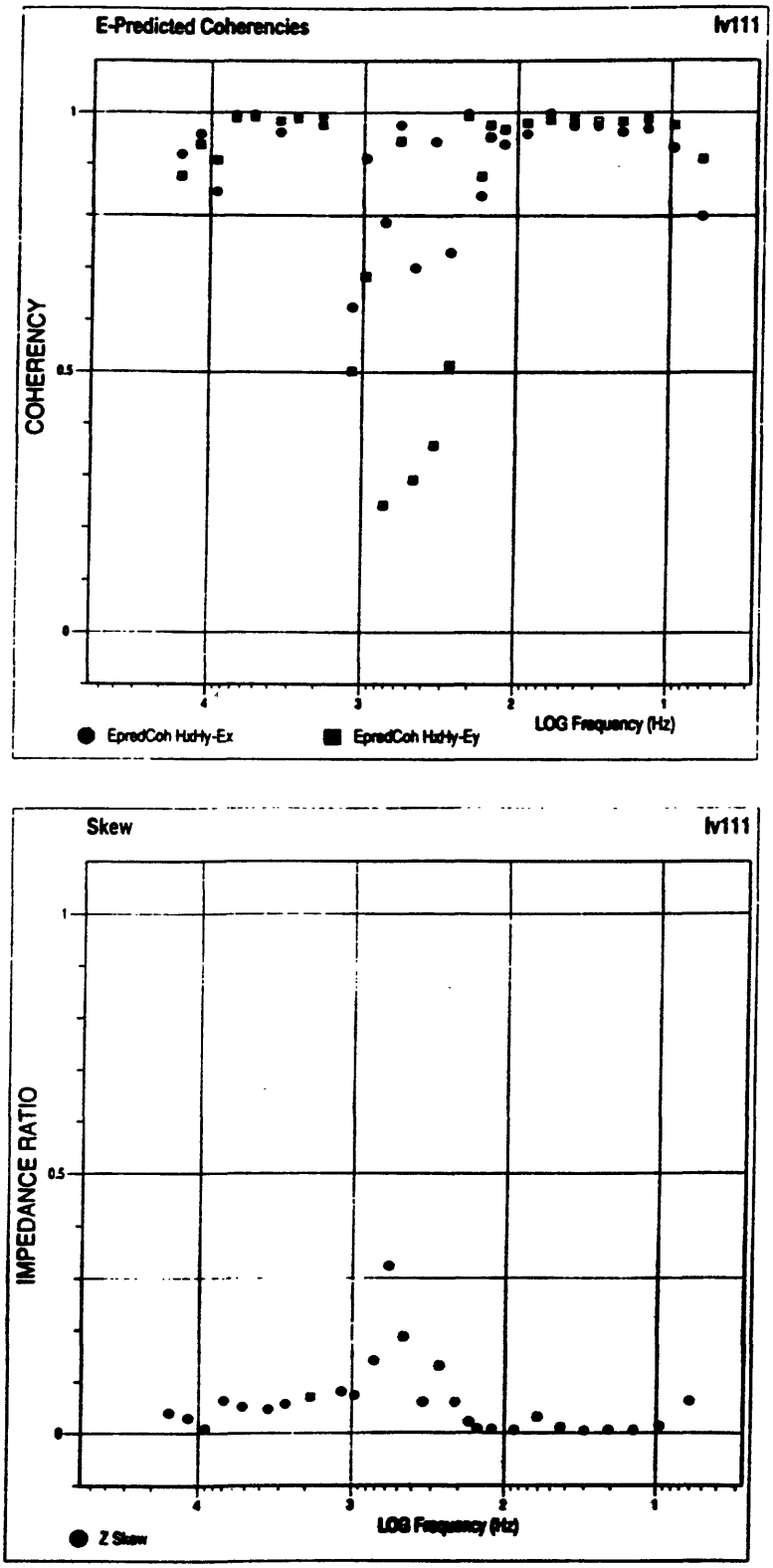

Figure 7-B--Site 111 continued. **TOP**: E-predicted multi-coherencies for XY or YX mode shown as symbols as labeled. **BOTTOM**: skew. Data plotted against frequency (decreasing toward right). Coherency and skew are dimensionless ratios. Coherency indicates absence of the noise (lower values indicate greater noise). Skew indicates relative magnitude of the XX and YY modes relative to XY and YX modes; skew greater than zero indicates 3-dimensional resistivity structure and (or) noise.

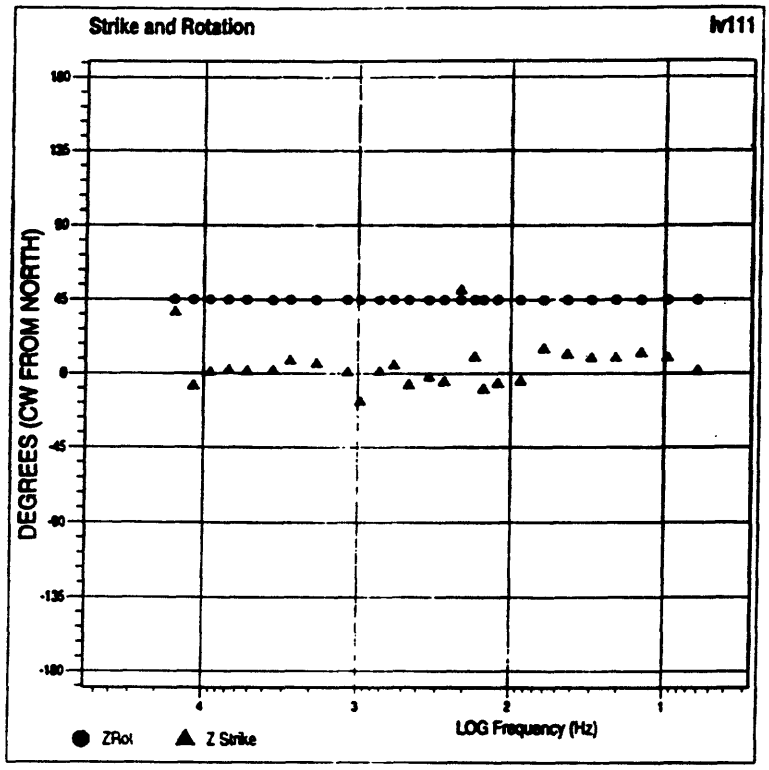

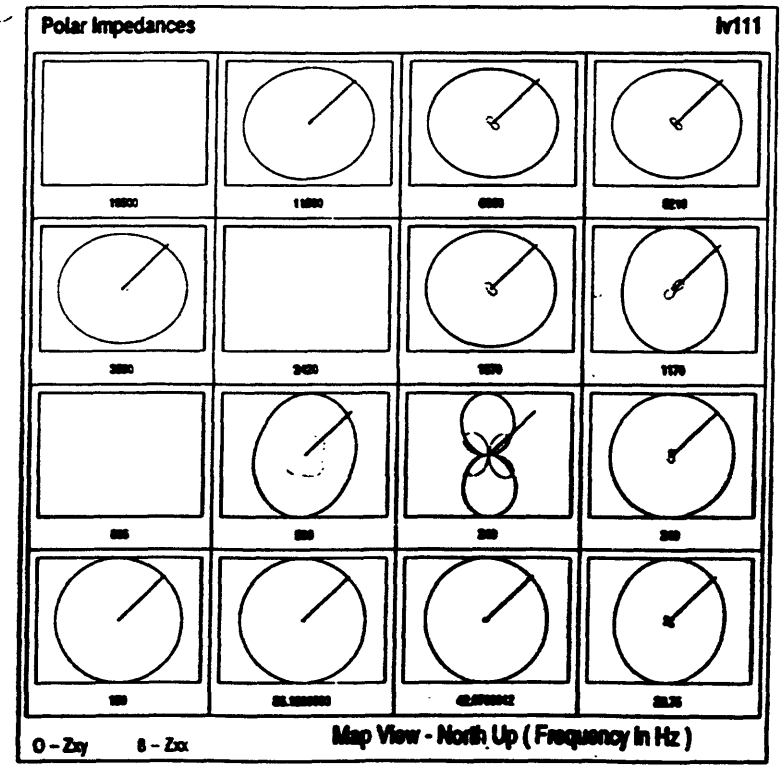

Figure 7-C–Site 111 continued. TOP: Estimated electrical strike and applied impedance rotation (both degrees clockwise from north) shown by symbols as labeled. **BOTTOM:** polar plots showing relative amplitudes of XY and XX impedance elements as labeled for rotation through 360°. Estimates of electrical strike uncertain by multiples of 90°. Zxx polar plots are larger for 3-dimensional environment and (or) noise.

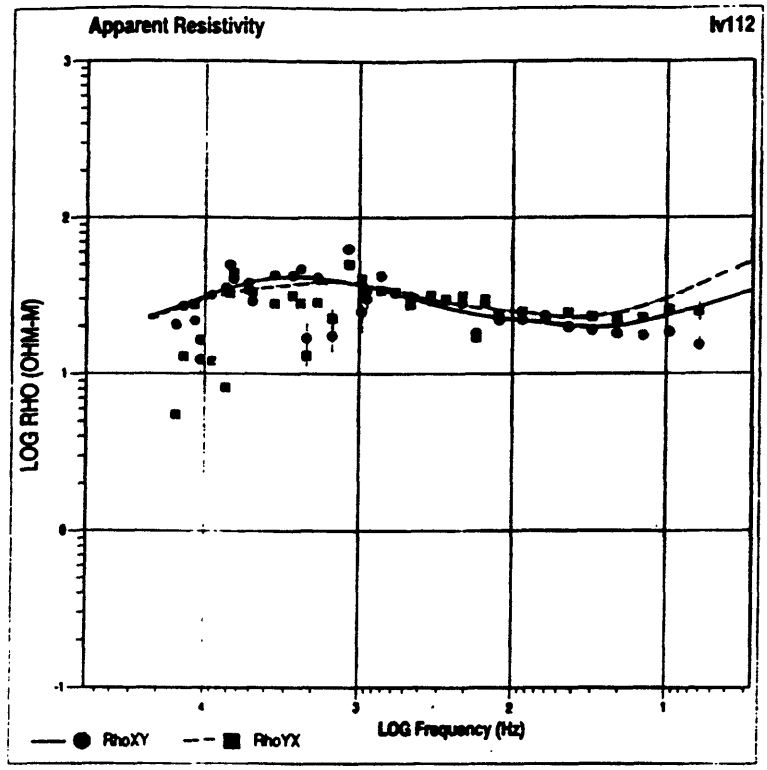

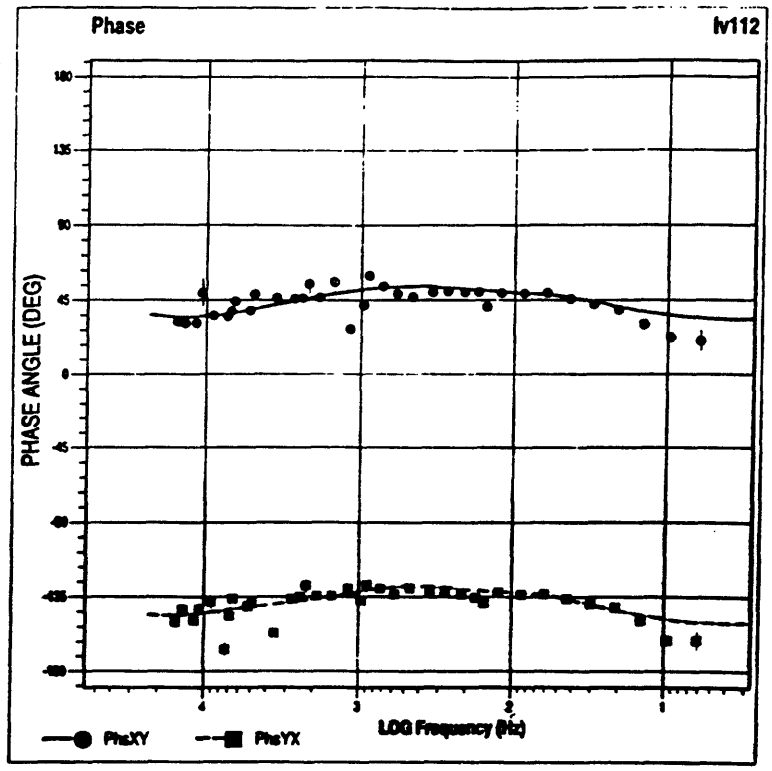

Figure 8-A--Data parameters for site 112; see caption figure 7-A.

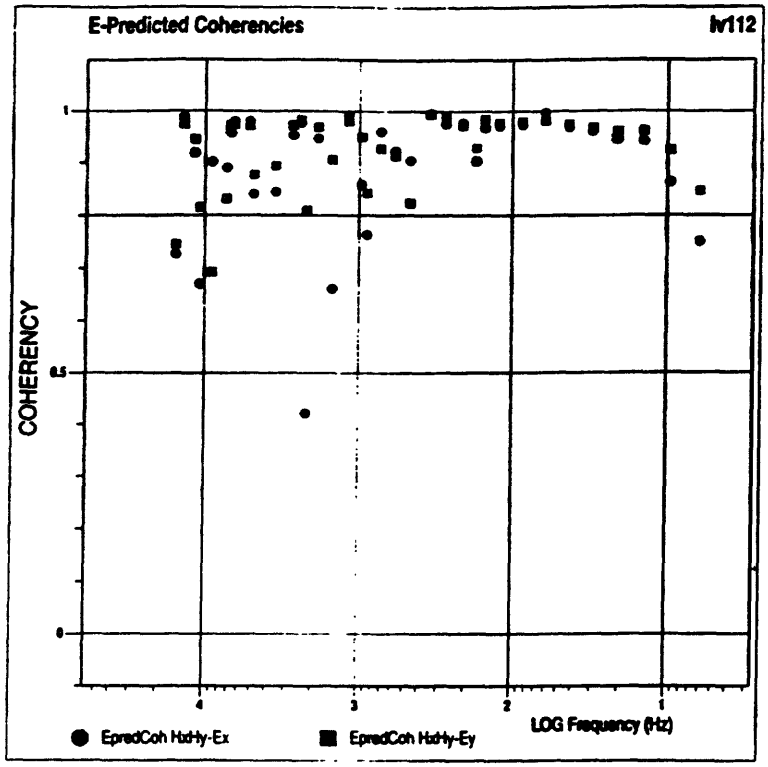

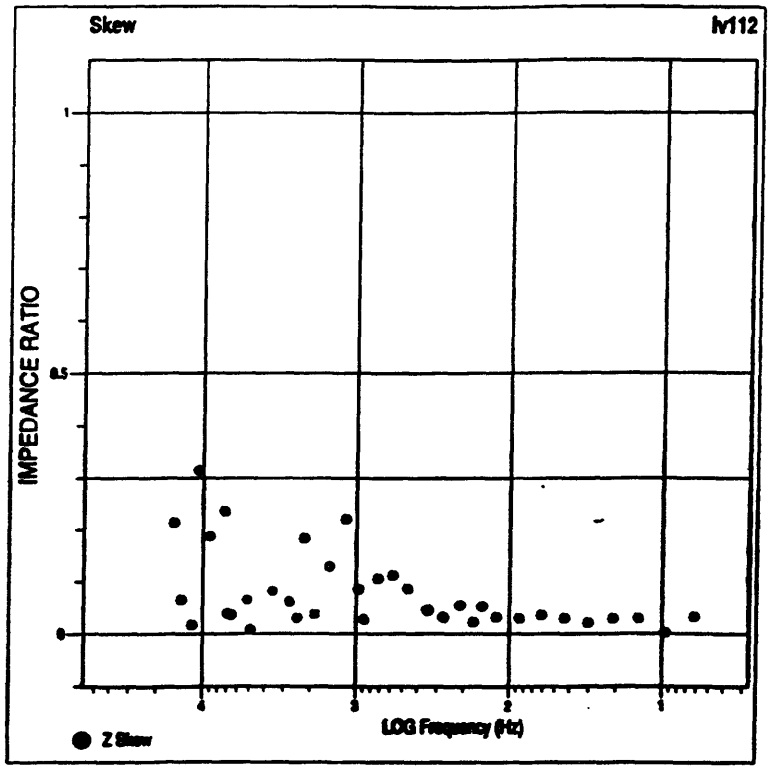

Figure 8-B--Site 112 continued; see caption figure 7-B.

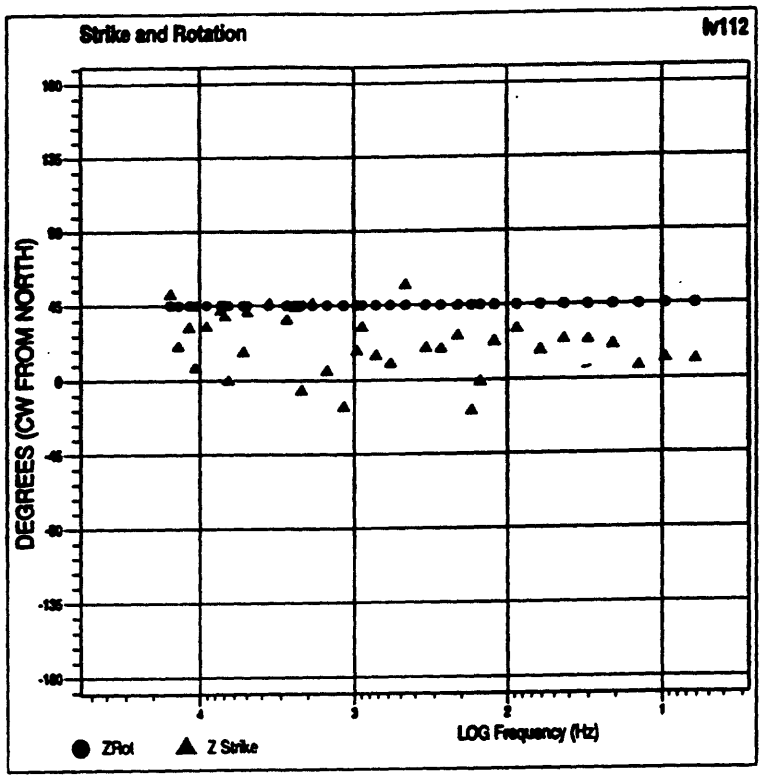

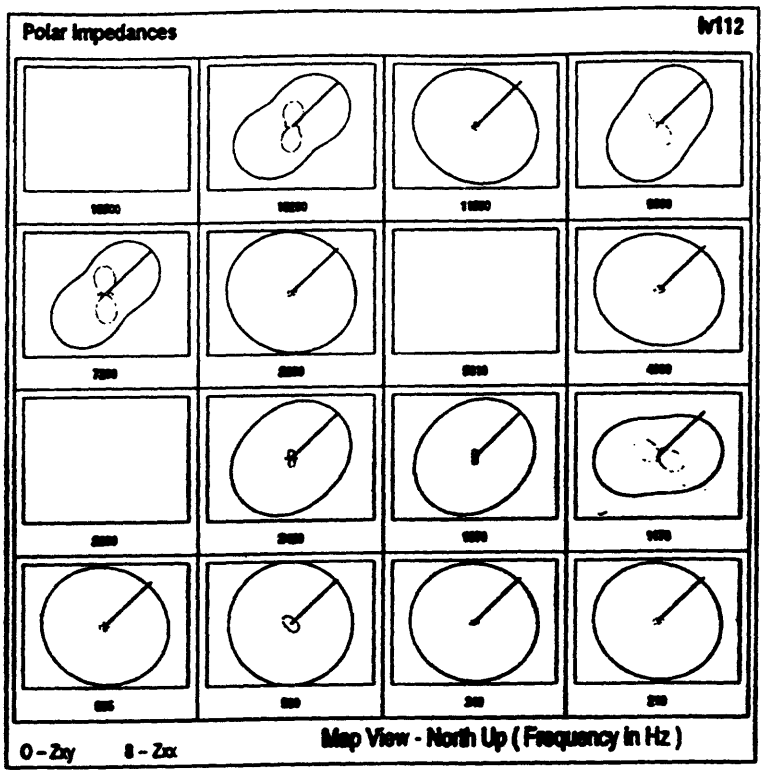

Figure 8-C--Site 112 continued; see caption figure 7-C.

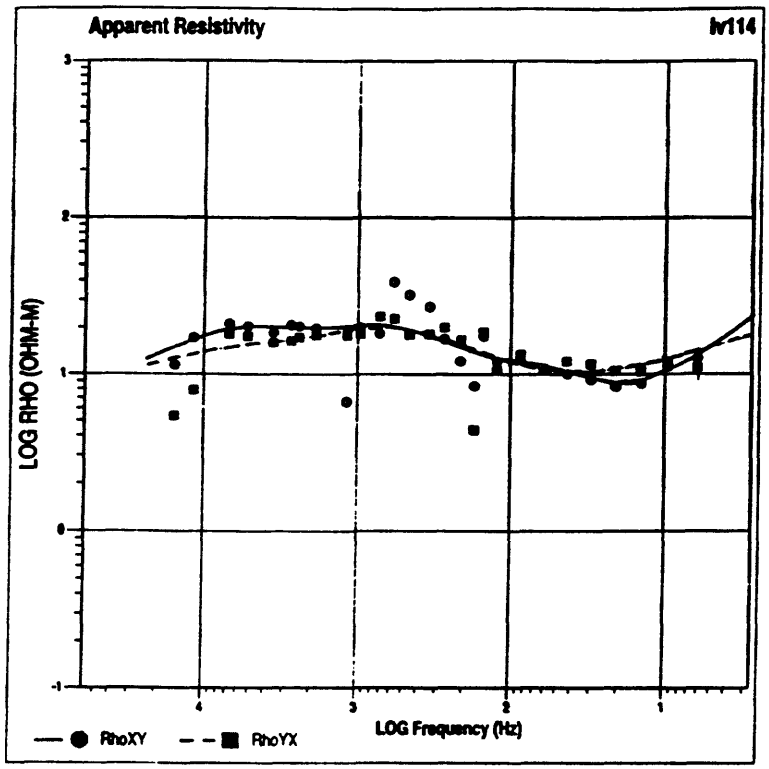

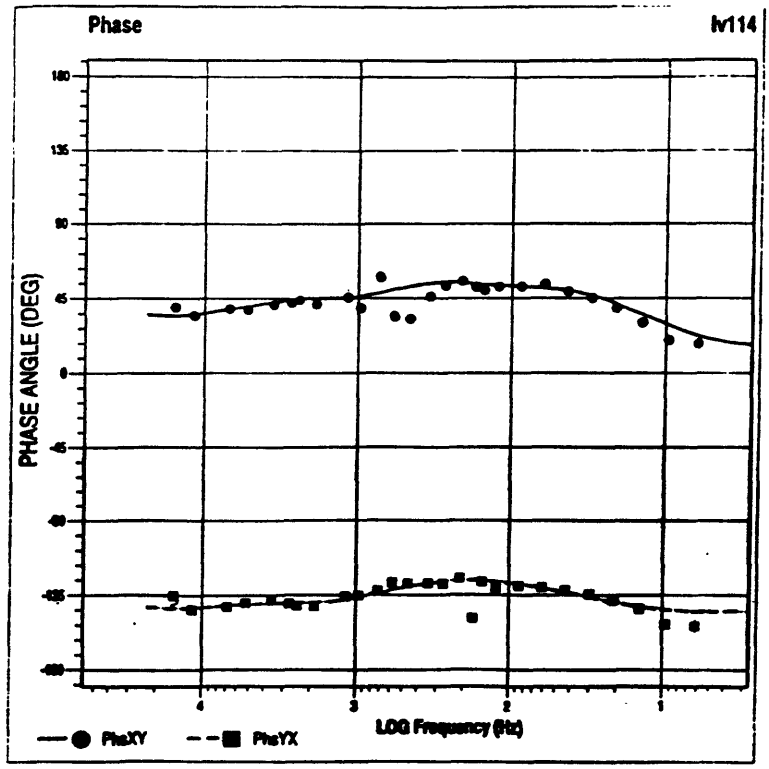

Figure 9-A--Data parameters for site 114; see caption figure 7-A.

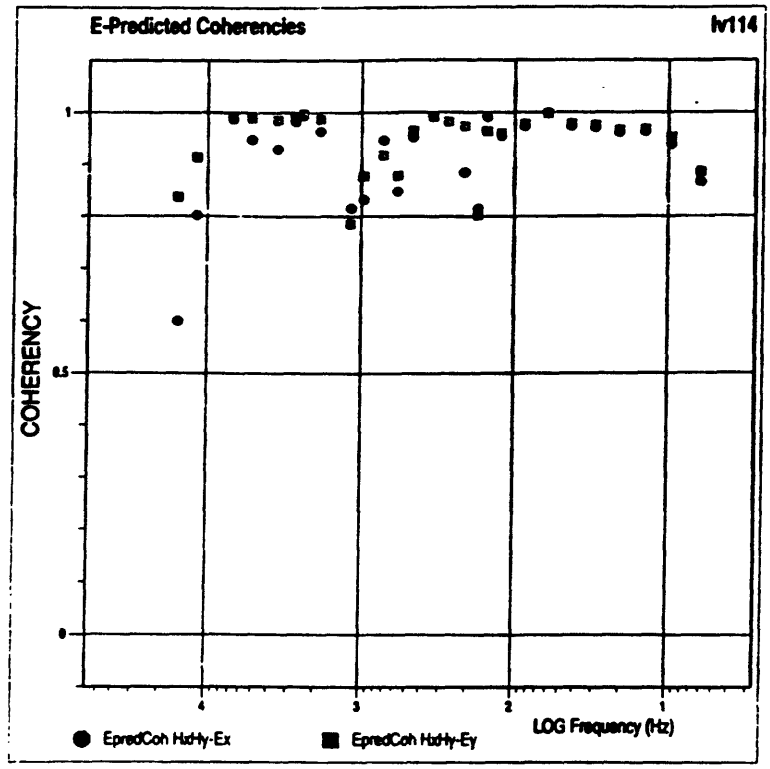

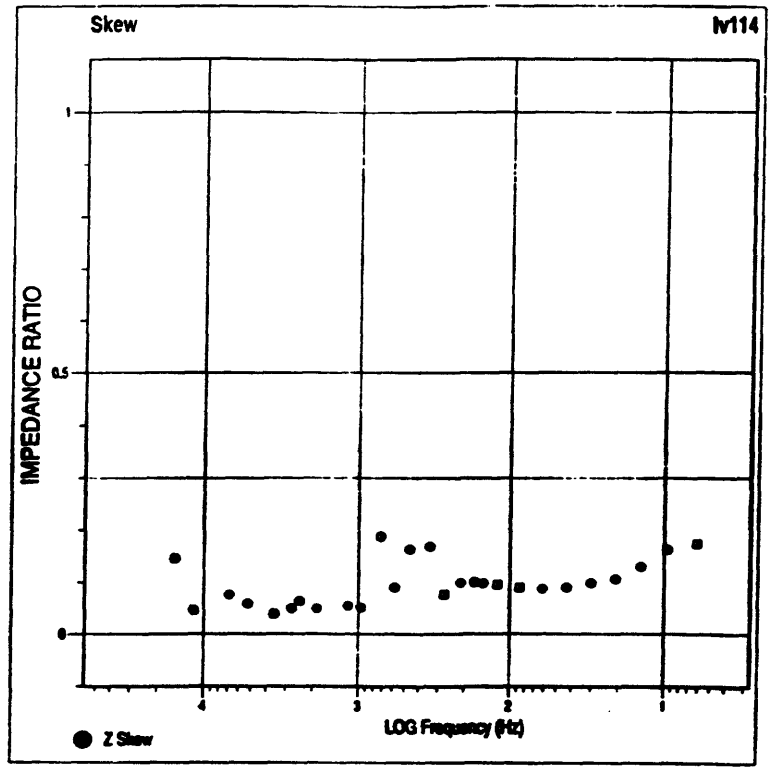

Figure 9-B--Site 114 continued; see caption figure 7-B.

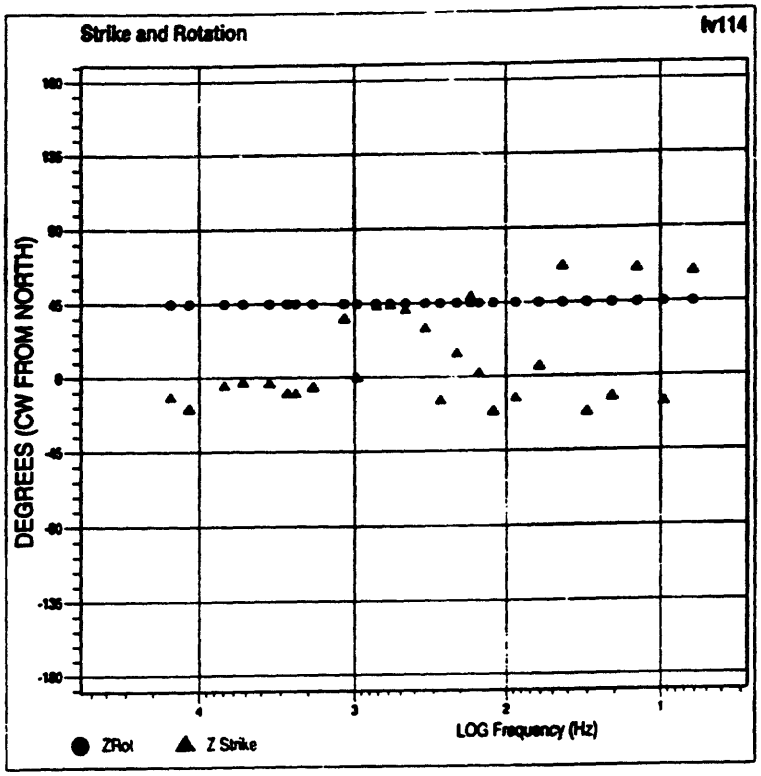

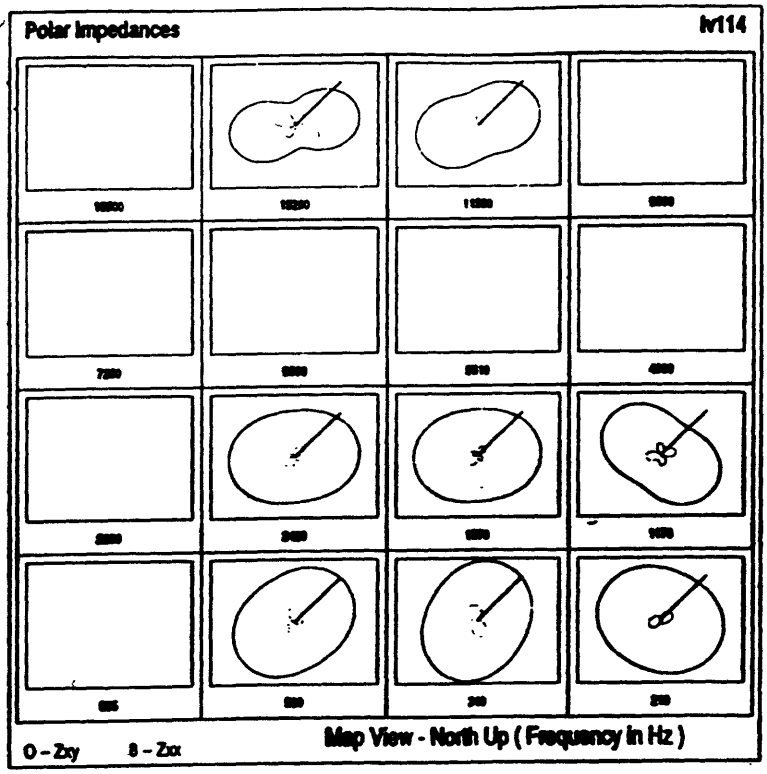

Figure 9-C--Site 114 continued; see caption figure 7-C.

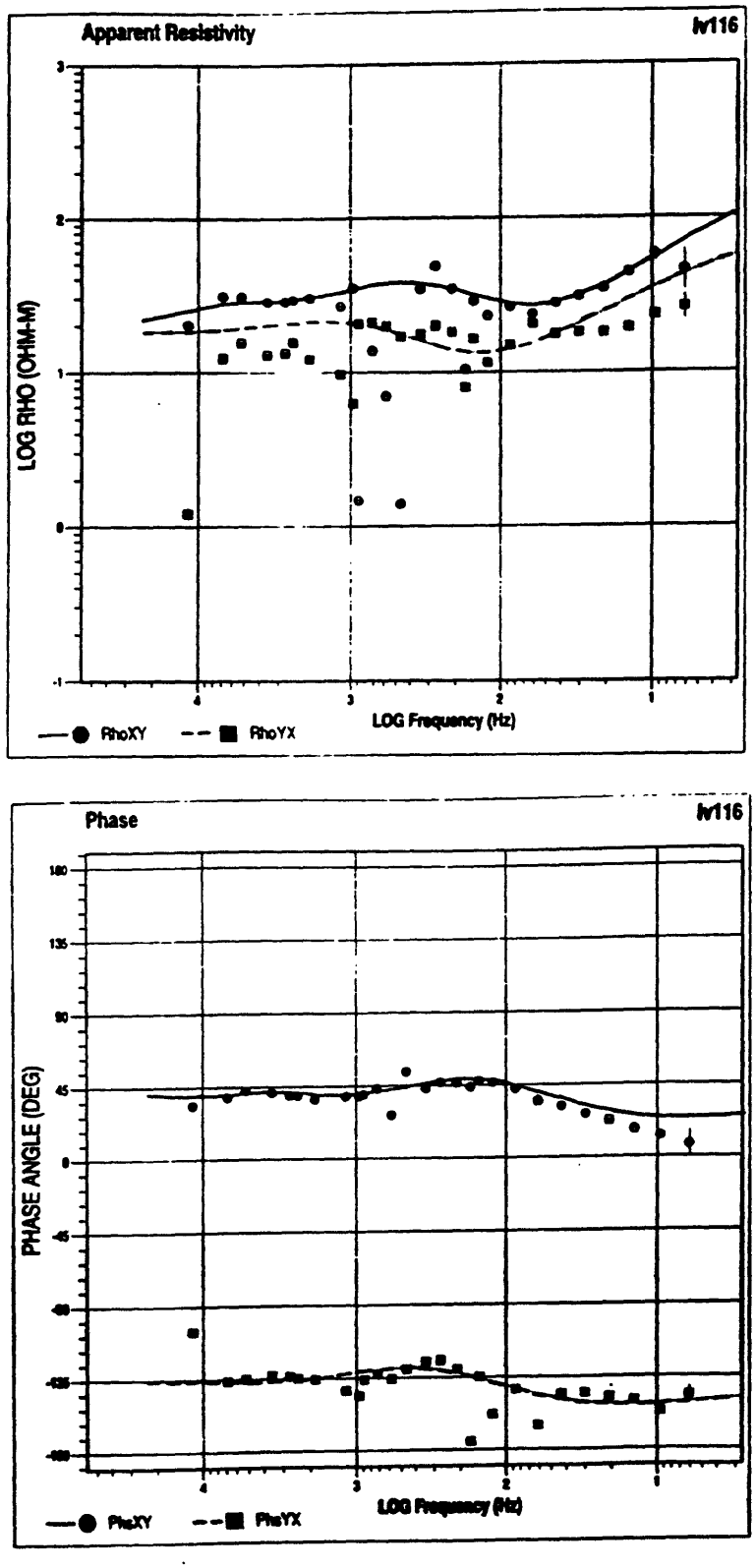

Figure 10-A--Data parameters for site 116; see caption figure 7-A.

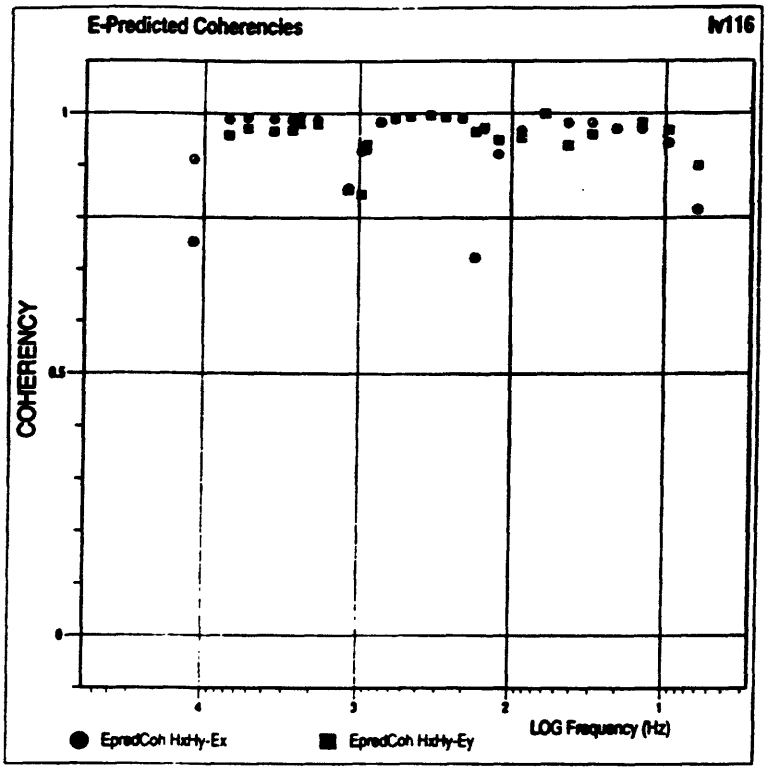

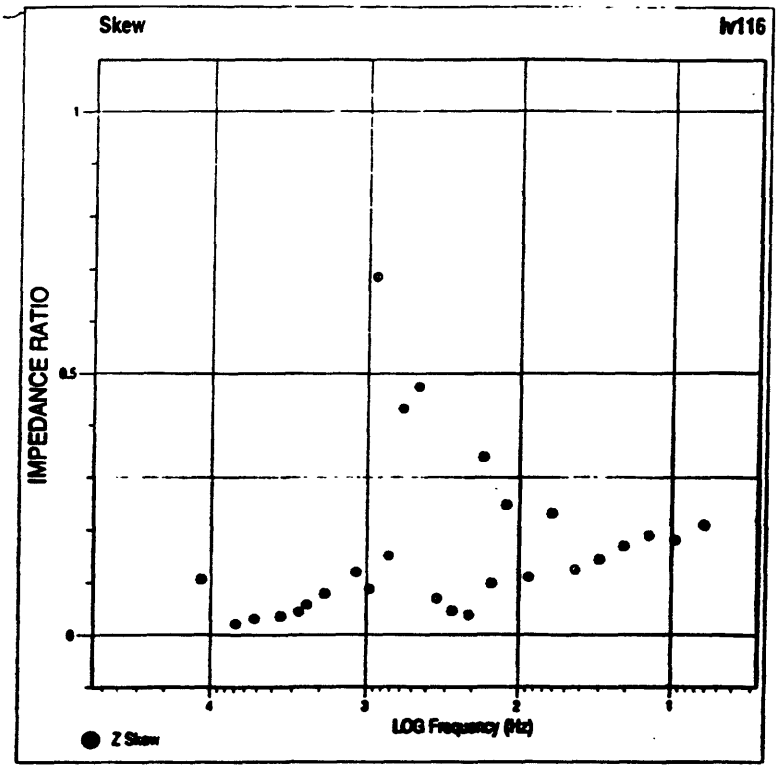

Figure 10-B–Site 116 continued; see caption figure 7-B.

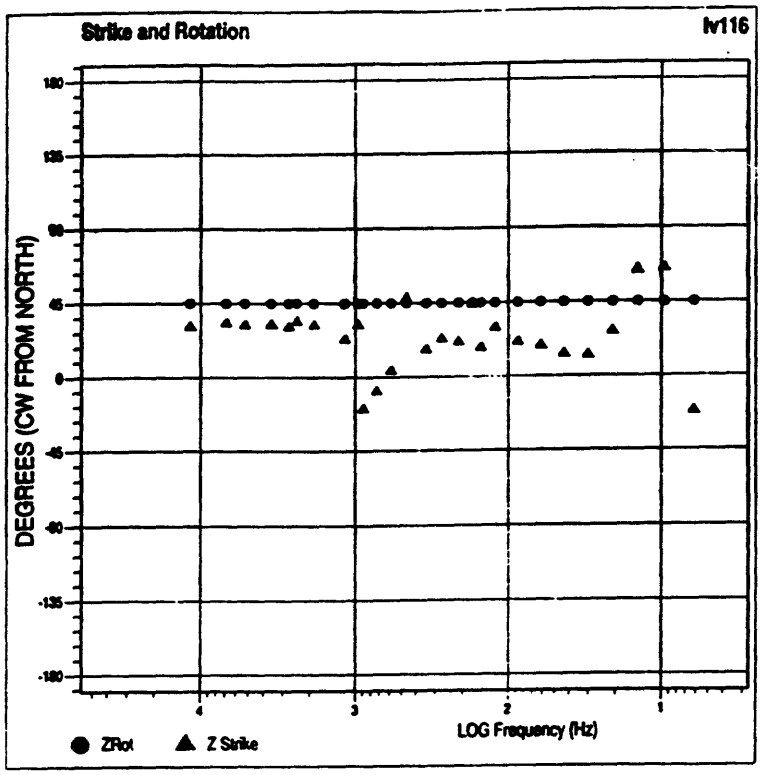

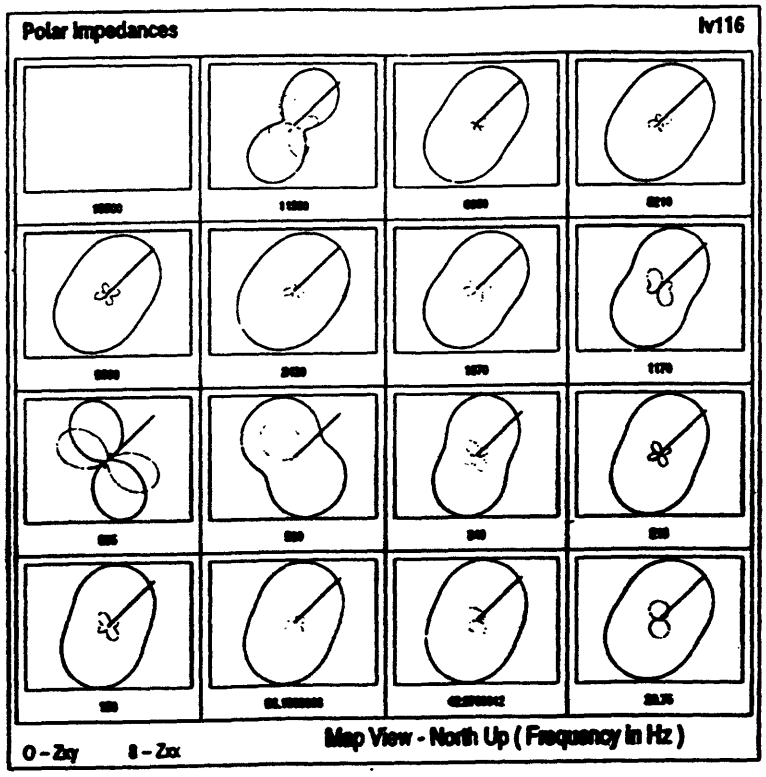

Figure 10-C--Site 116 continued; see caption figure 7-C.

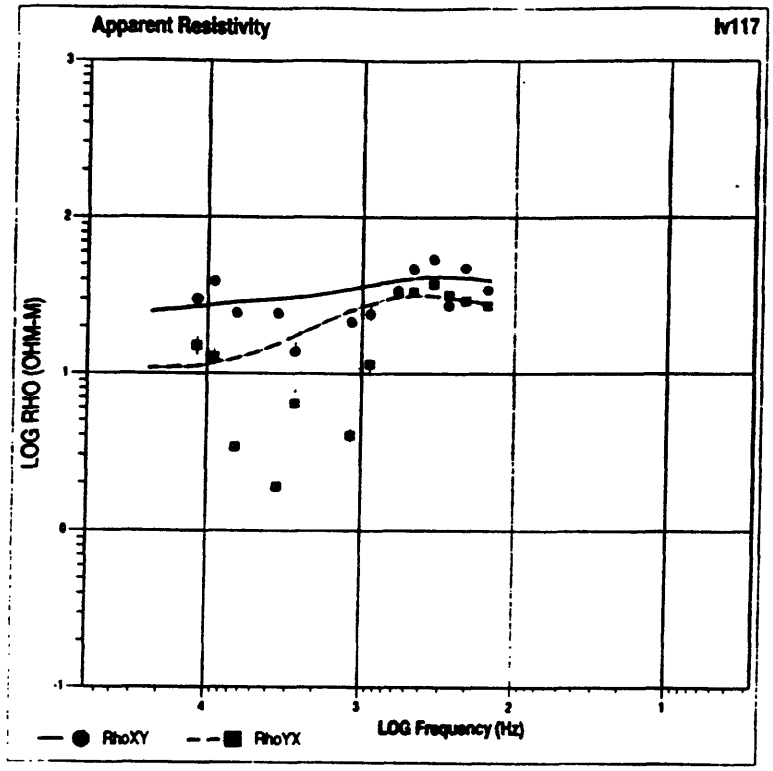

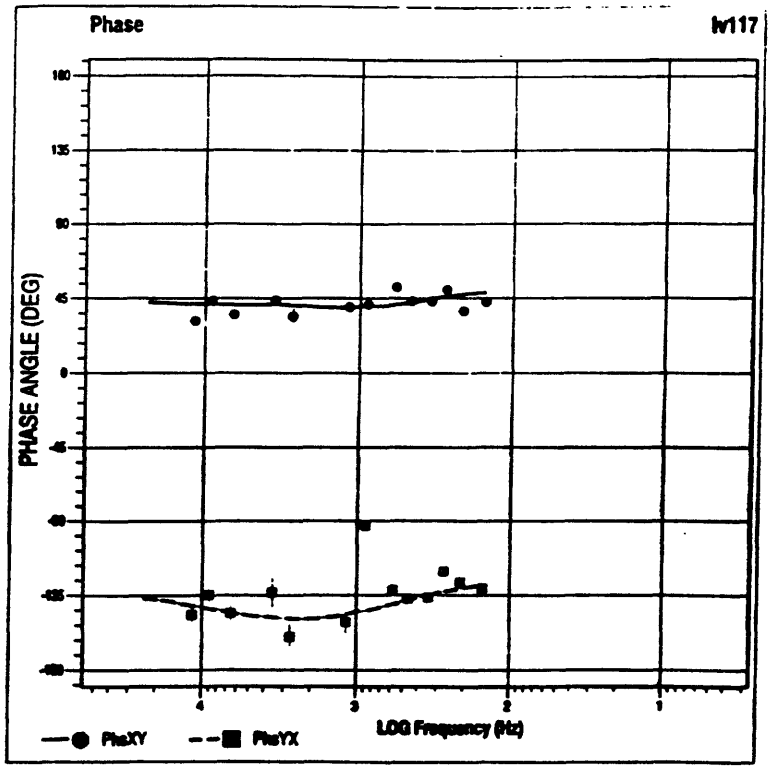

Figure 11-A--Data parameters for site 117; see caption figure 7-A.

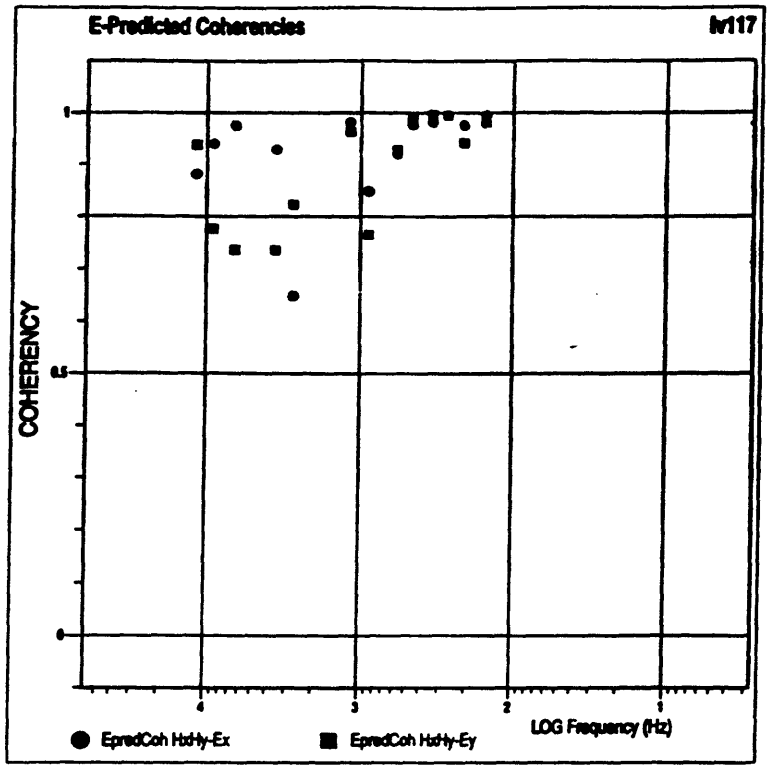

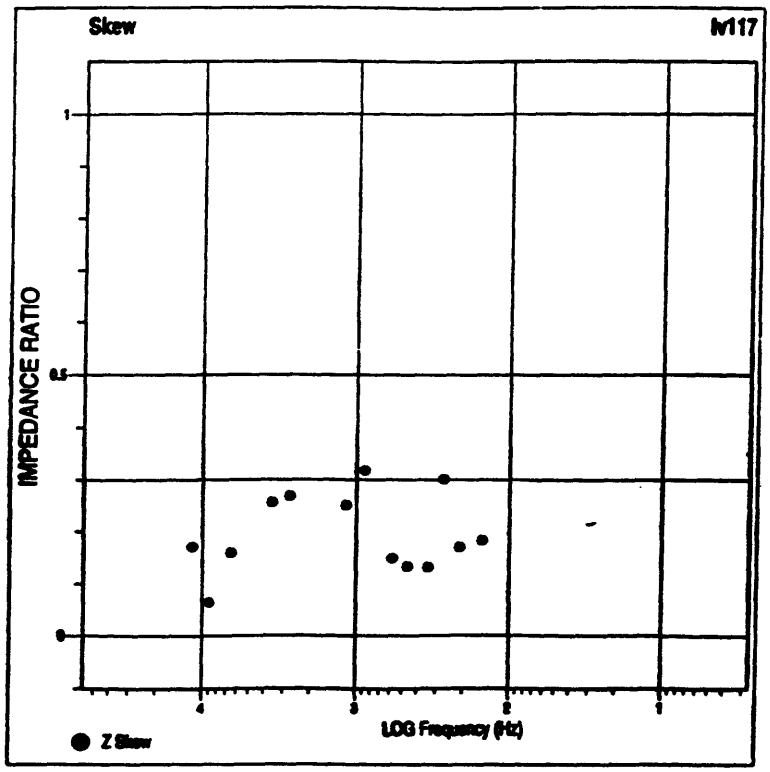

Figure 11-B--Site 117 continued; see caption figure 7-B.

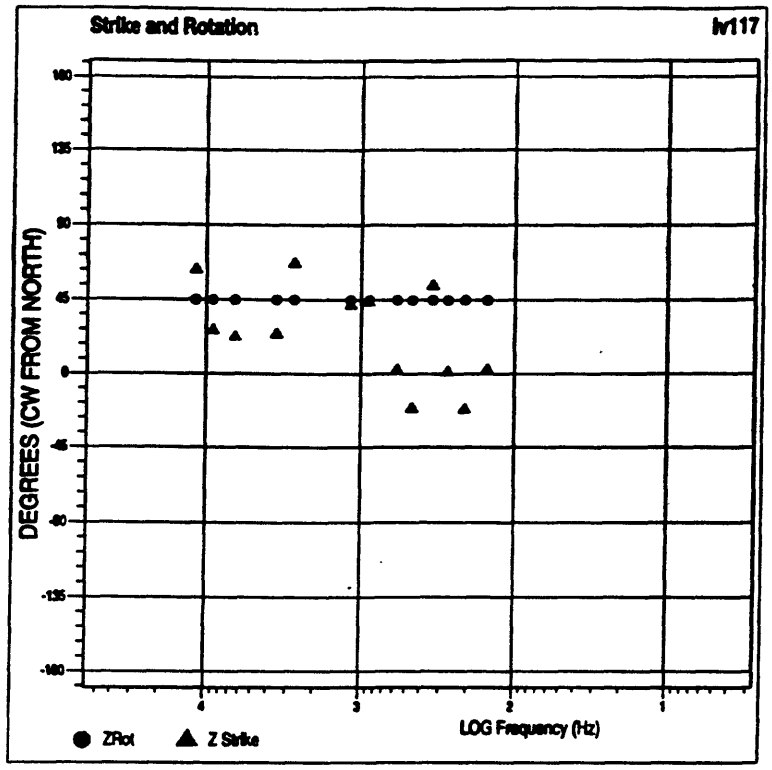

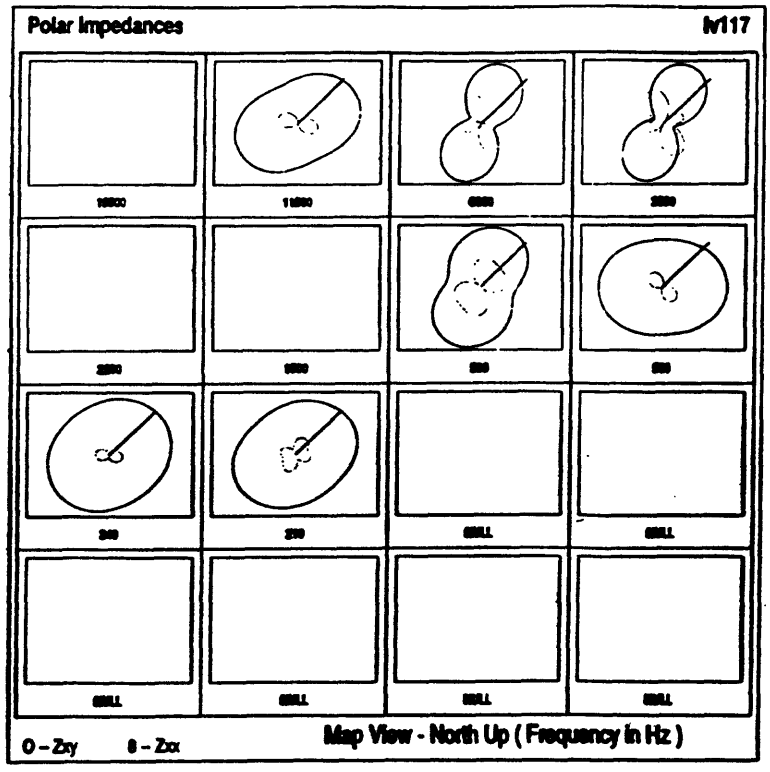

Figure 11-C--Site 117 continued; see caption figure 7-C.

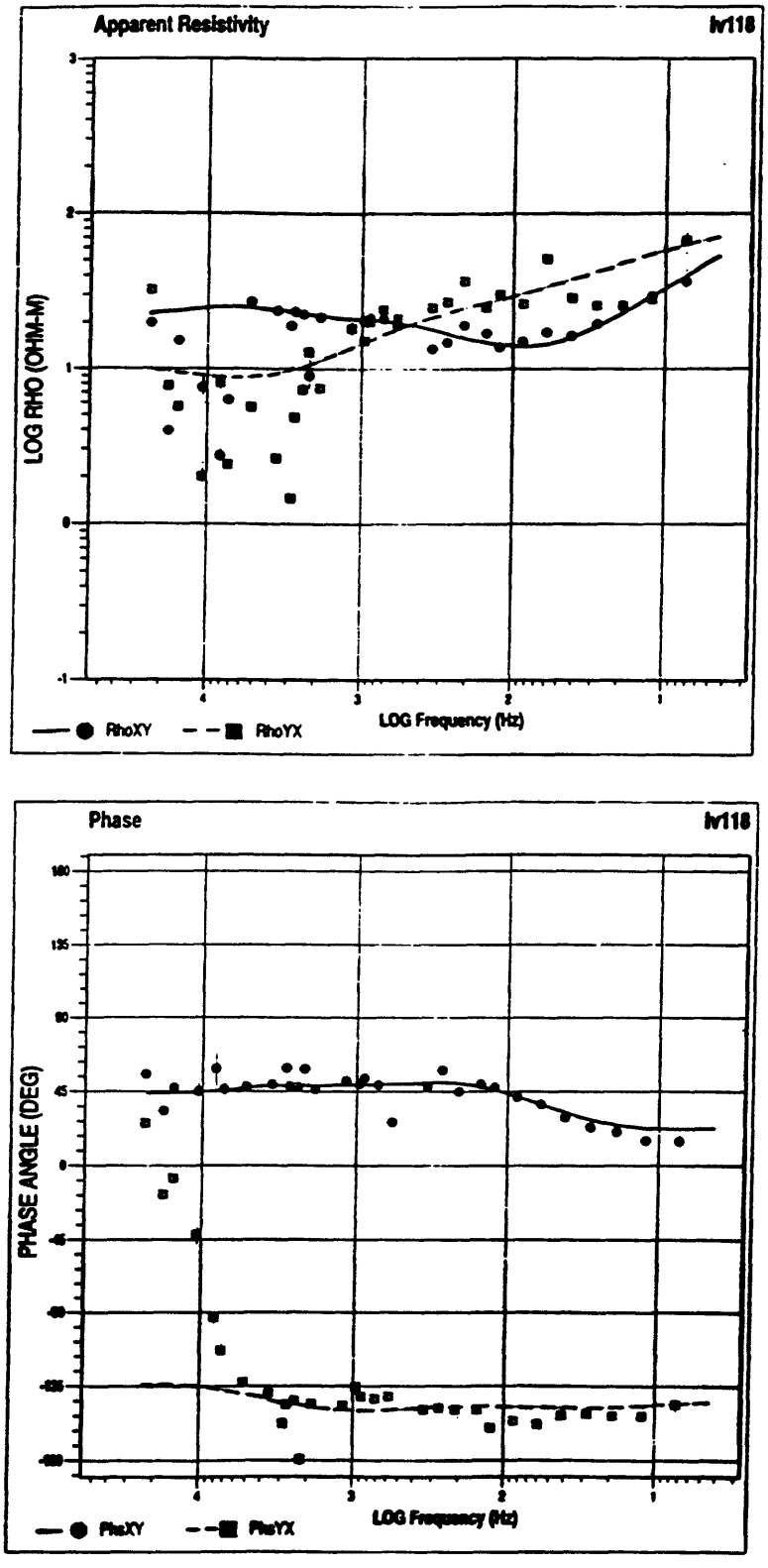

Figure 12-A--Data parameters for site 118; see caption figure 7-A.

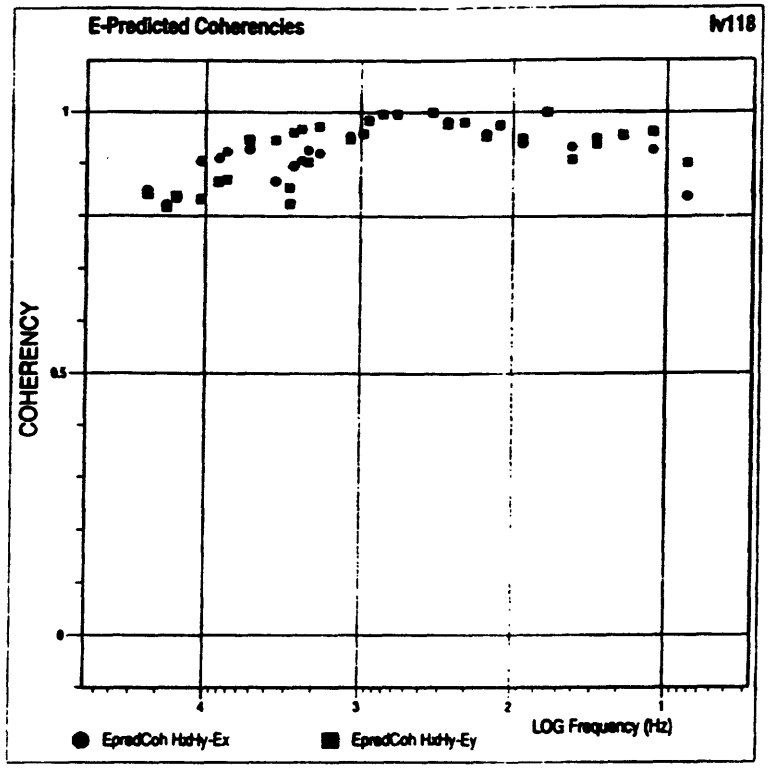

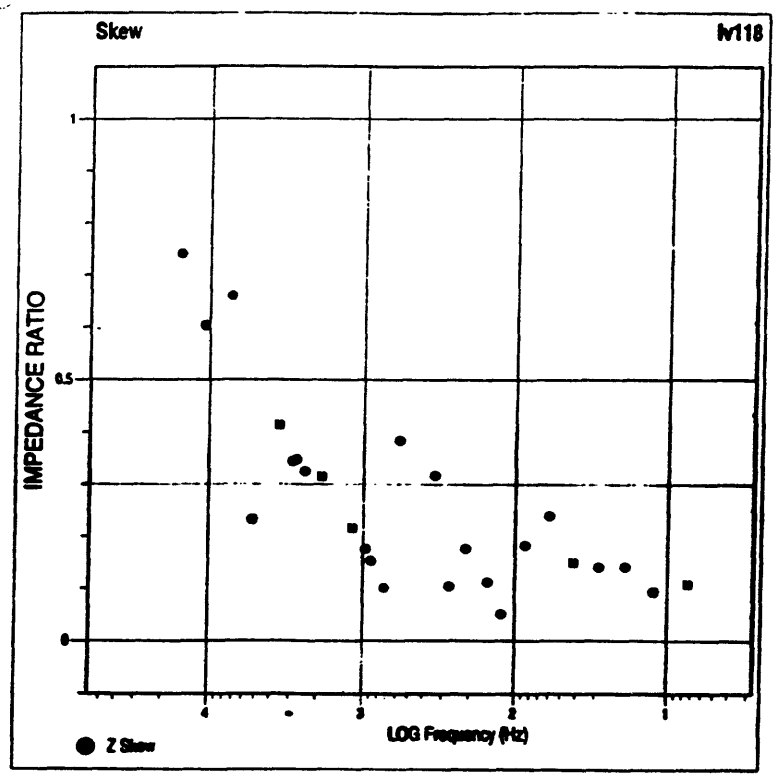

Figure 12-B--Site 118 continued; see caption figure 7-B.

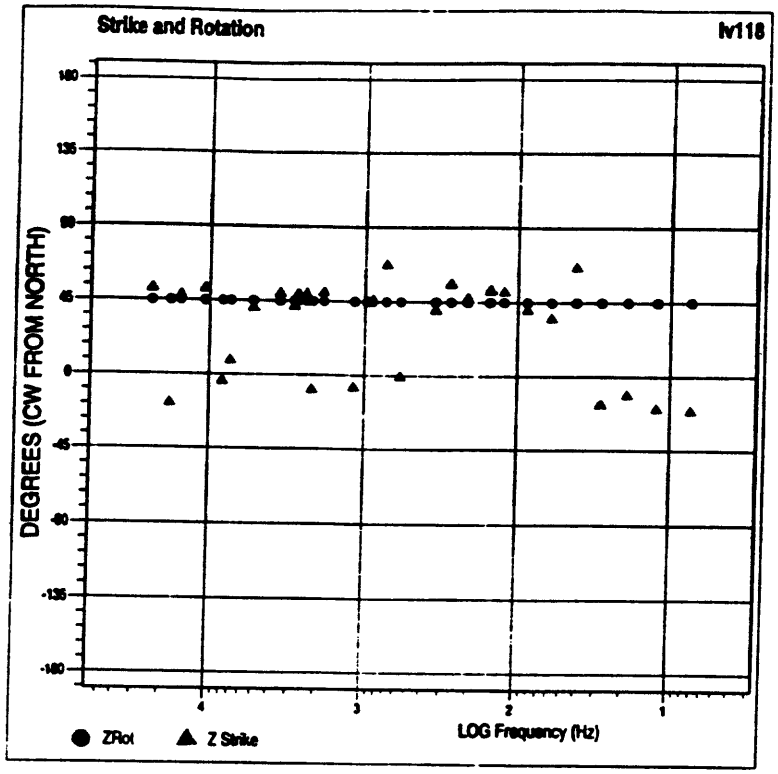

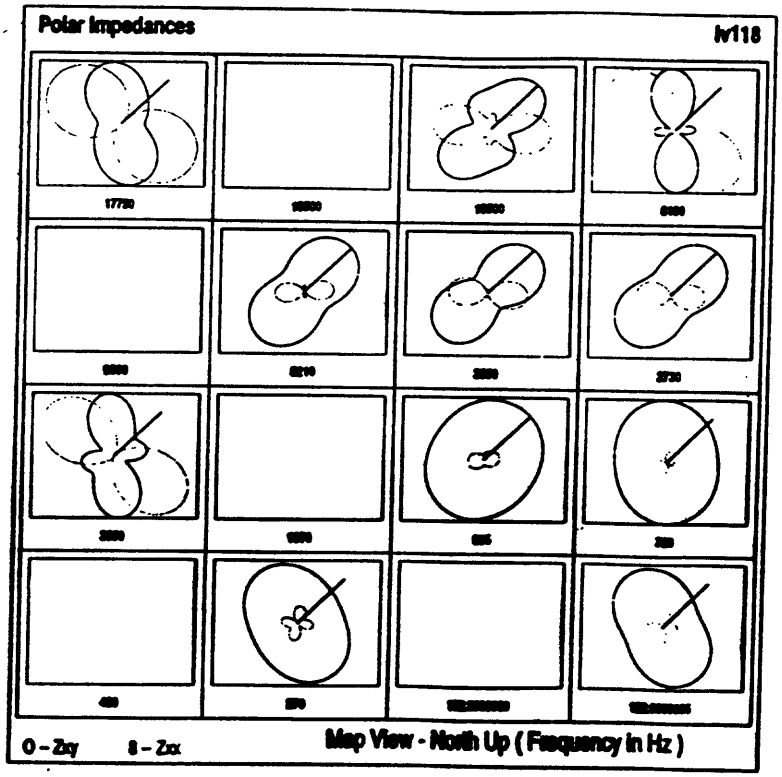

Figure 12-C--Site 118 continued; see caption figure 7-C.

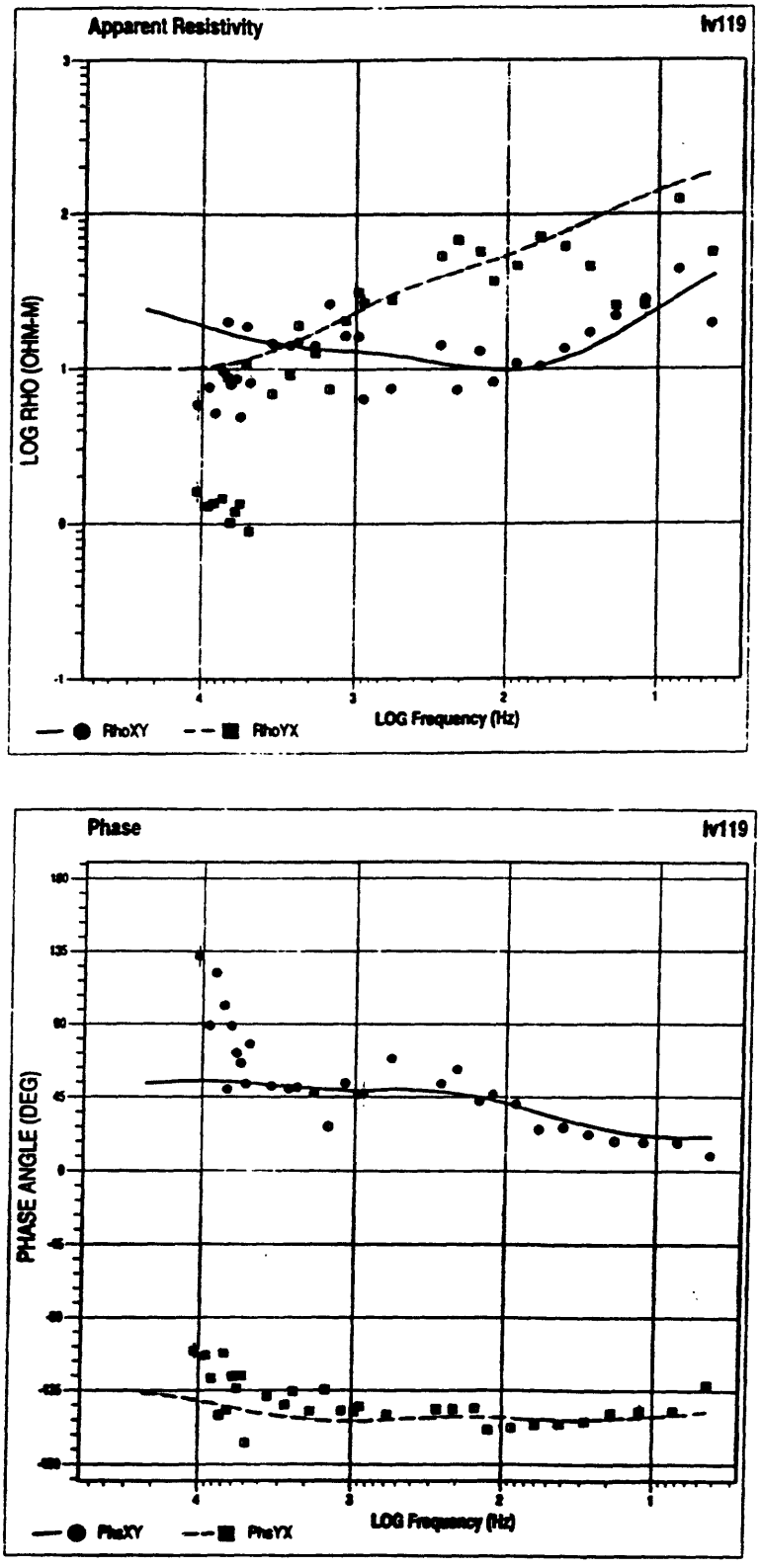

Figure 13-A--Data parameters for site 119; see caption figure 7-A.

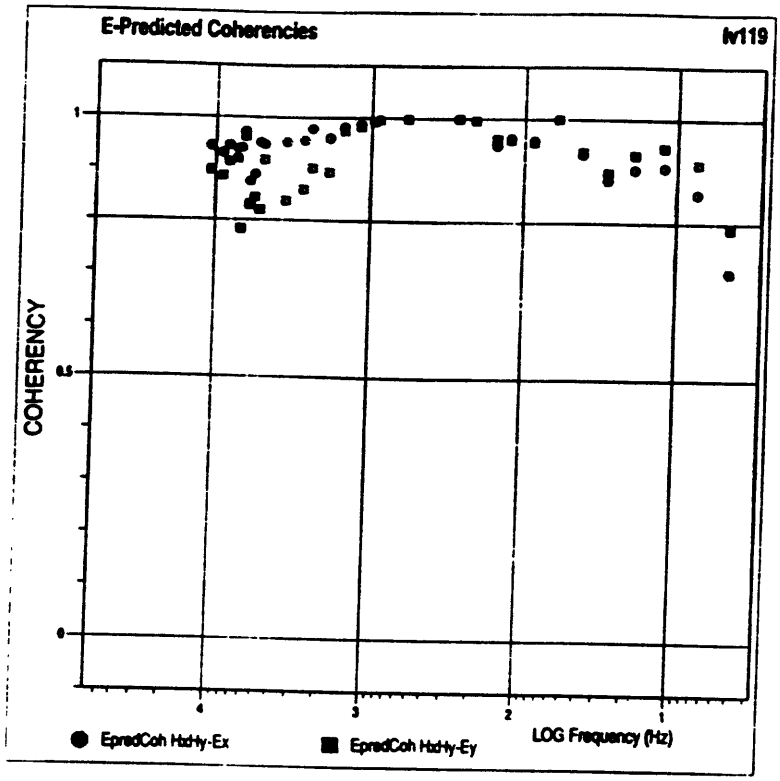

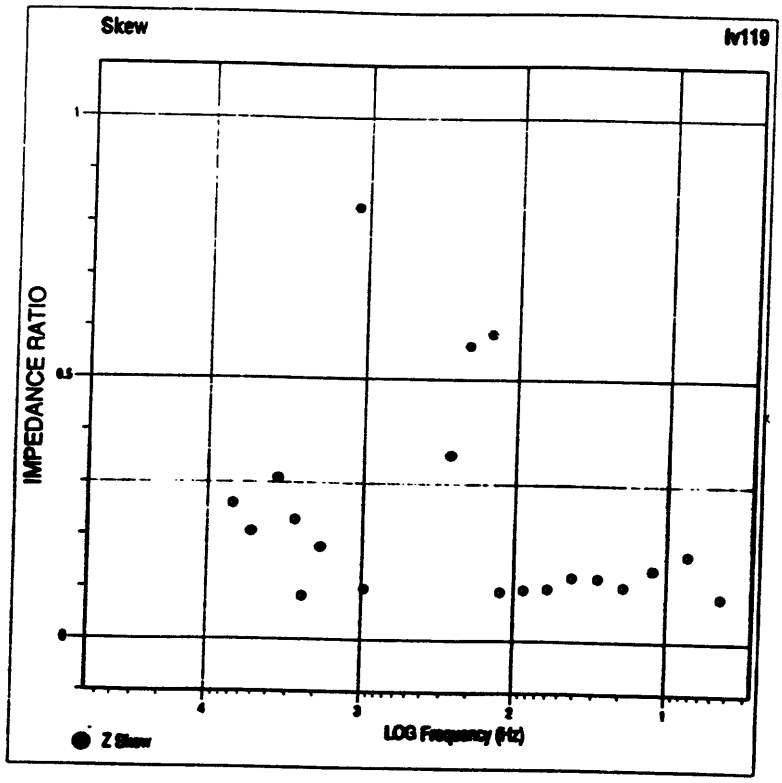

Figure 13-B--Site 119 continued; see caption figure 7-B.

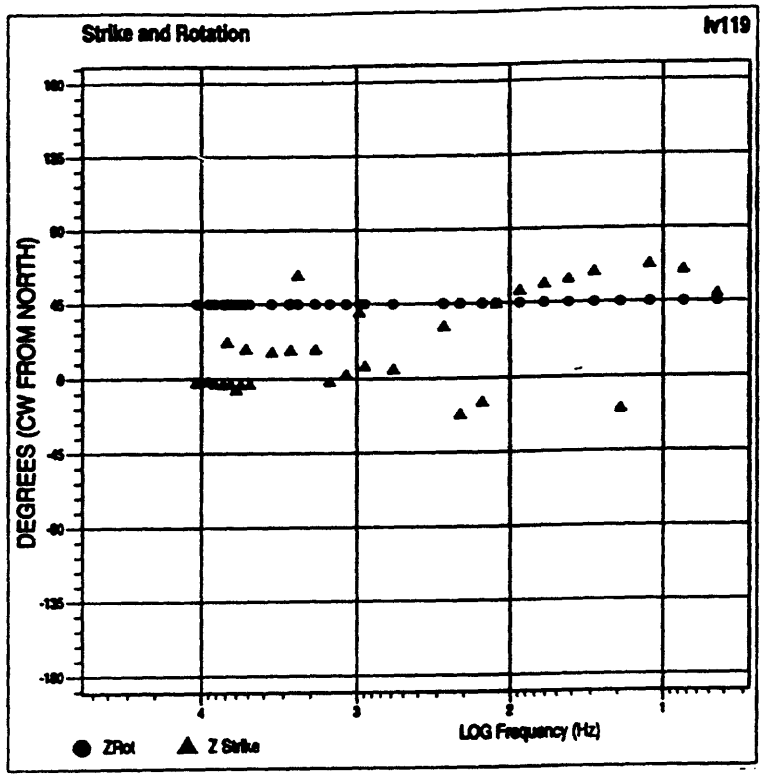

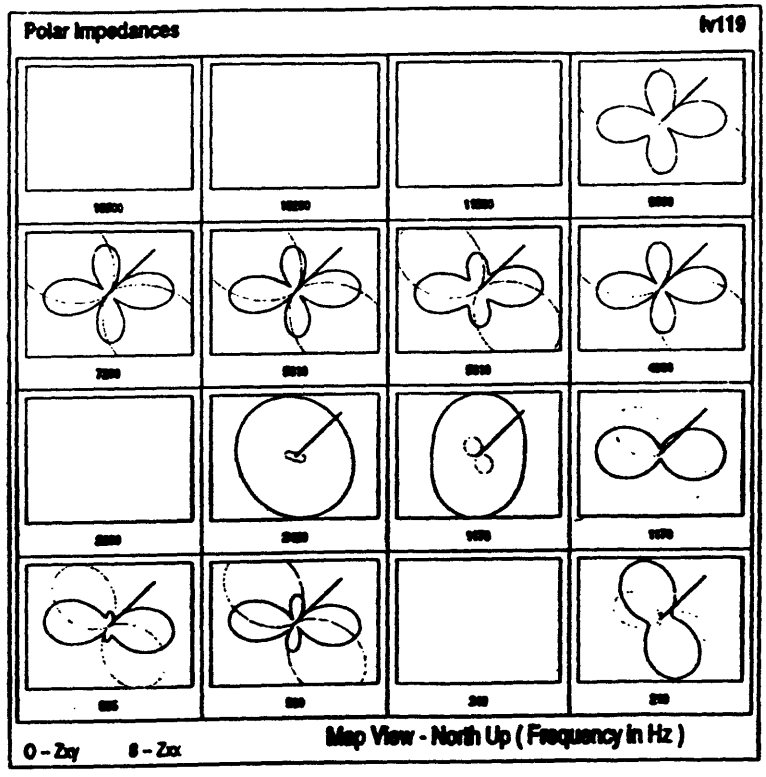

Figure 13-C--Site 119 continued; see caption figure 7-C.

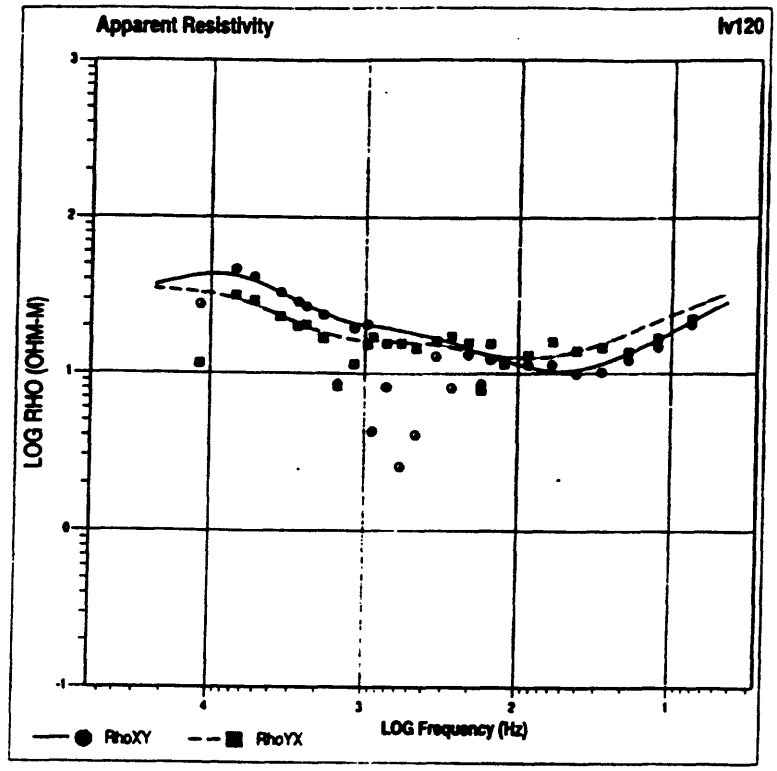

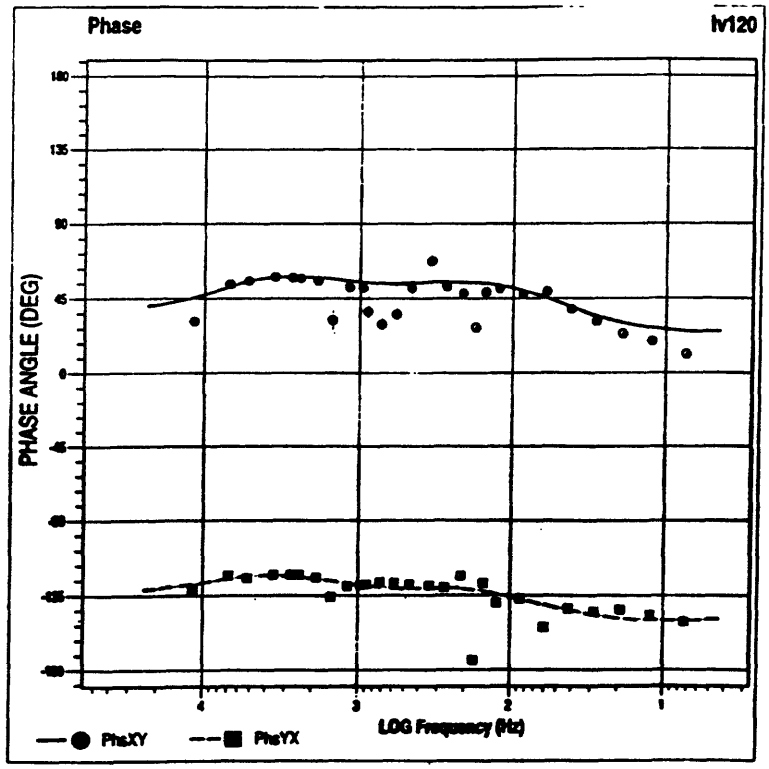

Figure 14-A--Data parameters for site 120; see caption figure 7-A.

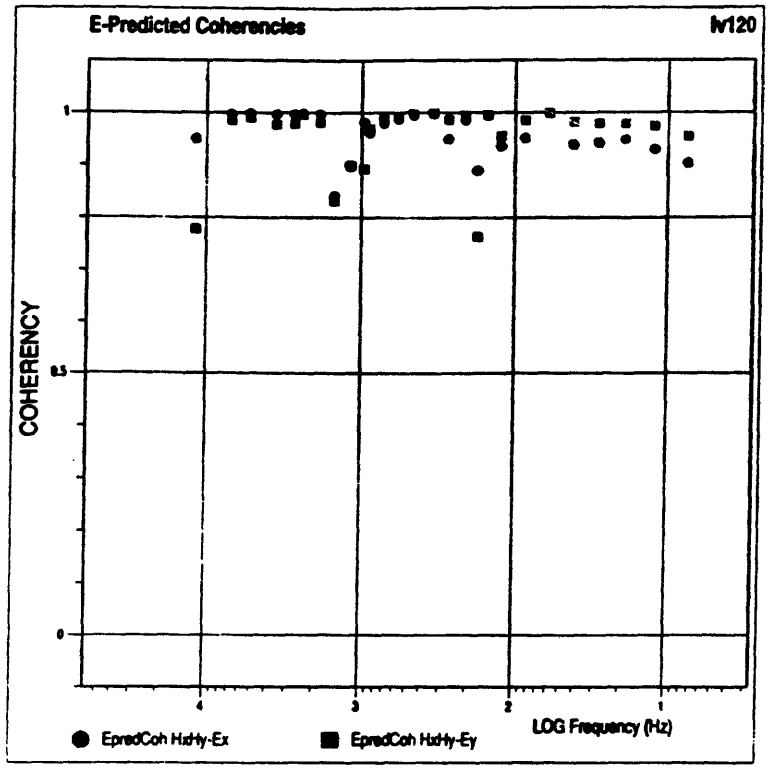

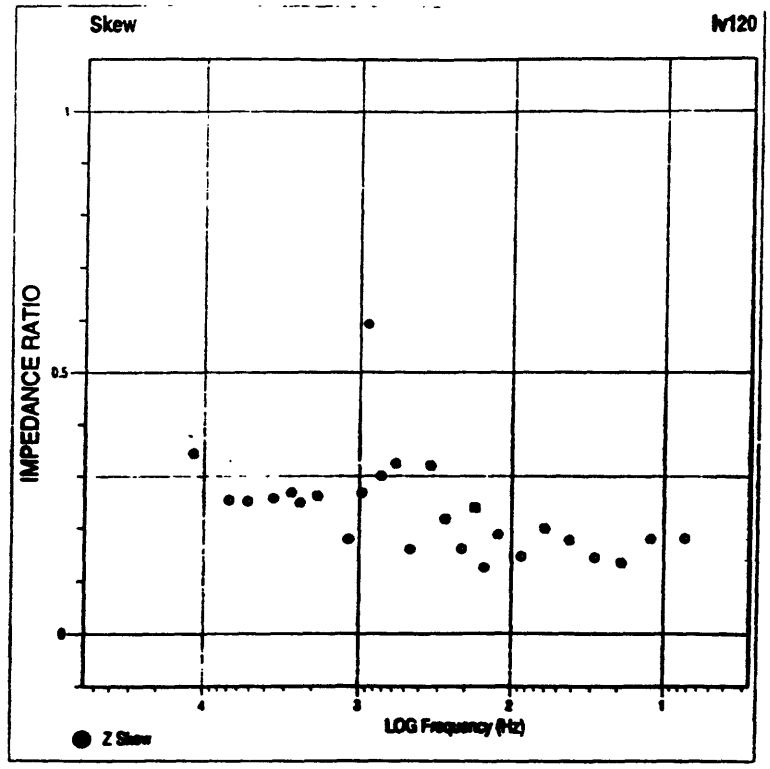

Figure 14-B--Site 120 continued; see caption figure 7-B.

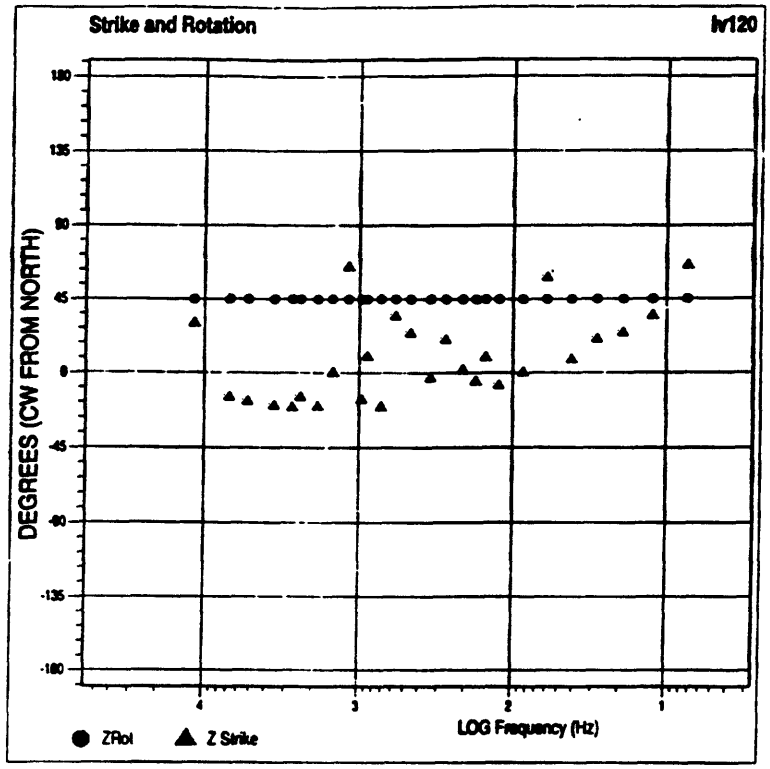

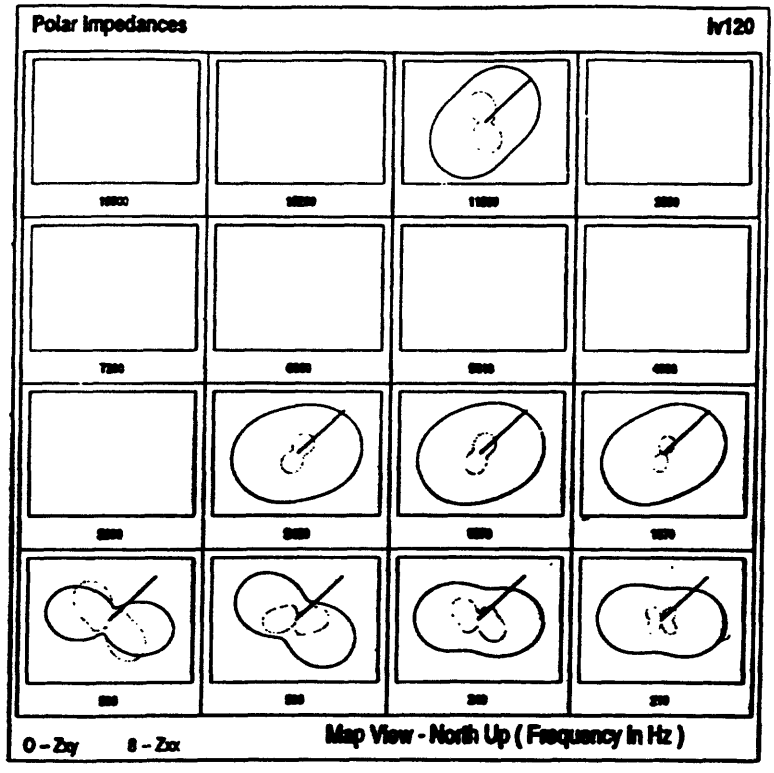

Figure 14-C--Site 120 continued; see caption figure 7-C.

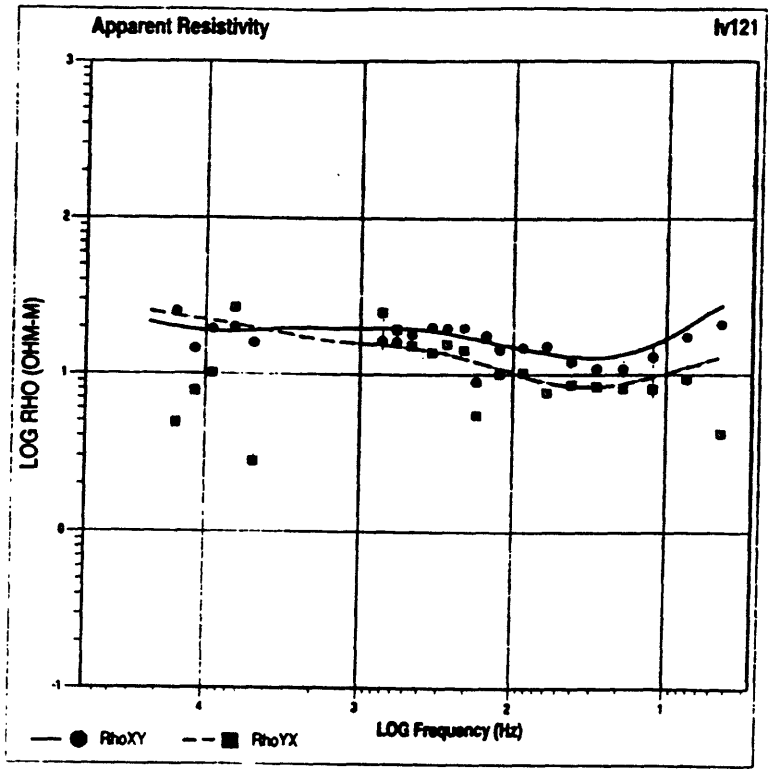

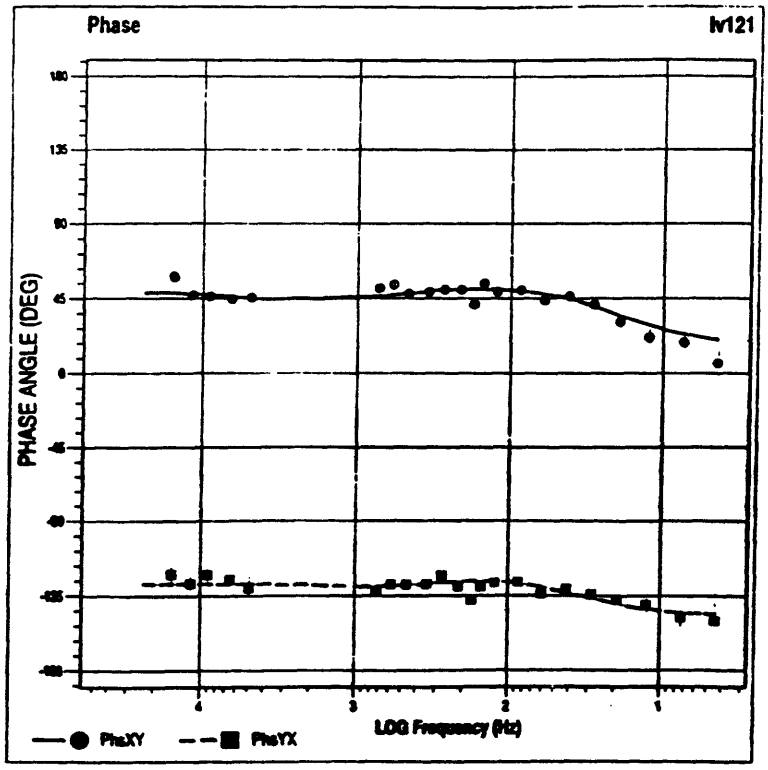

Figure 15-A--Data parameters for site 121; see caption figure 7-A.

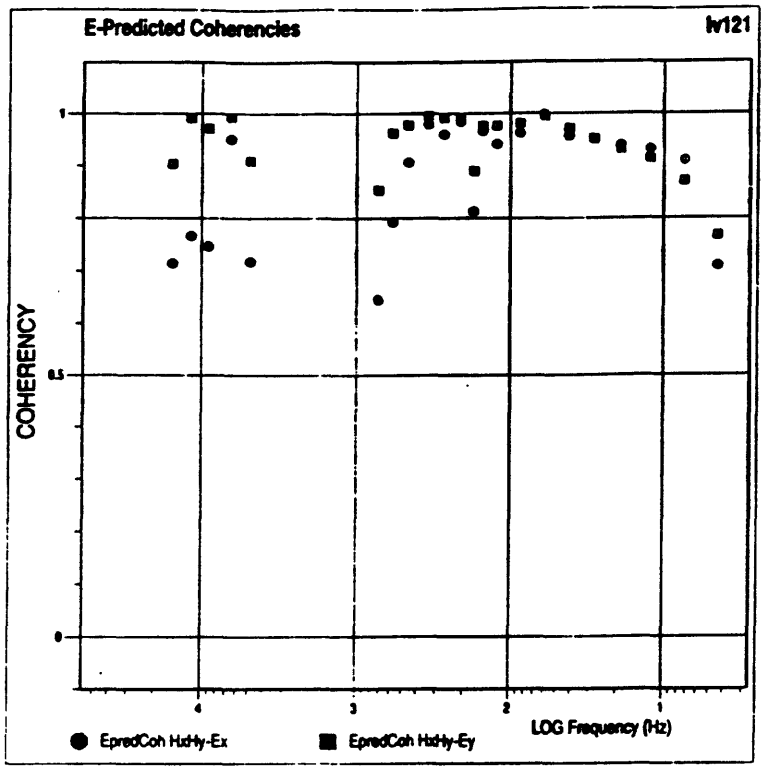

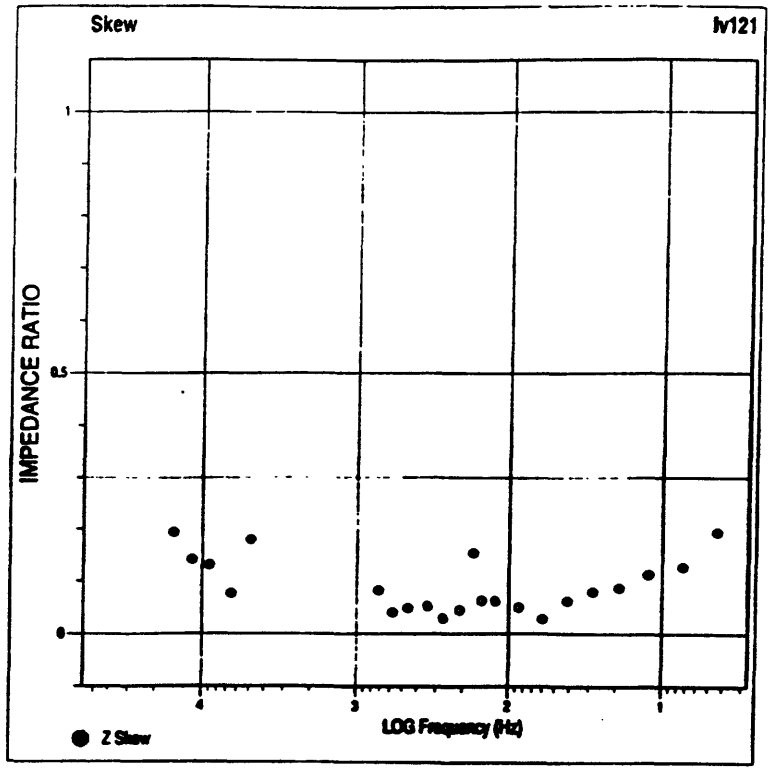

Figure 15-B--Site 121 continued; see caption figure 7-B.

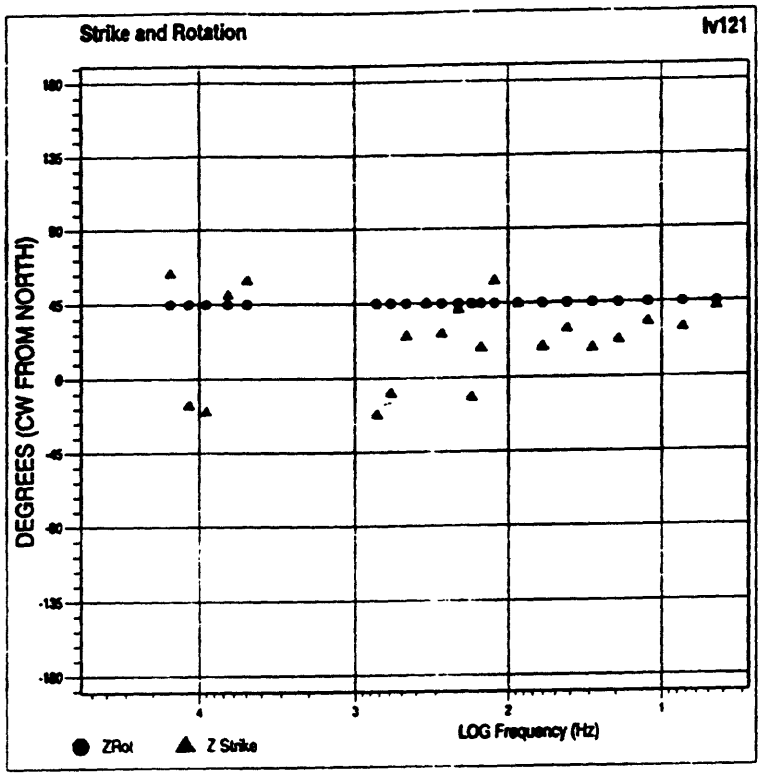

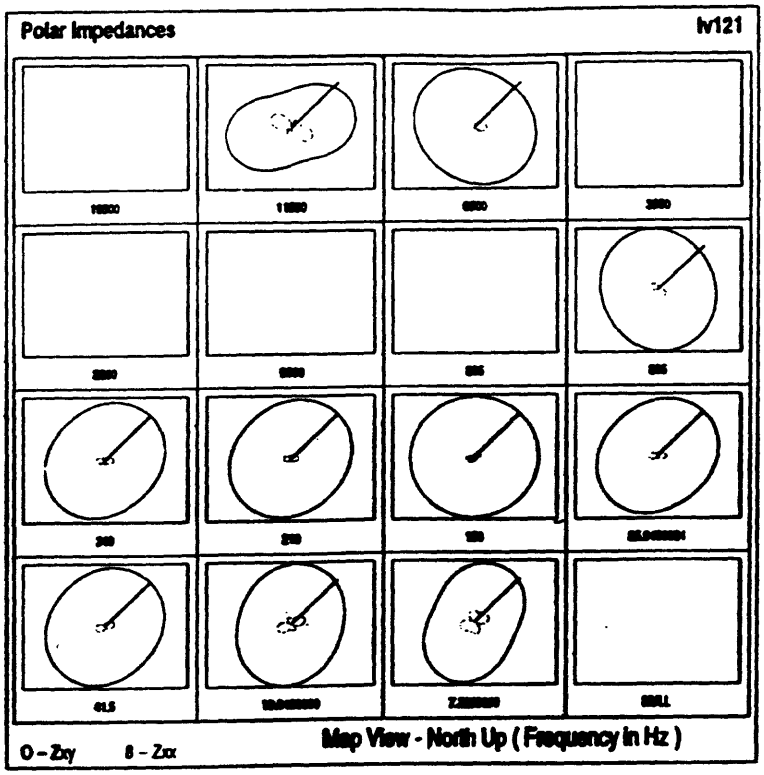

Figure 15-C--Site 121 continued; see caption figure 7-C.

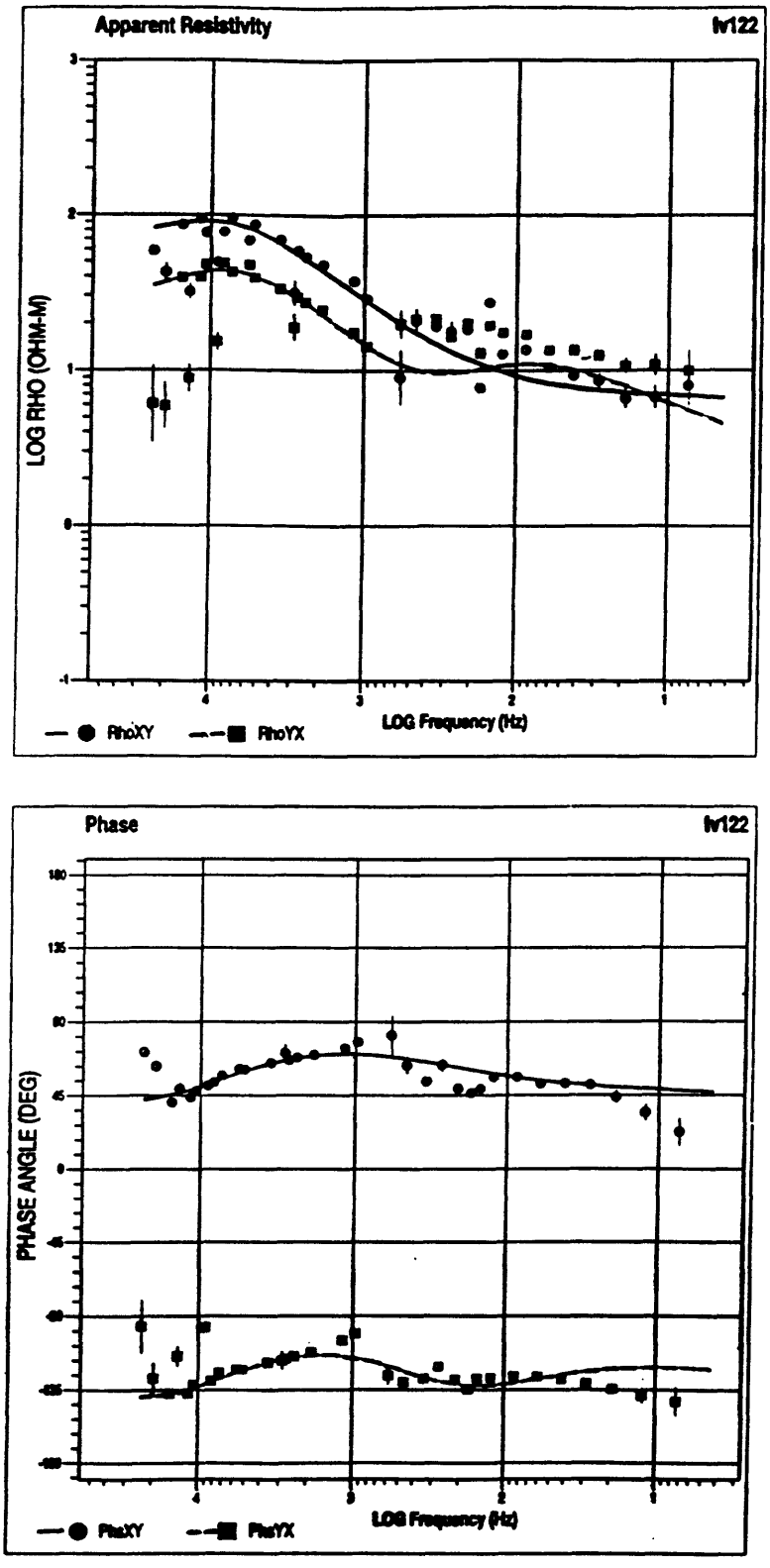

Figure 16-A--Data parameters for site 122; see caption figure 7-A.

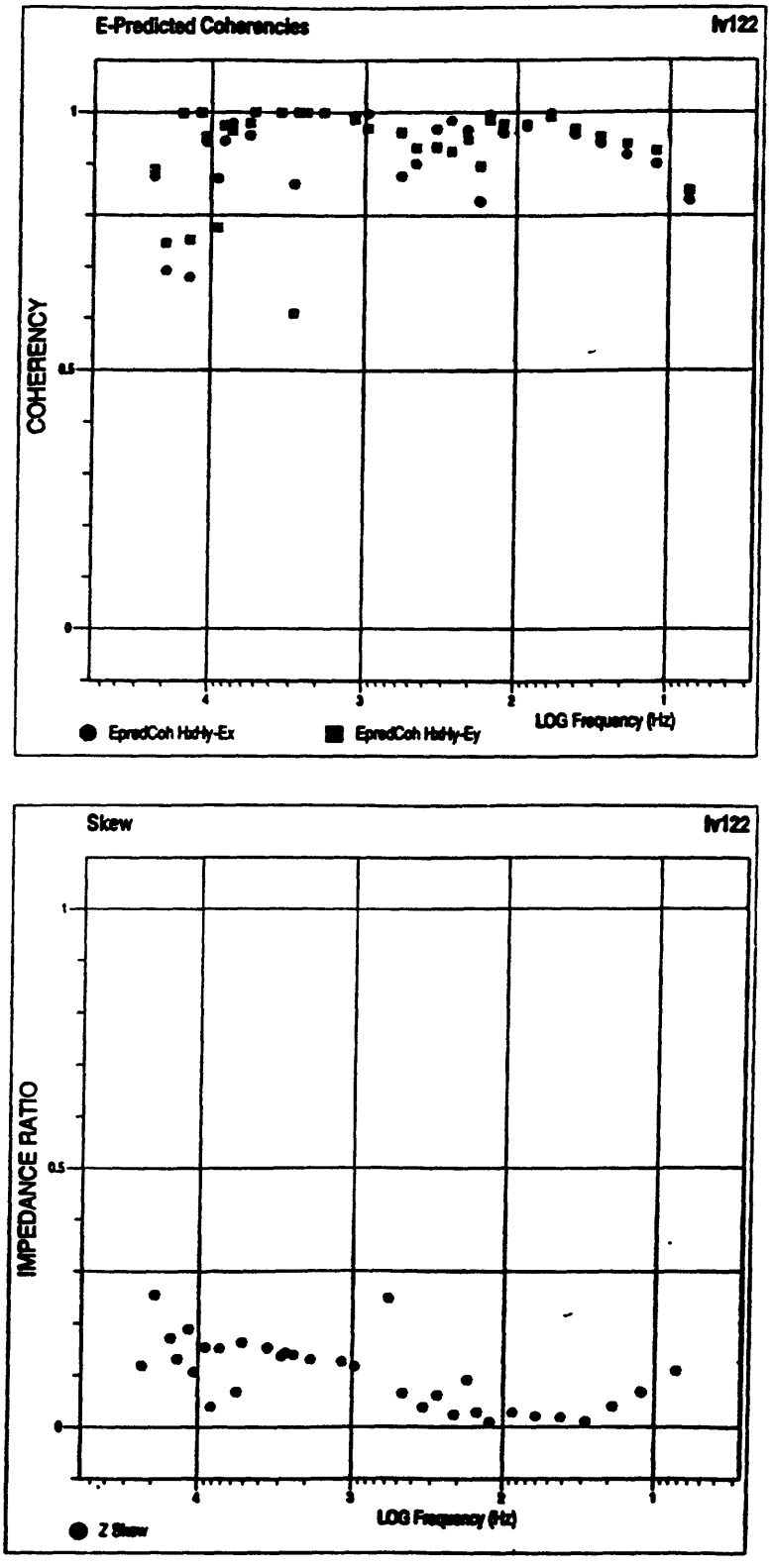

Figure 16-B--Site 122 continued; see caption figure 7-B.

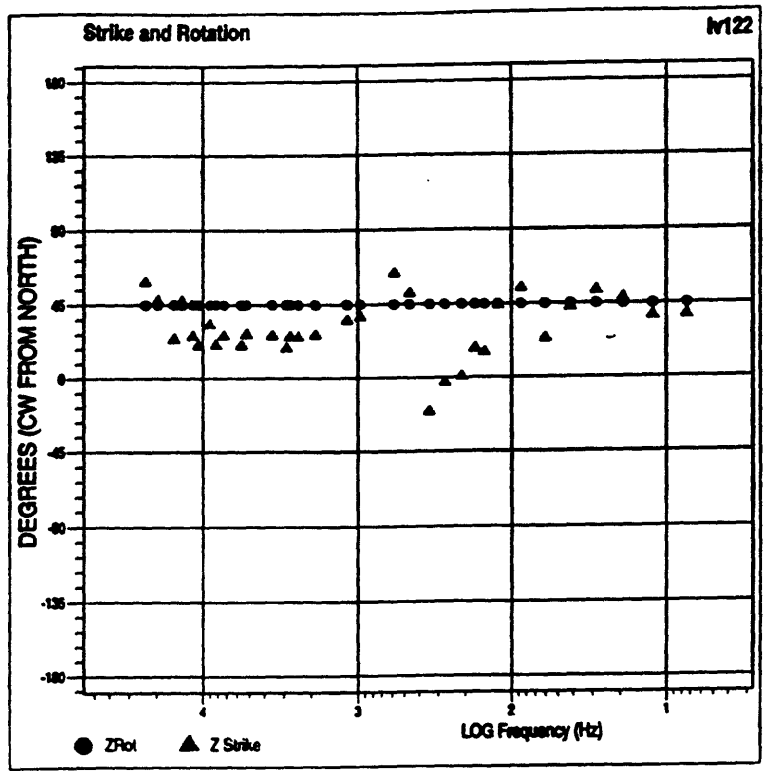

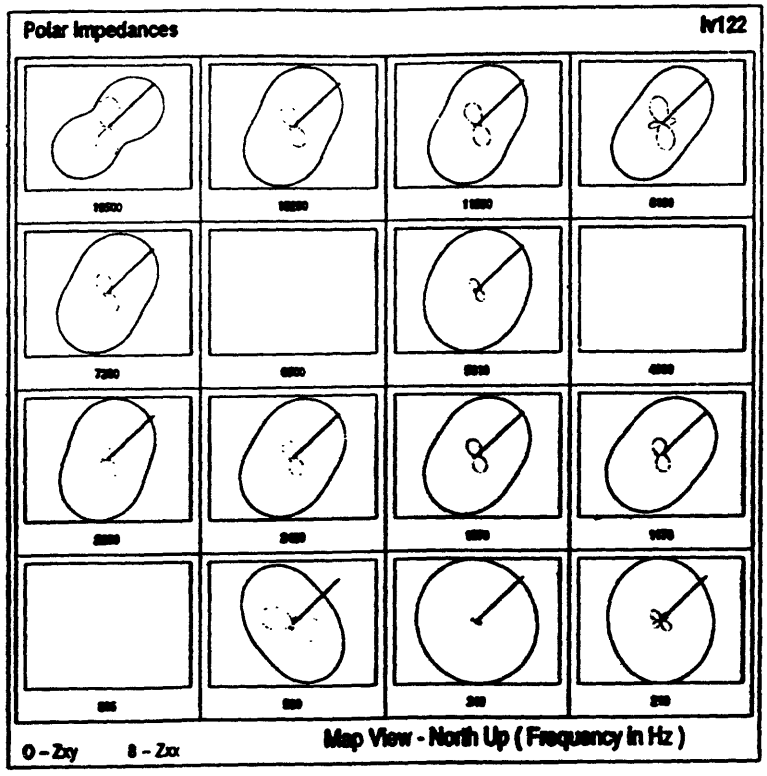

Figure 16-C--Site 122 continued; see caption figure 7-C.

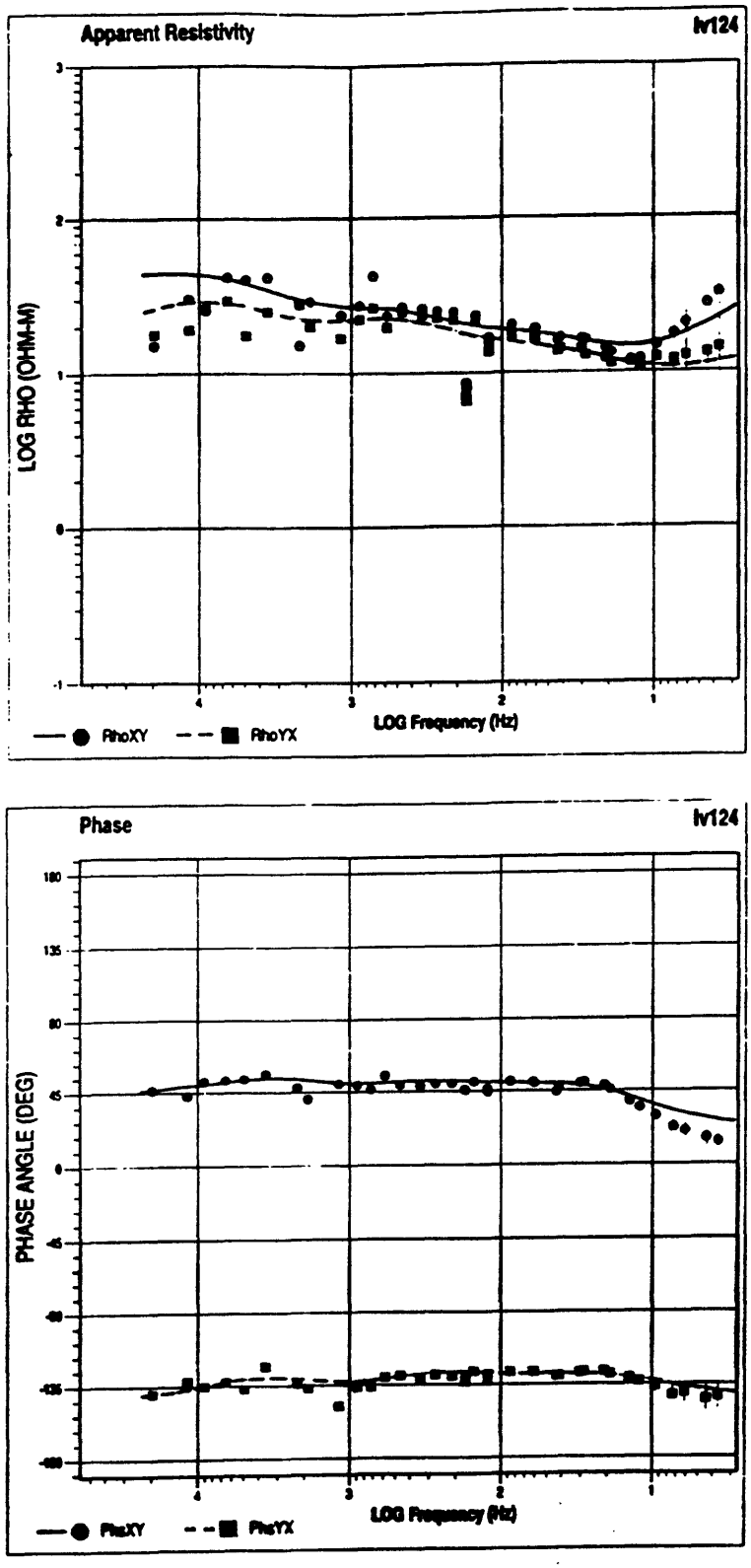

Figure 17-A--Data parameters for site 124; see caption figure 7-A.

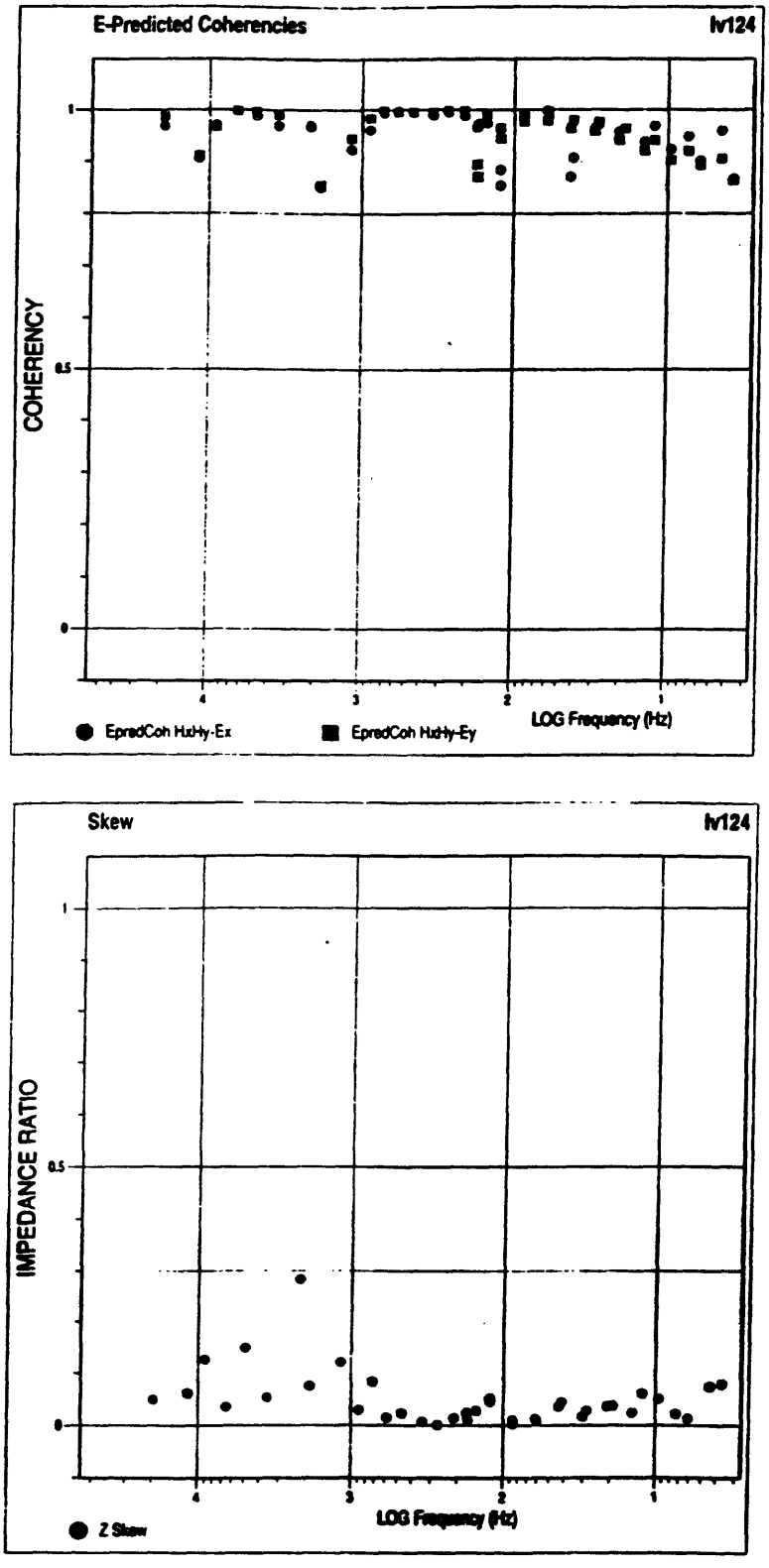

Figure 17-B--Site 124 continued; see caption figure 7-B.

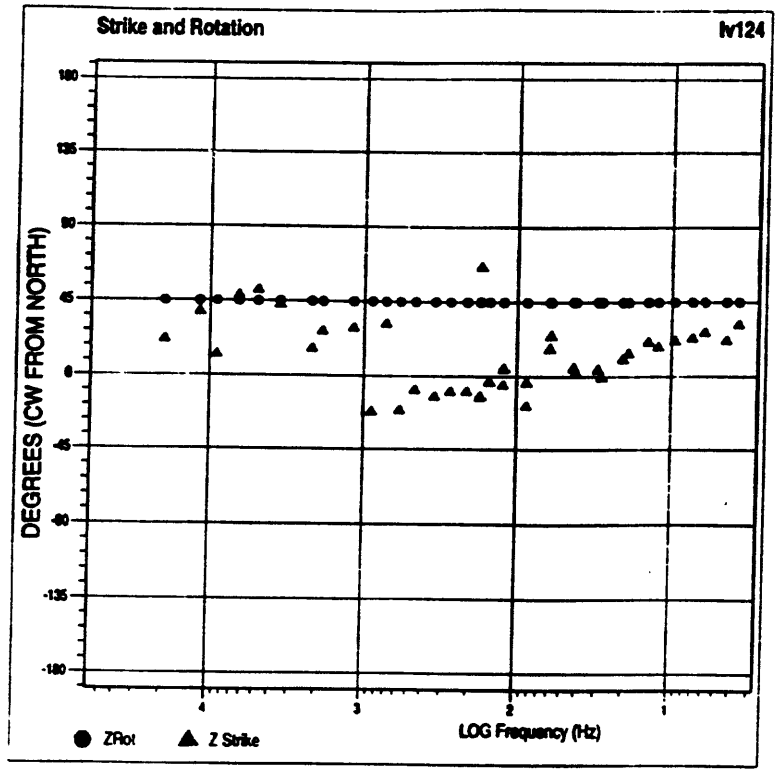

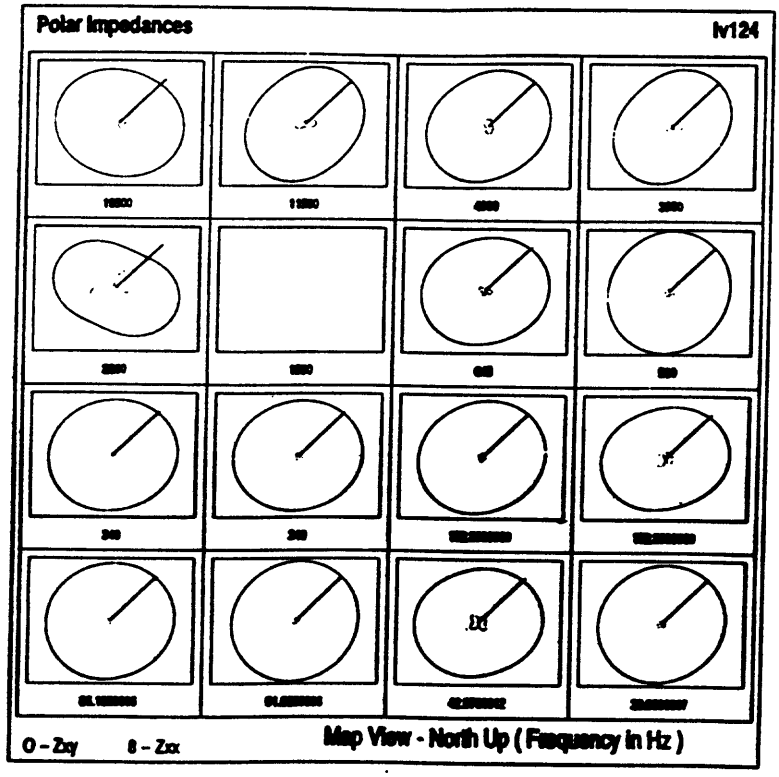

Figure 17-C--Site 124 continued; see caption figure 7-C.

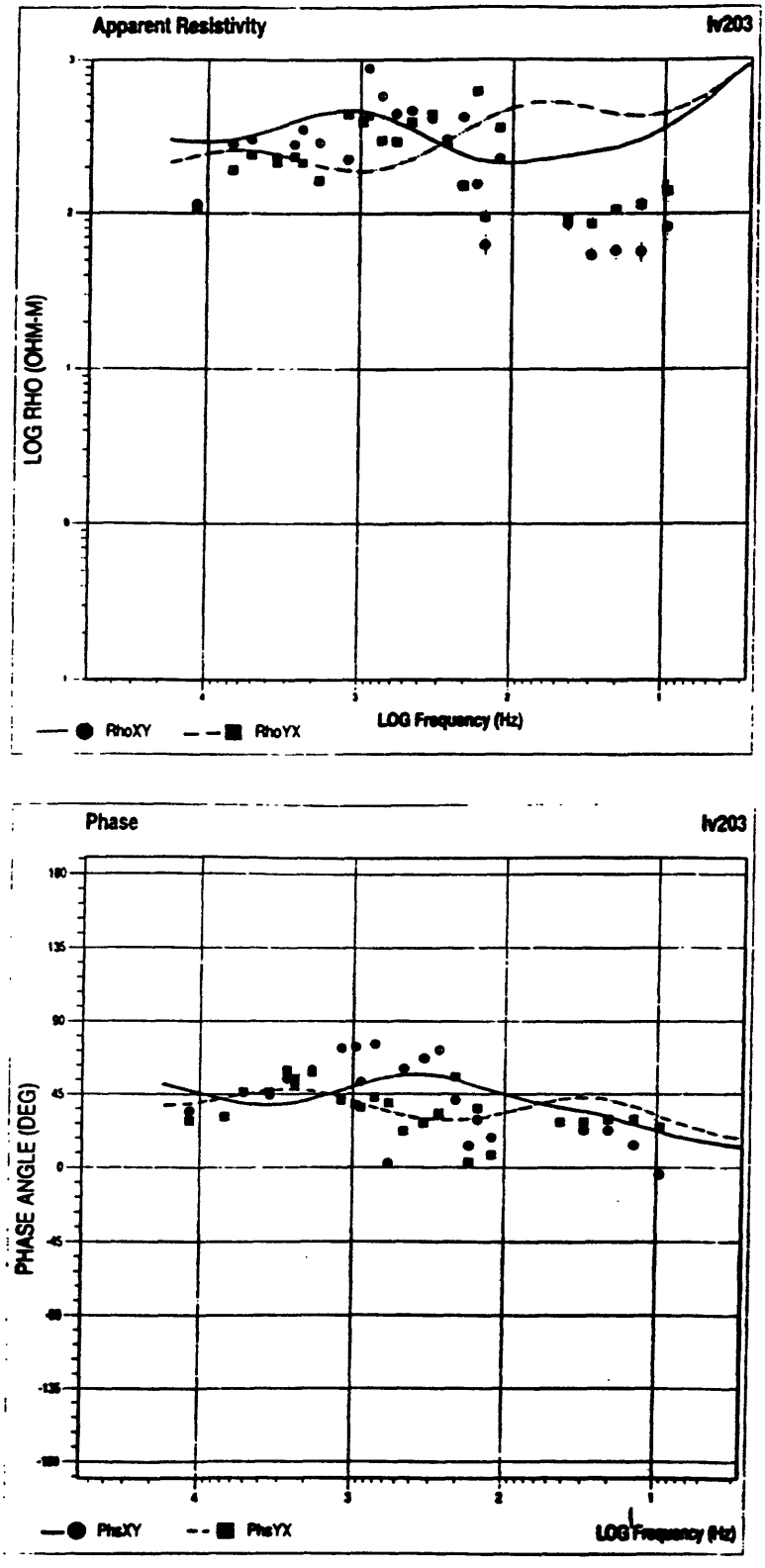

Figure 18-A--Data parameters for site 203; see caption figure 7-A.

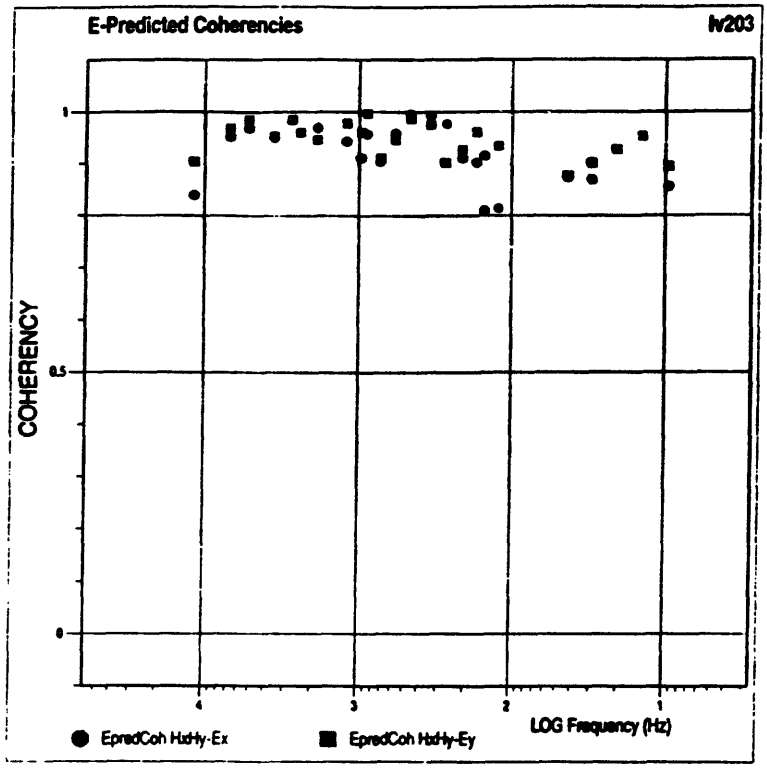

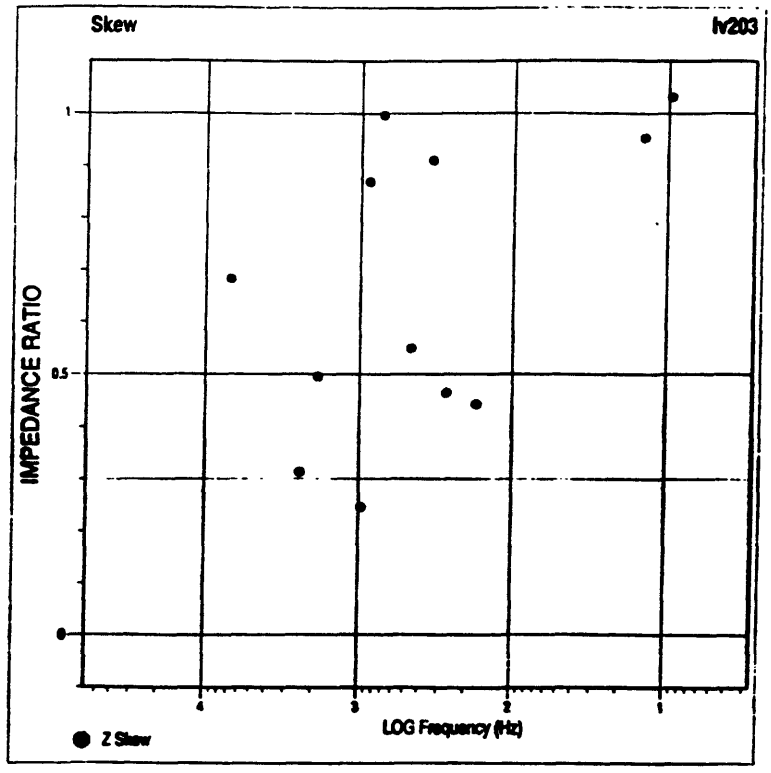

Figure 18-B--Site 203 continued; see caption figure 7-B.

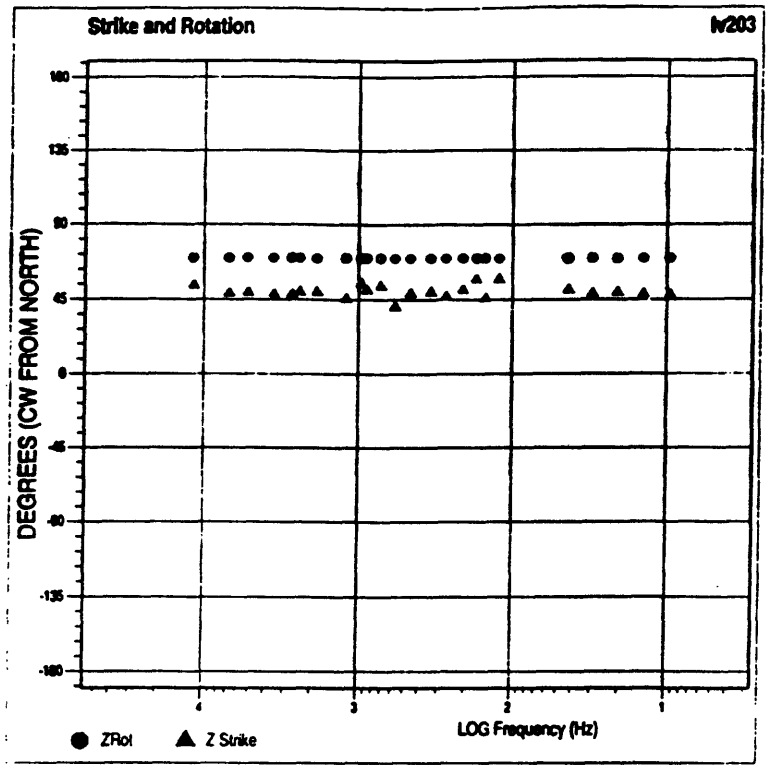

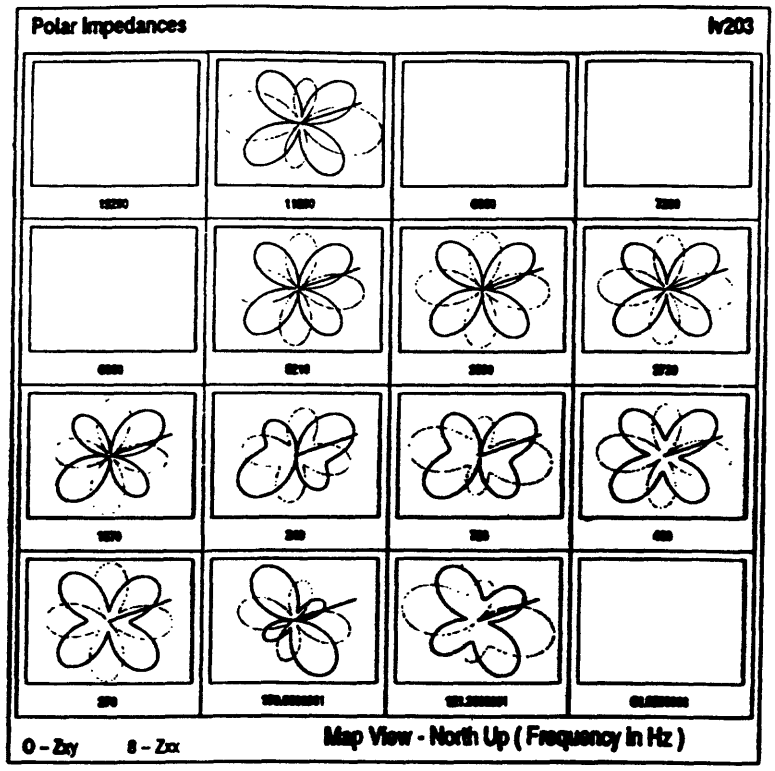

Figure 18-C--Site 203 continued; see caption figure 7-C.

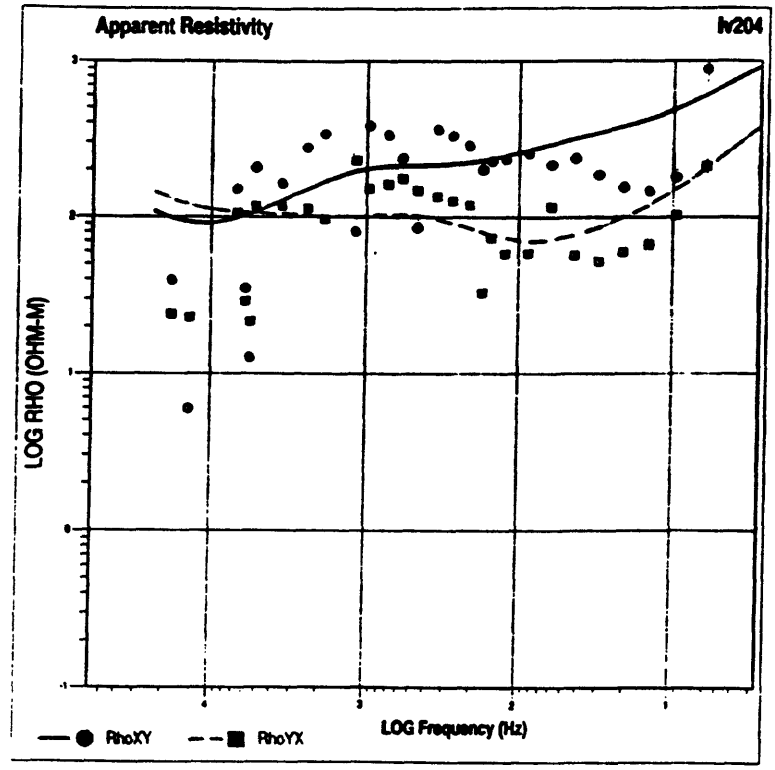

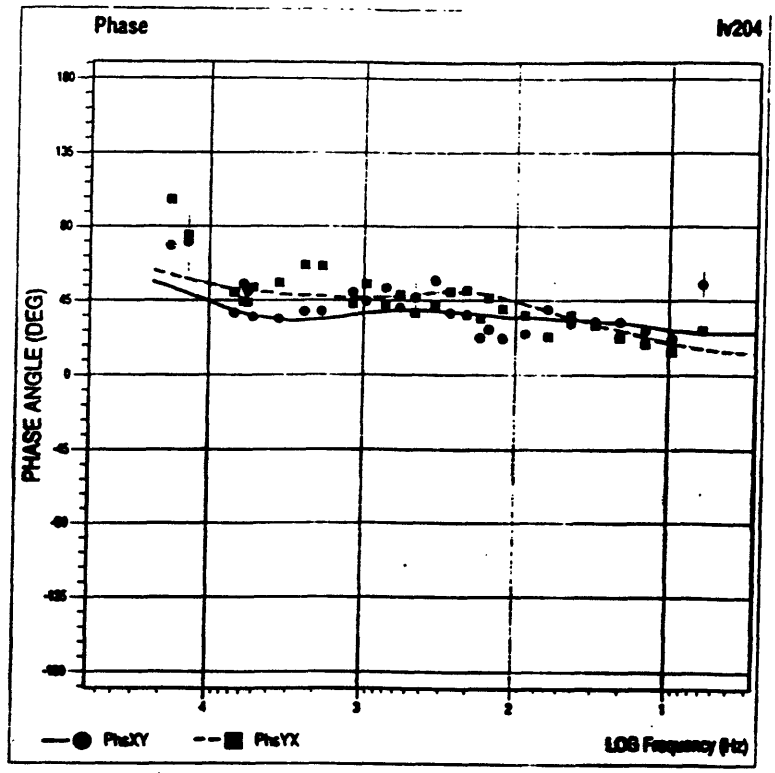

Figure 19-A--Data parameters for site 204; see caption figure 7-A.

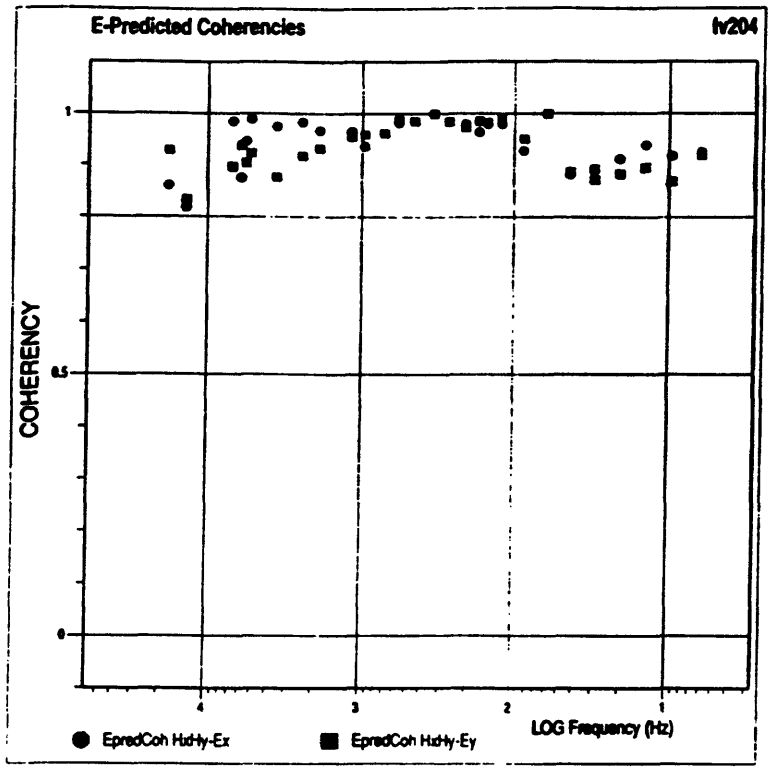

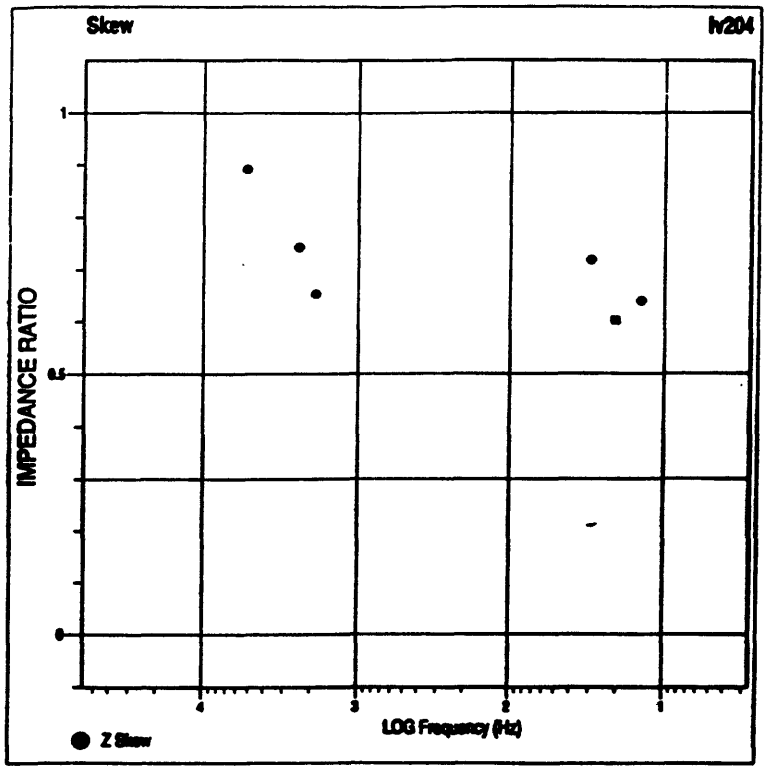

Figure 19-B--Site 204 continued; see caption figure 7-B.

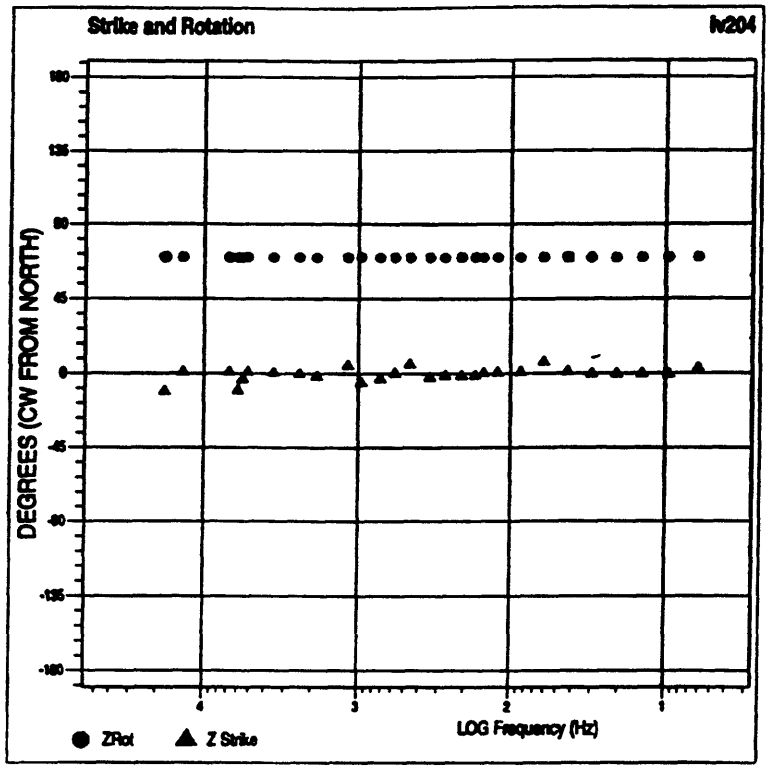

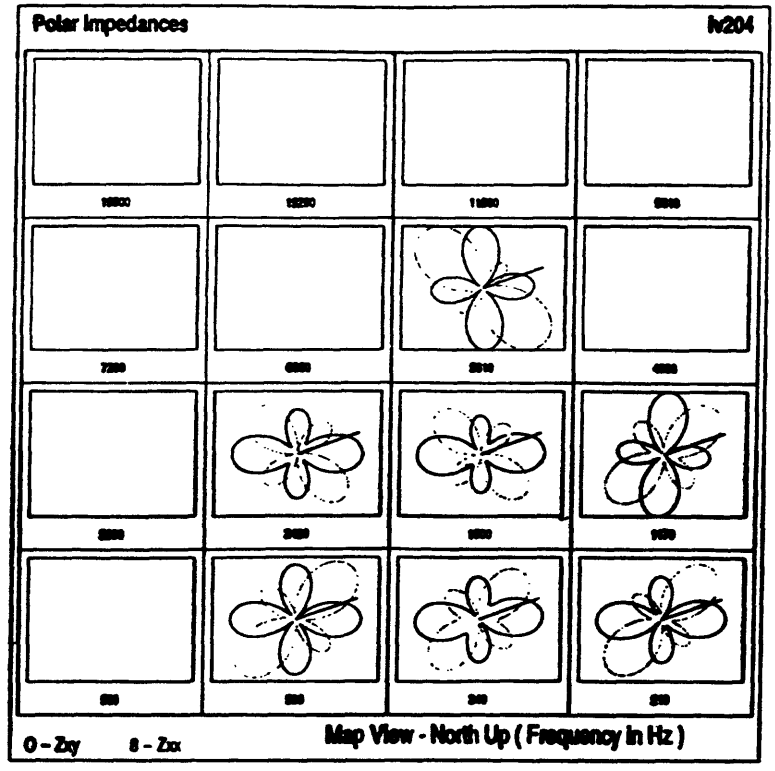

Figure 19-C--Site 204 continued; see caption figure 7-C.

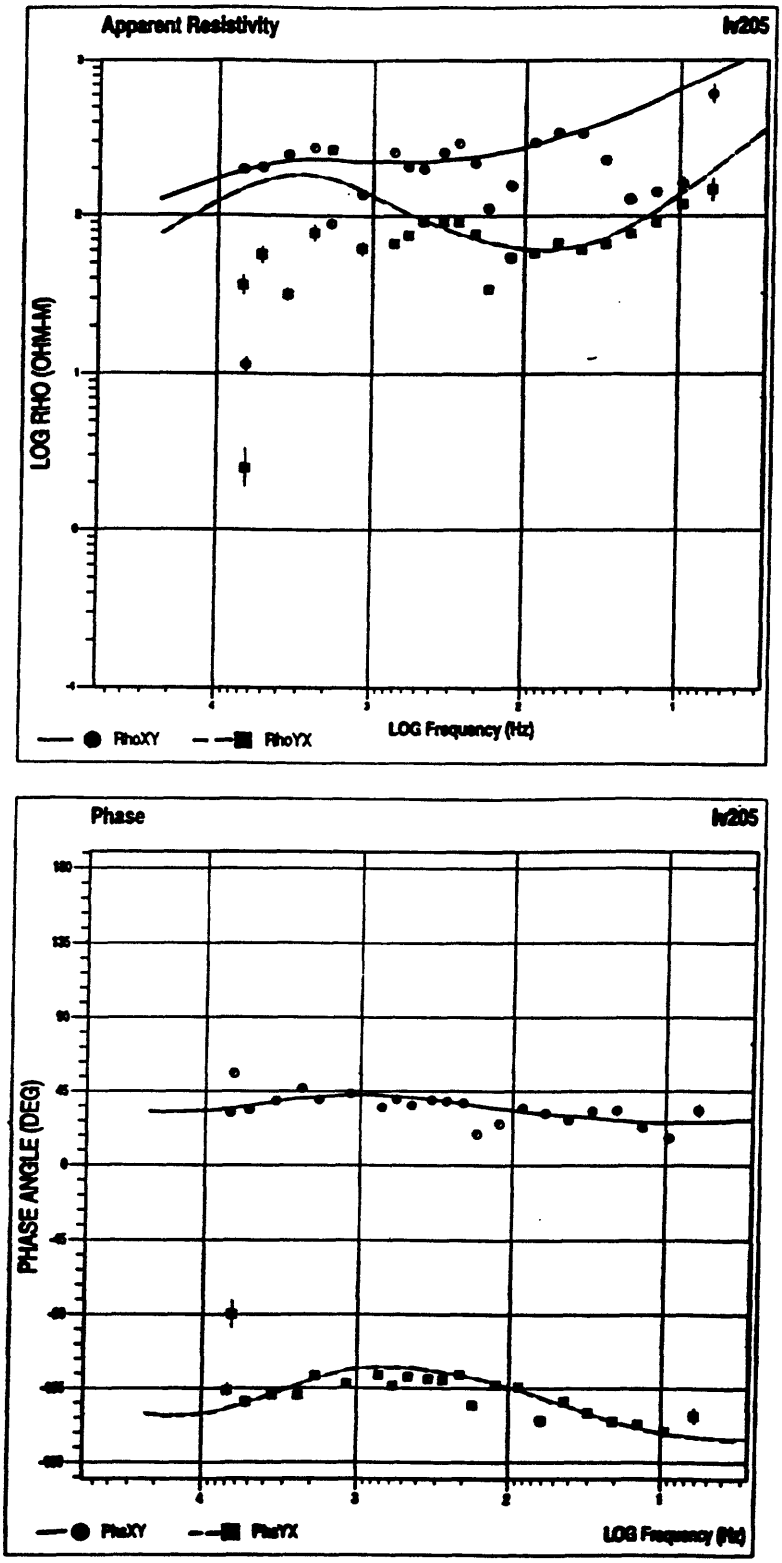

Figure 20-A--Data parameters for site 205; see caption figure 7-A.

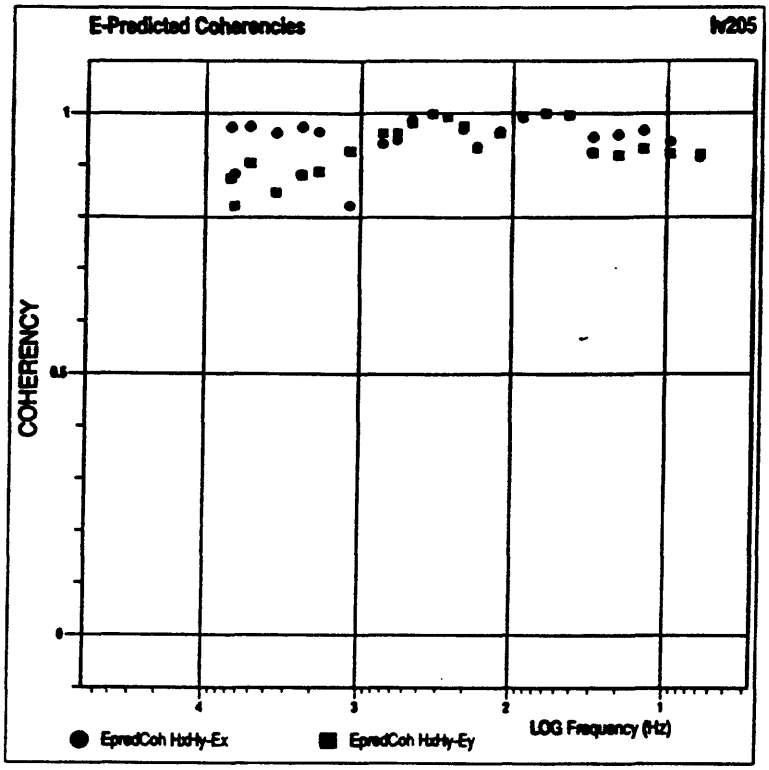

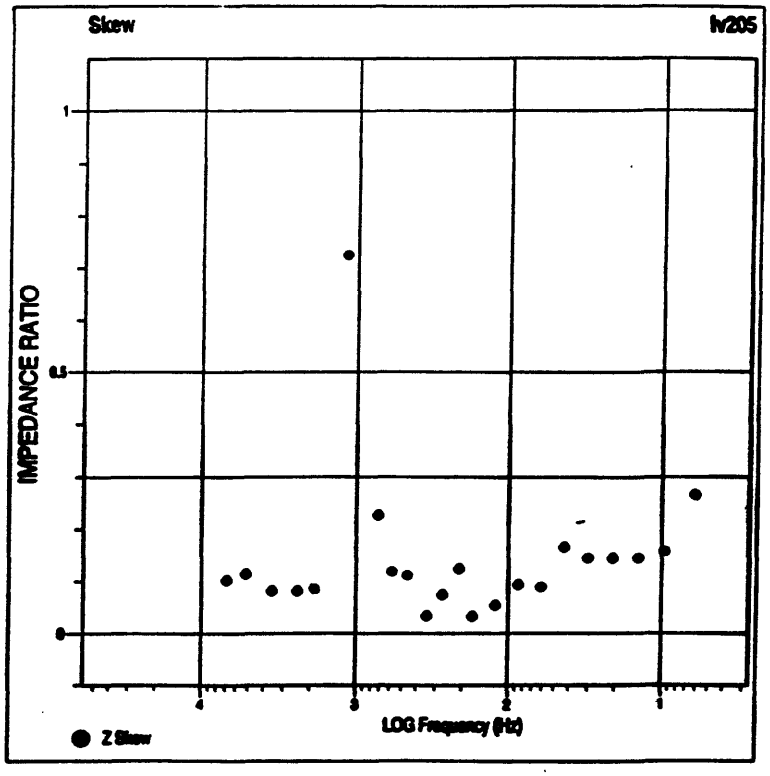

Figure 20-B--Site 205 continued; see caption figure 7-B.

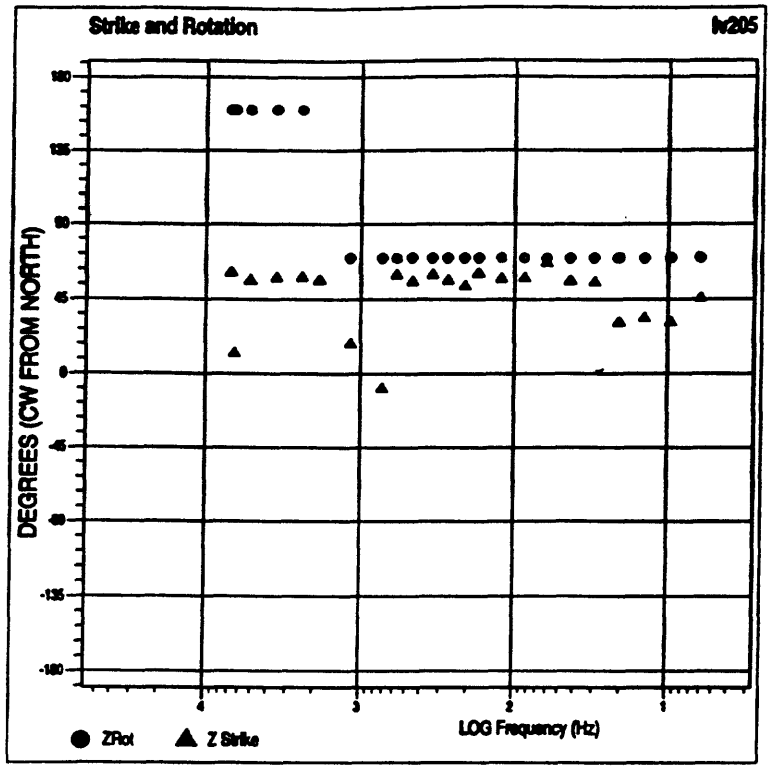

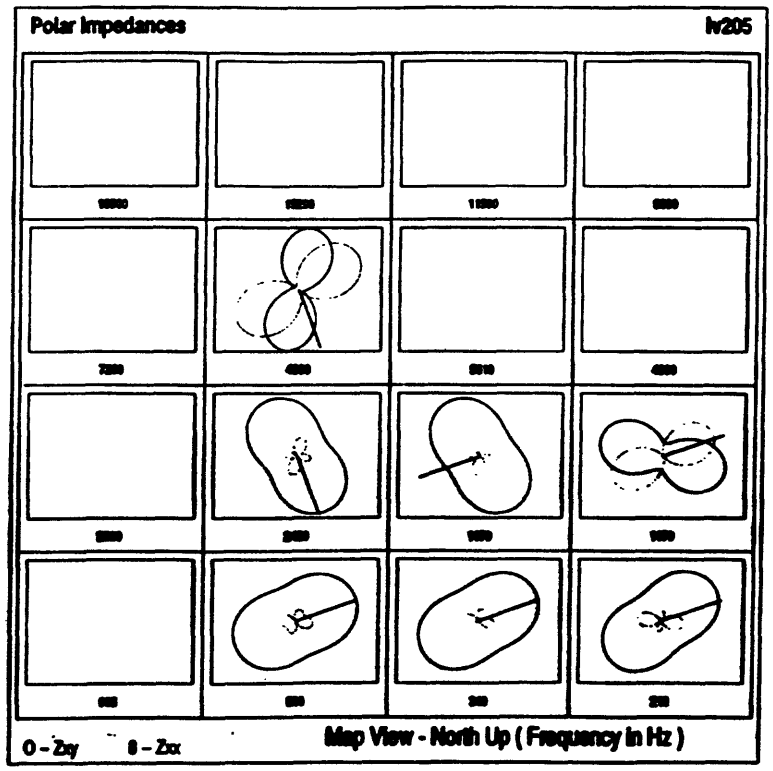

Figure 20-C–Site 205 continued; see caption figure 7-C.

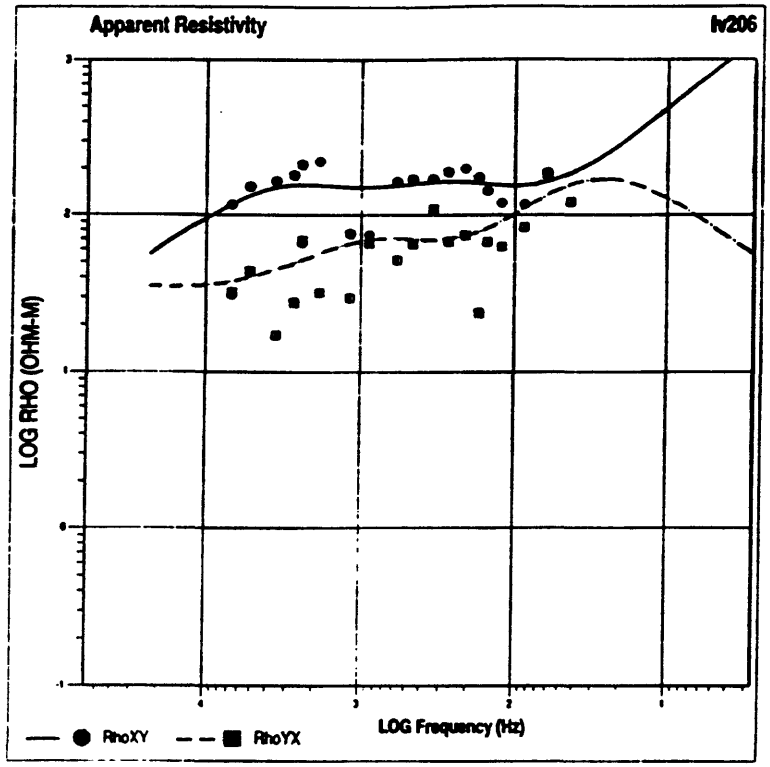

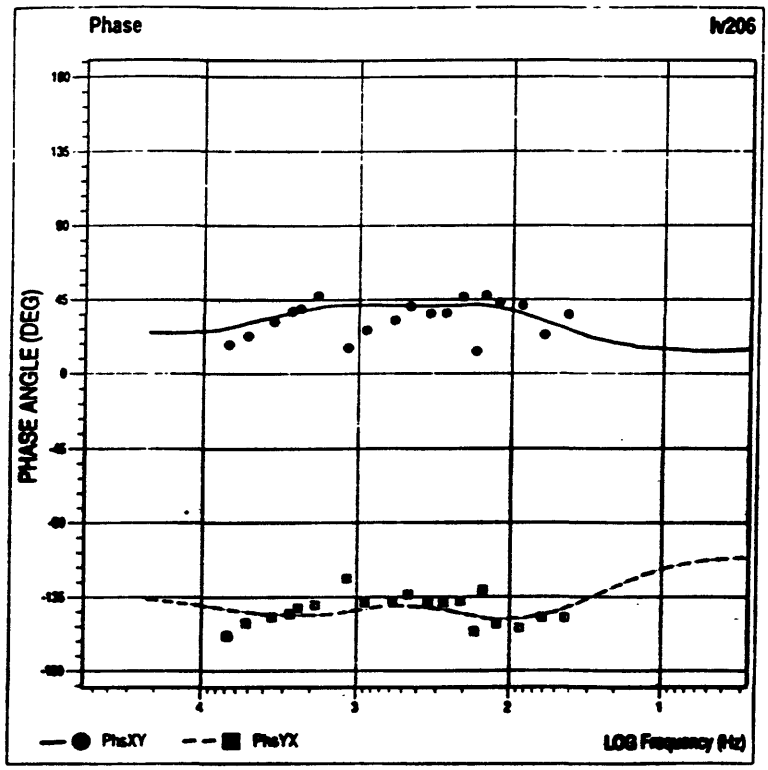

Figure 21-A--Data parameters for site 206; see caption figure 7-A.

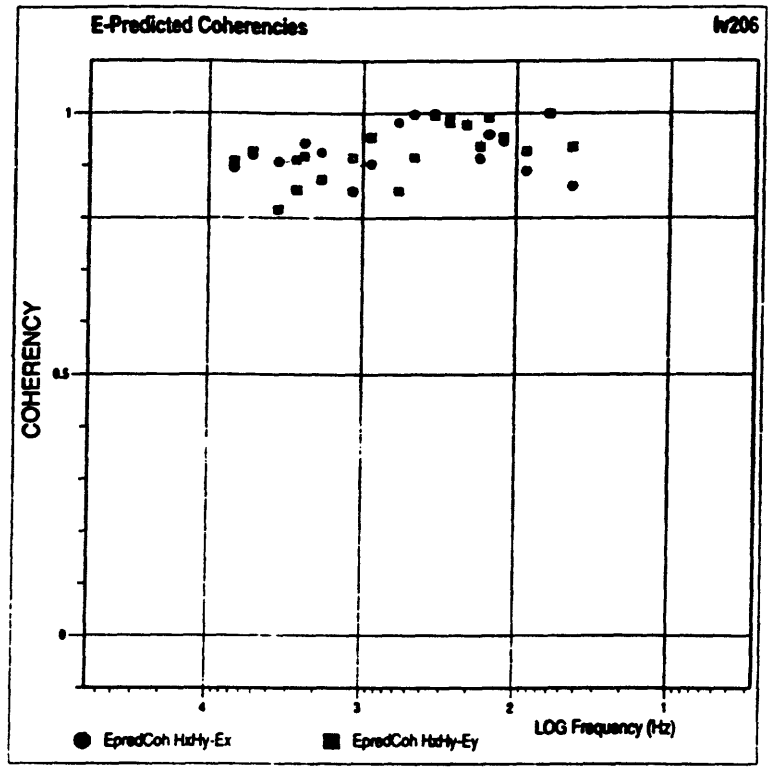

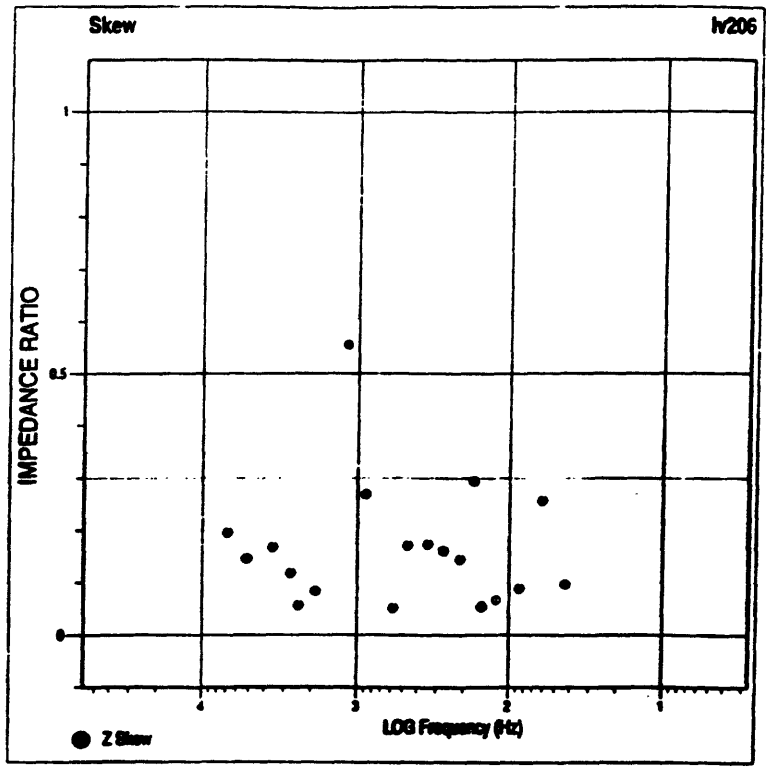

Figure 21-B--Site 206 continued; see caption figure 7-B.

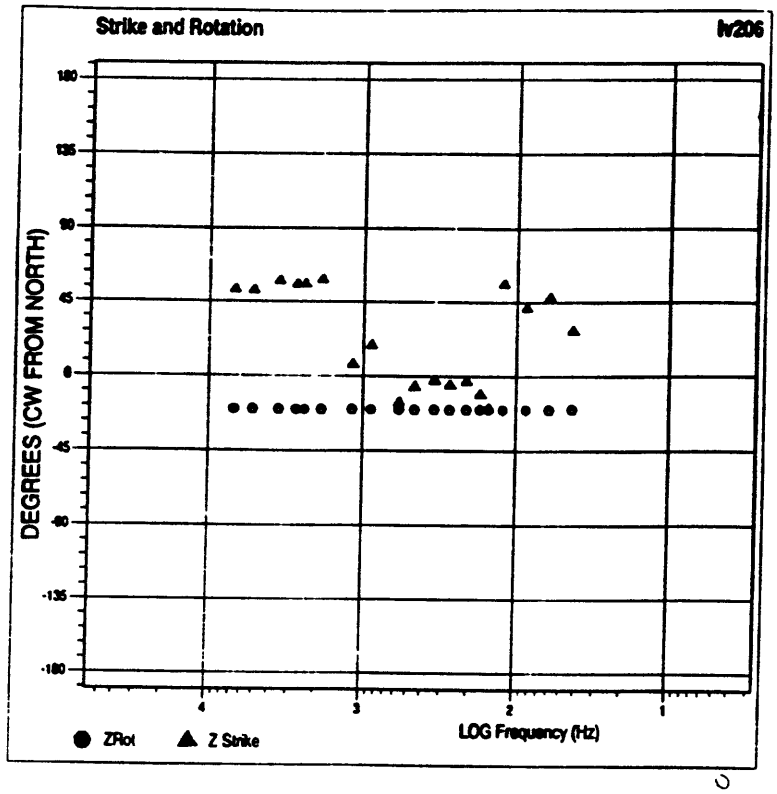

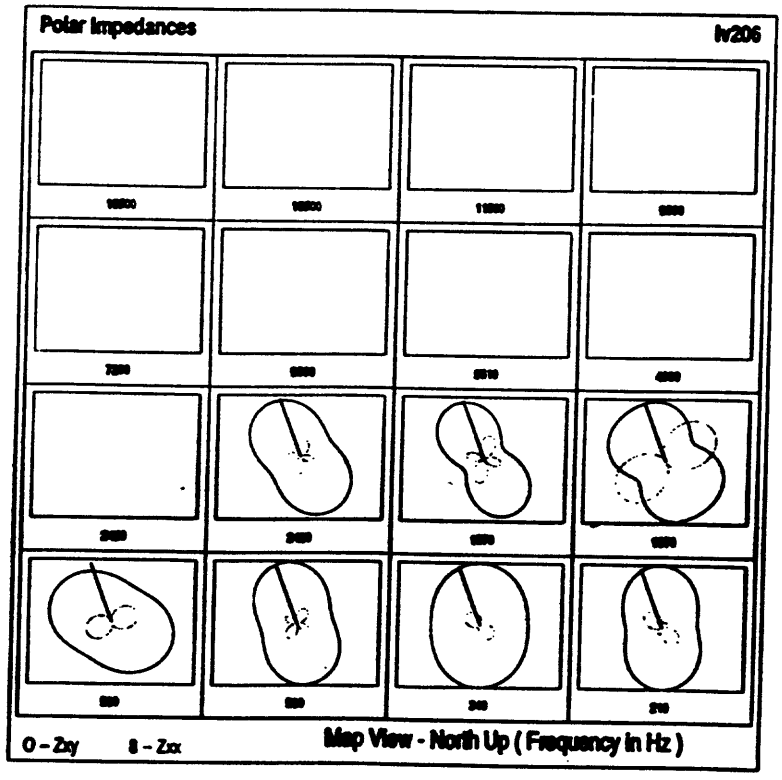

Figure 21-C--Site 206 continued; see caption figure 7-C.

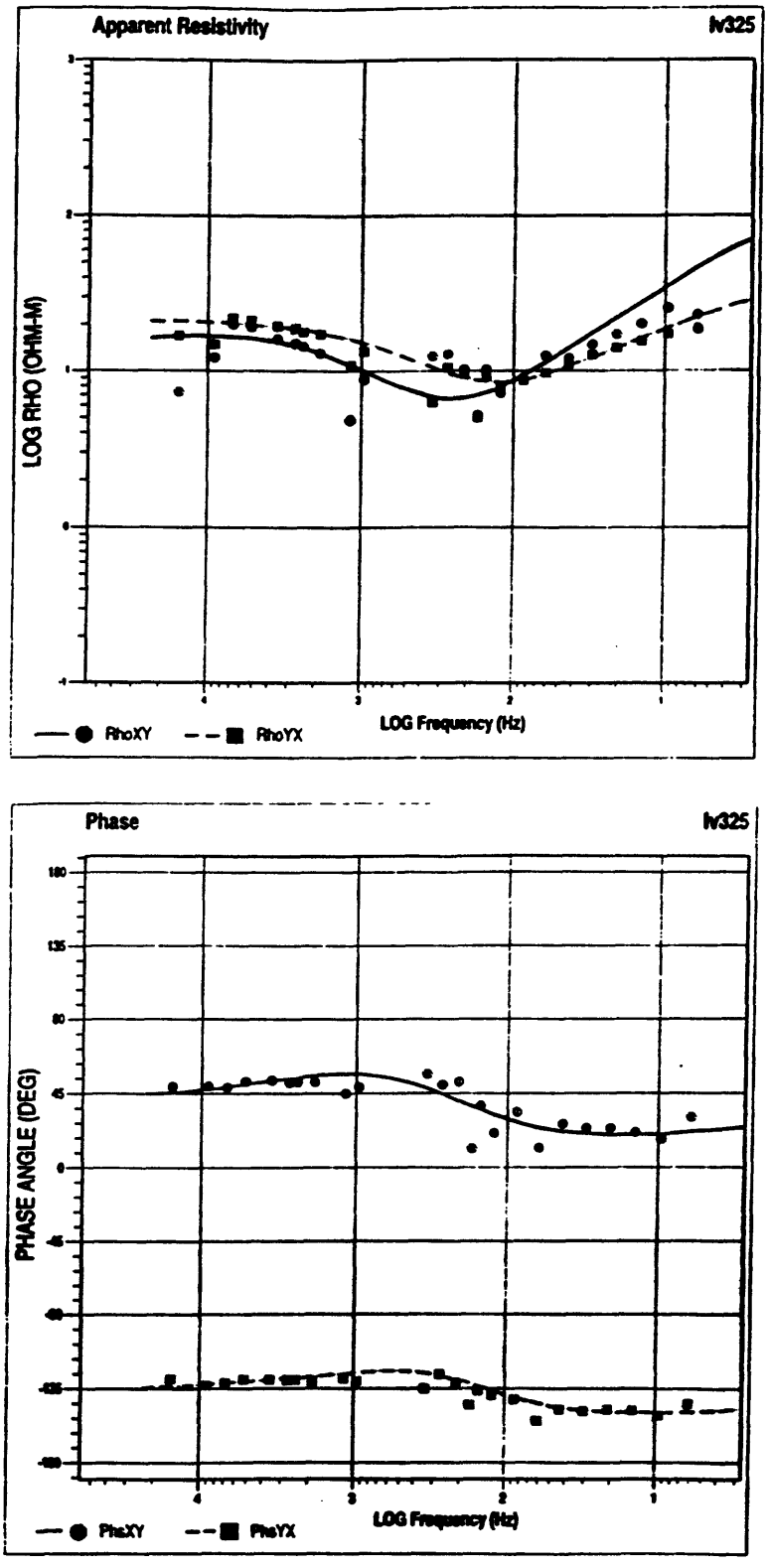

Figure 22-A--Data parameters for site 325; see caption figure 7-A.

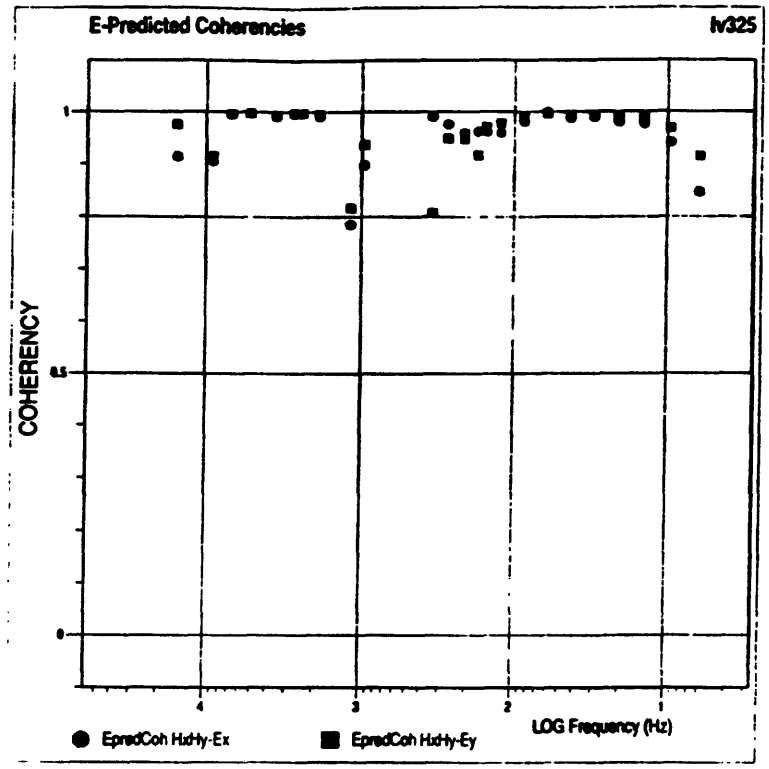

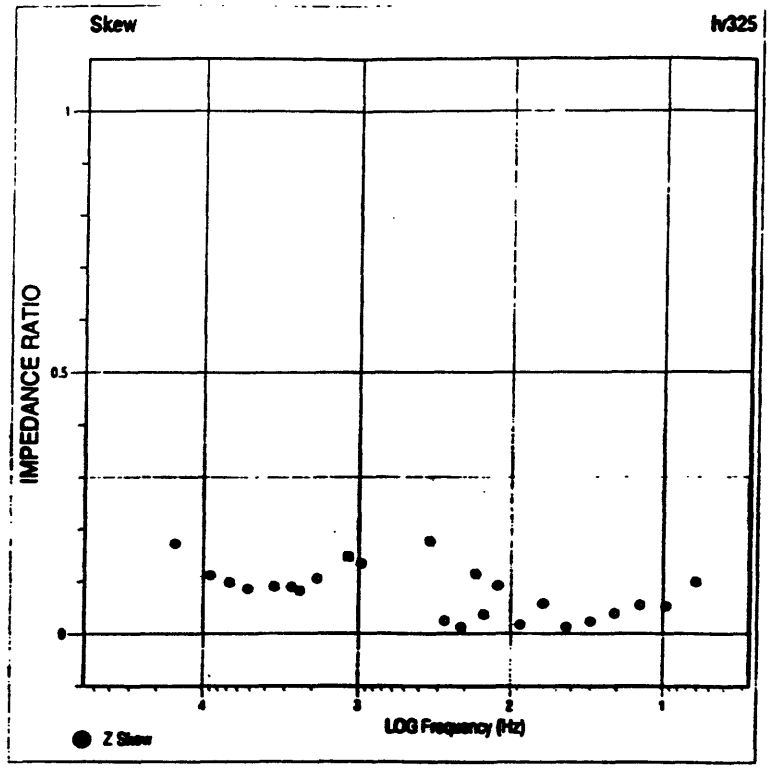

Figure 22-B--Site 325 continued; see caption figure 7-B.

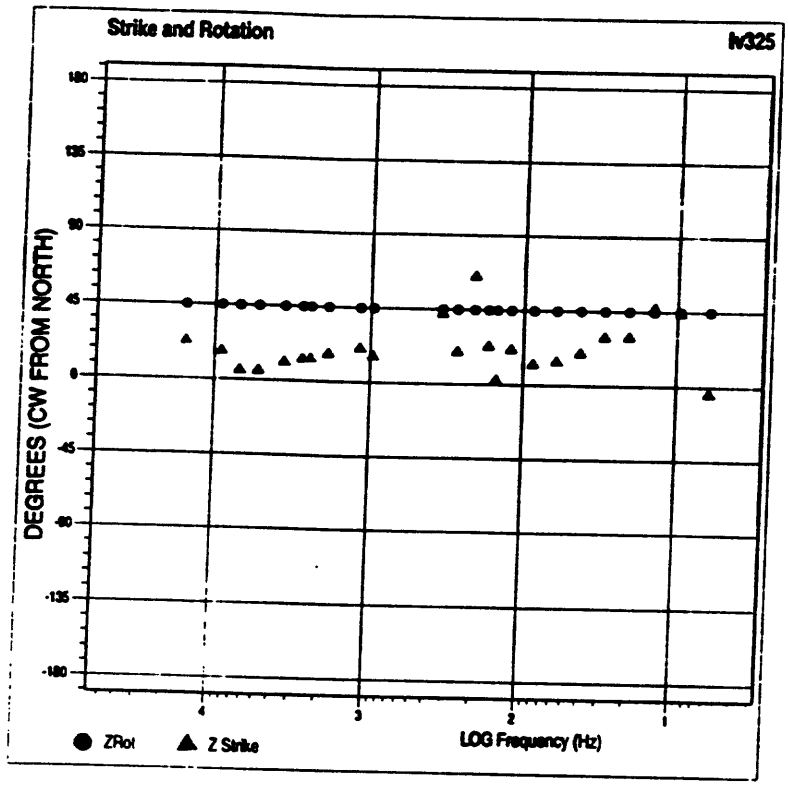

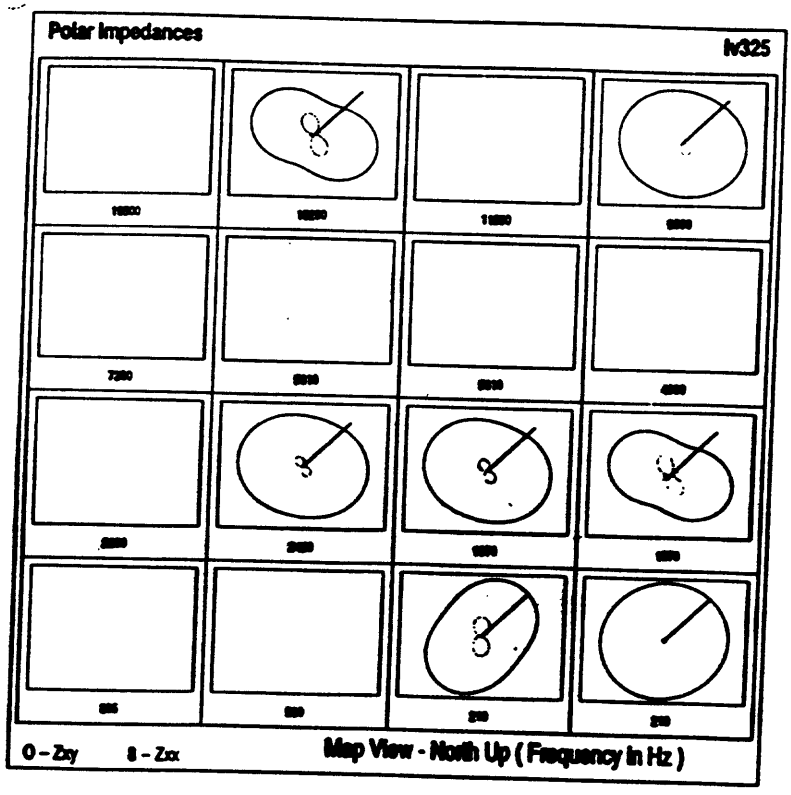

Figure 22-C--Site 325 continued; see caption figure 7-C.

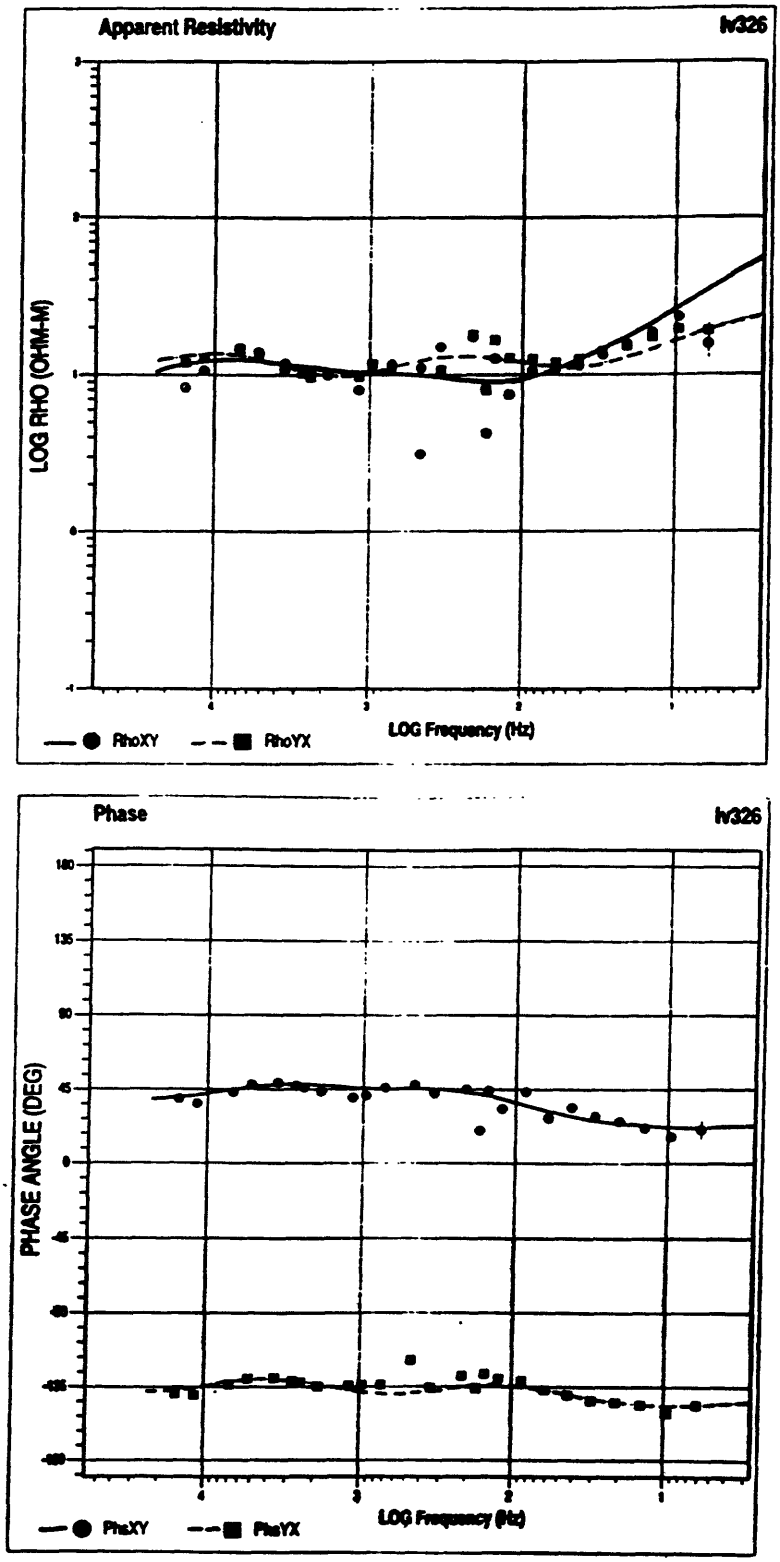

Figure 23-A–Data parameters for site 326; see caption figure 7-A.

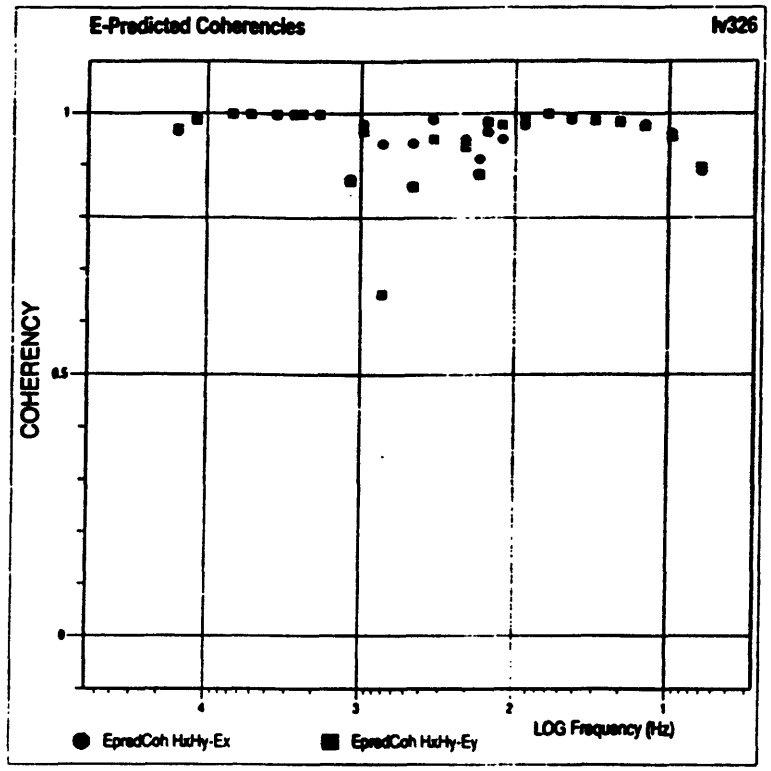

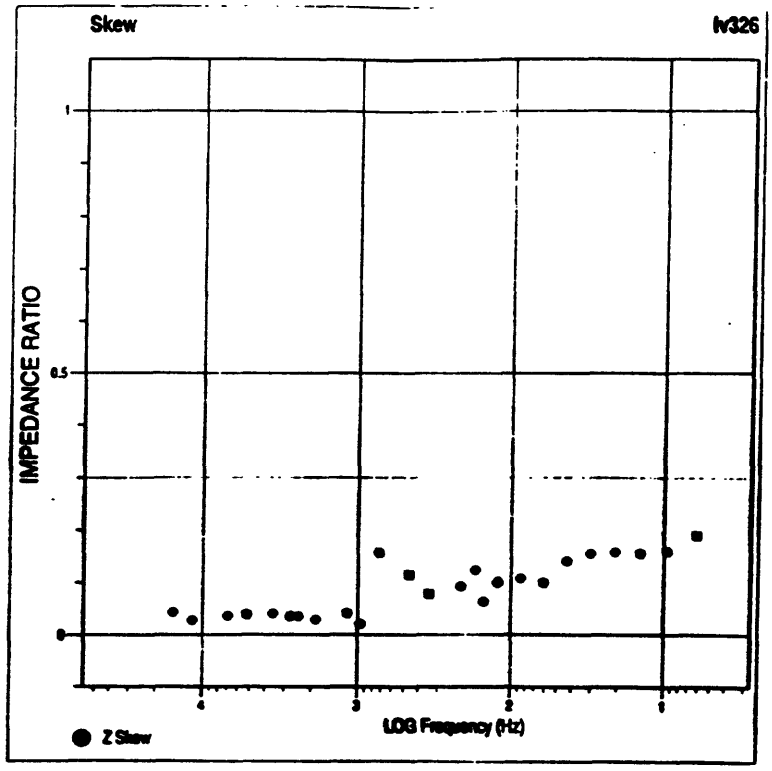

Figure 23-B–Site 326 continued; see caption figure 7-B.

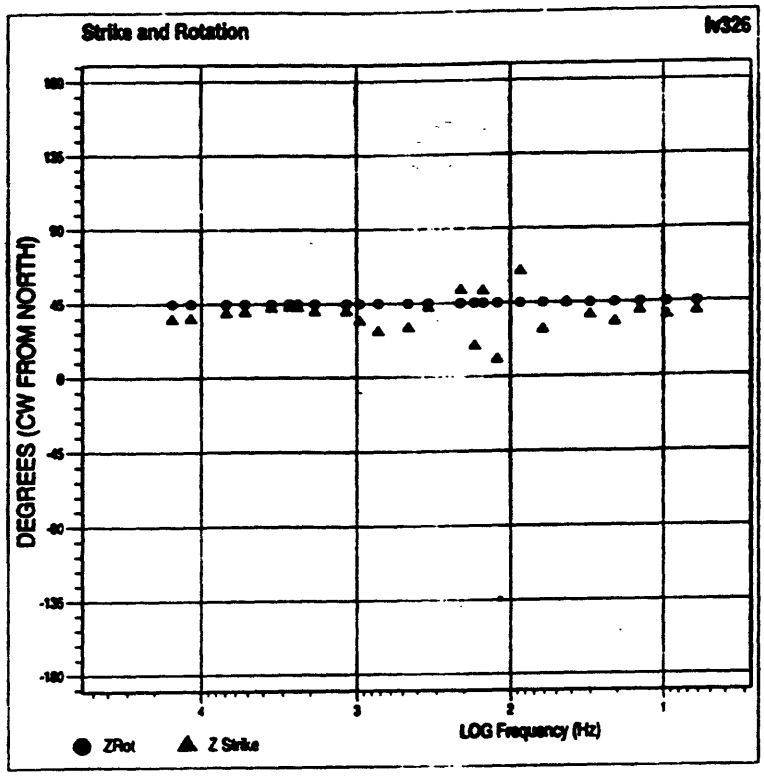

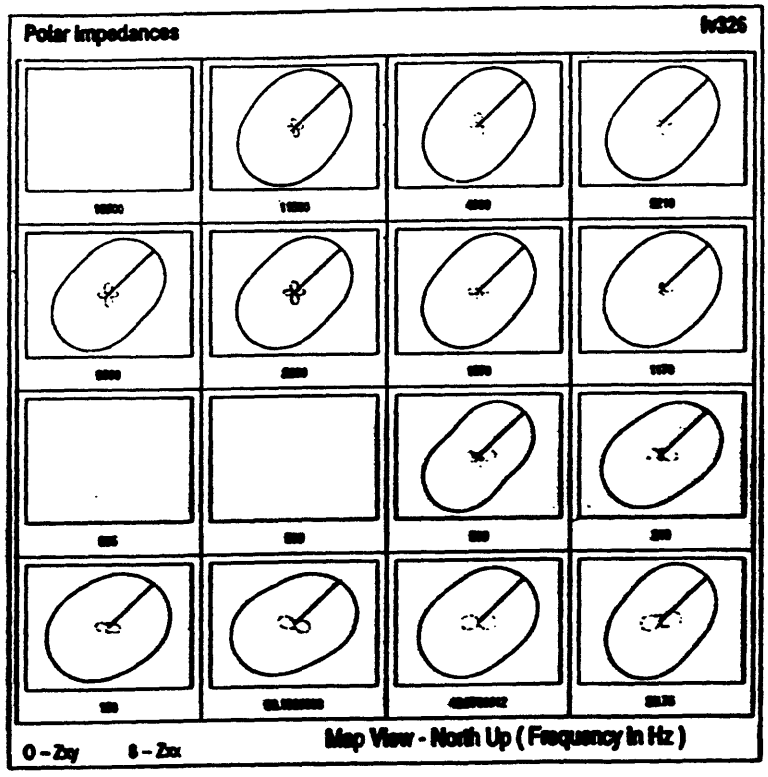

Figure 23-C--Site 326 continued; see caption figure 7-C.